PONTIFICAL CATHOLIC UNIVERSITY OF PARANÁ - PUCPR

POLYTECHNIC SCHOOL

GRADUATE PROGRAM IN MECHANICAL ENGINEERING - PPGEM

MASTER THESIS

DIFFERENTIAL MODELLING OF HEXANE DISPERSION WITHIN A ROOM

WILLIAM SCHINEIDER RABELO

Curitiba, February 5th, 2025

PONTIFICAL CATHOLIC UNIVERSITY OF PARANÁ – PUCPR

WILLIAM SCHINEIDER RABELO

DIFFERENTIAL MODELLING OF HEXANE DISPERSION WITHIN A ROOM

Thesis presented to the Graduate Program in Mechanical Engineering (PPGEM) of the Pontifical Catholic University of Paraná, as partial requirement to obtain the degree of Master in Mechanical Engineering.

Supervisor: Prof. PhD. Nathan Mendes
Co-Supervisor: Prof. PhD. Marcos Batistella Lopes

Curitiba, February 5th, 2025

Dados da Catalogação na Publicação
Pontifícia Universidade Católica do Paraná
Sistema Integrado de Bibliotecas – SIBI/PUCPR
Biblioteca Central
Gisele Alves – CRB 9/1578

R114d
2025

Rabelo, William Schineider
Differential modelling of hexane dispersion within a room / William Schineider Rabelo ; supervisor : Nathan Mendes ; co-supervisor : Marcos Batistella Lopes. – 2025.
105 f. : il. ; 30 cm

Dissertação (mestrado) – Pontifícia Universidade Católica do Paraná, Curitiba, 2025
Bibliografia: f. 79-84

1. Fluidodinâmica computacional. 2. Ar – Qualidade. 3. Hexano. 4. Gás. I. Mendes, Nathan. II. Lopes, Marcos Batistella. III. Pontifícia Universidade Católica do Paraná. Programa de Pós-Graduação em Engenharia Mecânica. IV. Título.

CDD 20. ed. – 620.1

Pontifícia Universidade Católica do Paraná–PUCPR
Escola Politécnica
Programa de Pós-Graduação em Engenharia Mecânica-PPGEM

APPROVAL TERM

William Schineider RABELO

Differential Modelling of Hexane Dispersion Within a Room

Master´s thesis approved as a partial requirement for obtaining a master's degree in the Master's Course in Mechanical Engineering, Postgraduate Program in Mechanical Engineering, of the Polytechnic School at the Pontifical Catholic University of Paraná, by the following examining board:

Prof. Dr. Carsten RODE
Technical University of Denmark, DTU

Dr. Daniela Andresa MORTARI
CEREMA Centre-Est - L'Isle d'Abeau, França, Rapporteur

Documento assinado digitalmente
gov.br MARCOS BATISTELLA LOPES
Data: 06/02/2025 09:21:06-0300
Verifique em https://validar.iti.gov.br

Prof. Dr. Marcos Batistella LOPES
Pontifícia Universidade Católica do Paraná, PUCPR, Co-Supervisor

Documento assinado digitalmente
gov.br NATHAN MENDES
Data: 06/02/2025 09:56:45-0300
Verifique em https://validar.iti.gov.br

Prof. Dr. Nathan MENDES
Pontifícia Universidade Católica do Paraná, PUCPR, Supervisor

Curitiba, Brazil, 5.February.2025

ACKNOWLEDGEMENTS

I would first like to thank my advisor, Nathan Mendes and my co-advisor Marcos Batistella Lopes. Their help in carrying out this work was indispensable, always providing valuable insights into how to approach the themes of this work.

I would also like to thank CAPES and PUCPR for their financial support and for giving me the opportunity to study in such a rich and intellectually stimulating environment. I would also like to thank the PPGEM teachers and staff who were always willing to help me when I needed it.

I would like to thank my family, my mother Zeni Leal and my father Celso Bracale Rabelo, for their love and support during these years, which were challenging in many ways, but which I was able to overcome alongside them (and away from them), and it is to them that I dedicate this work.

This study was financed in part by the Coordenação de Aperfeiçoamento de Pessoal de Nível Superior - Brasil (CAPES) - Finance Code 001

“Essentially, all models are wrong, but some are useful.”

(Box; Draper, 1987)

TABLE OF CONTENTS

LIST OF FIGURES

LIST OF TABLES

NOMENCLATURE

Latin Alphabet:

C	Constant for Tetrahedron Mesh 124.70765802	[-]
C_μ	Constant with value of 0.09	[-]
c_p	Specific Heat at Constant Pressure	$[J \cdot kg^{-1} \cdot K^{-1}]$
$C_{1\varepsilon}$	Constant with value 1.44	[-]
C_2	Constant with value 1.9	[-]
$C_{3\varepsilon}$	This variable determines the degree of buoyancy effect. It is zero when buoyant shear layers are perpendicular to the gravitational vector	[-]
G_k	Generation of turbulence kinetic energy due to mean velocity gradient	[-]
G_b	Generation of turbulence kinetic energy due to buoyancy	[-]
$\vec{J}_i$	The diffusion flux of species *i*	$[mol/m^2 \cdot s]$
k	Thermal Conductivity	$[W/(m \cdot K)]$
p	Static Pressure	[Pa]
q''	Volumetric Rate of Thermal Energy Generation	$[W/m^3]$
R_i	The net rate of production of species *i* by chemical reaction	[-]
S_i	The rate of creation by addition from the dispersed phase plus any user-define sources.	[-]
S_ε	User-defined source term	[-]
S_k	User-defined source term	[-]
T	Temperature	[K]
t	Time	[s]
u	Component of the mass average velocity	[-]
$\vec{v}$	The three-dimensional velocity components	[m/s]
v	Component of the mass average velocity	[m/s]
w	Component of the mass average velocity	[m/s]
x	Component of the mass average velocity	[m/s]
Y_i	The mass fraction of species *i*	[-]
Y_M	Contribution of the fluctuating dilatation in compressible turbulence to the overall dissipation rate. In this work the airflow is incompressible	$[kg/m^3]$

y	Component of the mass average velocity	[m/s]
z	Component of the mass average velocity	[m/s]

Greek Alphabet:

μ_t	Turbulent Viscosity	[Pa·s]
ρ	Density of species i	[kg/m^3]
μ	Dynamic Viscosity	[Pa·s]
ρ	Fluid Density	[kg/m^3]
$\sigma\varepsilon$	Constant with value 1.2	[-]
σ_k	Constant with value 1.0	[-]

Subscripts:

i	Chemical Specie

Acronyms:

ACH	Air Changes per Hour
ASHRAE	American Society of Heating, Refrigerating and Air Conditioning Engineers
BBRI	Belgian Building Research Institute
BSD	Berkeley Software Distribution
CAD	Computer-Aided Design
CFD	Computational Fluid Dynamics
CPU	Central Processing Unit
DALY	Disability-Adjusted Life-Years
DES	Detached Eddy Simulation
DFVLR	German Test and Research Institute for Aviation and Space Flight
DNS	Direct Numerical Simulation
EPS	Expanded Polystyrene
FDM	Finite Difference Method
FVM	Finite Volume Method
GC-FID	Gas Chromatography-Fame Ionization Detection

GC-MS	Gas Chromatography-Mass Spectrometry
HVAC	Heating, Ventilation, and Air Conditioning
IAQ	Indoor Air Quality
IEA-EBC	Energy Agency - Energy in Buildings and Communities Program
LES	Large Eddy Simulation
MDF	Medium-Density Fiberboard
MVHR	Mechanical Ventilation with Heat Recovery
NV	Natural Ventilation
OAPEC	Organization of Arab Petroleum Exporting Countries
OECD	Organization for Economic Co-operation and Development
PPM	Parts per Million
PM	Particulate Matter
PH	Passive House
PU	Polyurethane
RAM	Random Access Memory
RANS	Reynolds Average Navier-Stokes
RNG	Re-Normalization Group
RSTM	Reynolds Stress Transport Model
SBR	Styrene-Butadiene Rubber
TVOC	Total Volatile Organic Compound
UDF	User Defined Function
VOC	Volatile Organic Compound
ZEB	Zero Energy Buildings

RESUMO

Este estudo investiga a modelagem diferencial da dispersão de hexano em um ambiente interno usando a Dinâmica de Fluidos Computacional (CFD). Os modelos tradicionais dependentes do tempo pressupõem uma condição bem misturada dentro do ambiente, muitas vezes ignorando a variabilidade espacial das concentrações de poluentes. Esta pesquisa tem como objetivo preencher essa lacuna implementando uma abordagem diferencial para simular a distribuição espacial do hexano, um poluente transportado pelo ar, sob condições variáveis de ventilação na célula de teste Passys. As simulações de CFD foram conduzidas usando o software Fluent, considerando as propriedades físicas e o comportamento dinâmico do hexano e das misturas de ar. Os resultados comparados a outros resultados do exercício comum número 1 do Anexo 68 da Agência internacional de Energia, destacam as vantagens da análise espacial em relação aos modelos de parâmetros lumped, fornecendo informações detalhadas sobre áreas com possível acúmulo de poluentes. Os resultados de concentração máxima são: Teste de Campo 2.31e-2 [kg/m^3], Matlab HAMFitPlus 1e1 [kg/m^3], TRNSYS16 1e-8 [kg/m^3], Matlab ODE23S 1e1 [kg/m^3], CONTAM-TRNSYS 1e-8 [kg/m^3], DELPHIN6 9.25e-6 [kg/m^3] e FLUENT 1.55e-1 [kg/m^3]. Essas informações são essenciais para otimizar as estratégias de ventilação e garantir a qualidade do ar interno. As descobertas sugerem que, embora os modelos CFD ofereçam maior precisão, suas demandas computacionais representam um desafio para simulações de larga escala ou de longo prazo, enfatizando a necessidade de abordagens equilibradas em aplicações práticas.

Palavras-chave: Dinâmica de Fluidos Computacional, Dispersão de Gás, Qualidade do Ar Interior, Hexano, Otimização da Ventilação.

ABSTRACT

This study investigates the differential modeling of hexane dispersion within an indoor environment using Computational Fluid Dynamics (CFD). Traditional time-dependent models assume a well-mixed condition within the room, often overlooking the spatial variability of pollutant concentrations. This research aims to bridge this gap by implementing a differential approach to simulate the spatial distribution of hexane, an airborne pollutant, under varying ventilation conditions in the Passys test cell. The CFD simulations were conducted using the software Fluent, considering the physical properties and dynamic behavior of hexane and air mixtures. The results compared to other results from the common exercise number 1 of Annex 68 of the International Energy Agency, highlight the advantages of spatial analysis over lumped parameter models, providing detailed insights into areas with potential pollutant accumulation. The maximum concentration results are: Field Test 2.31e-2 [kg/m^3], Matlab HAMFitPlus 1e1 [kg/m^3], TRNSYS16 1e-8 [kg/m^3], Matlab ODE23S 1e1 [kg/m^3], CONTAM-TRNSYS 1e-8 [kg/m^3], DELPHIN6 9.25e-6 [kg/m^3] and FLUENT 1.55e-1 [kg/m^3]. This information is crucial for optimizing ventilation strategies to ensure indoor air quality. The findings suggest that while CFD models offer enhanced precision, their computational demands pose a challenge for large-scale or long-term simulations, emphasizing the need for balanced approaches in practical applications.

Keywords: Computational Fluid Dynamics, Gas Dispersion, Indoor Air Quality, Hexane, Ventilation Optimization.

CHAPTER 1
INTRODUCTION

1.1 MOTIVATION

Humanity is now facing two critical challenges in our history on this planet. One in the broader context as species and another more localized in time, within the realm of geopolitics. The first is the natural climate change in geological timescale, with possible anthropic components associated with it, while the second is the need of States to be as energy efficient as possible in a very unstable world. Since both the industrial sector and residential sector accounts for more the 50% of global energy use today (U.S. Energy Information Administration Office of Energy Analysis, 2019, p. 14), we have two ways to increase our energy efficiency, reduce our greenhouse gas emissions and improve our resilience, one by practicing nearshoring (Fernández-Miguel *et al.*, 2022, p. 10), while the other is by reducing the energy consumption of the residential sector.

Coupled with climate and geopolitical challenges, we have an unprecedented demographic phenomenon happening globally. While most countries in western hemisphere will face an abrupt demographic decline, Africa and Asia will rise as the youngest continents on Earth. The United Nations (World Population Prospects 2024, 2024, p. 3) estimate that world population will stabilize around 10.2 billion people towards the end of the century as shown in the Figure 1.

Figure 1 - Global population, according to United Nations (World Population Prospects) in 2013 and 2024, 1995-2100

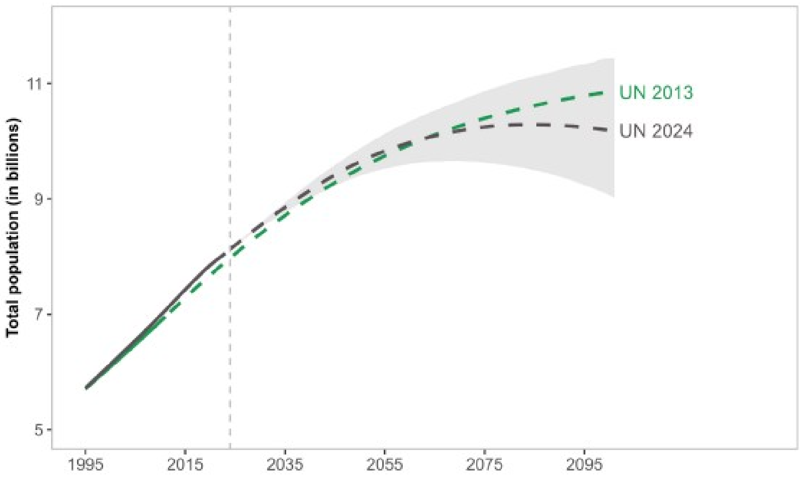

Sources: United Nations (2013; 2024a).
Notes: Estimates correspond to the period from 1995 to 2023 in United Nations (2024) and from 1995 to 2010 in United Nations (2013); projections correspond to the period from 2024 to 2100 (with 95 per cent prediction intervals) in United Nations (2024) and from 2010 to 2100 in United Nations (2013). United Nations has been abbreviated as UN.

Source: (World Population Prospects 2024, 2024)

This increase in population will change today's demographic distribution around the world. In 2015, the world population was 1 billion in the Americas, North and South combined; 1 billion in Europe and Russia; 1 billion in Africa and 4 billion in Asia and Oceania. For the end of the century, projections estimate a completely different scenario, 1 billion in the Americas, North and South combined; 1 billion in Europe and Russia; 4 billions in Africa and 5 billions in Asia and Oceania (Don't Panic - The Facts About Population, 2013).

Africa and Asia will go through an unprecedented industrialization and urbanization process due to the abrupt increase in its population. The effects on global energy consumption for the next decades will make the non-OECD countries by far the biggest consumers of the global energy production already in 2050 (U.S. Energy Information Administration Office of Energy Analysis, 2019, p. 23) as shown in Figure 2.

Figure 2 - World Energy Consumption from 2010 until 2050

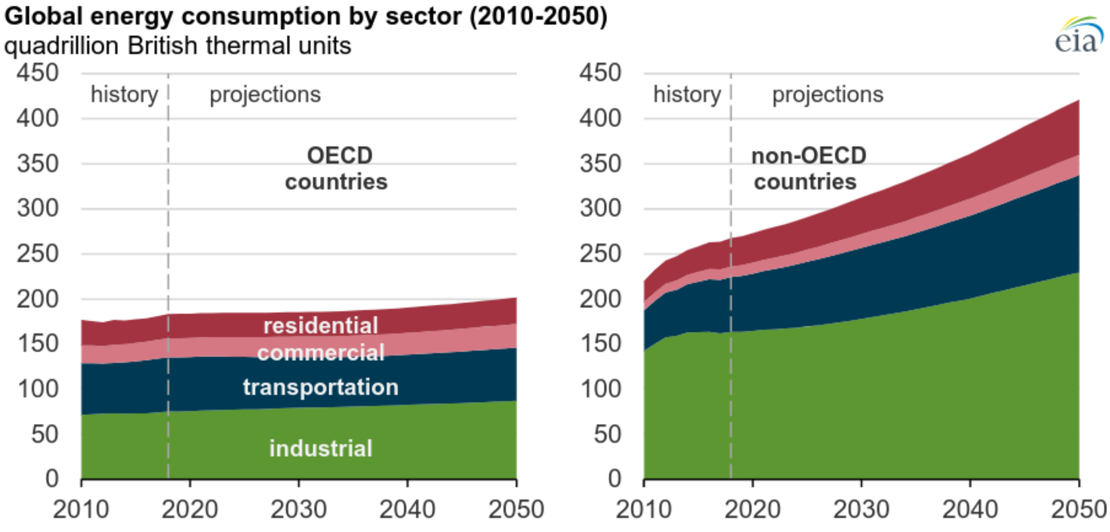

Source: (EIA projects nearly 50% increase in world energy usage by 2050, led by growth in Asia - U.S. Energy Information Administration (EIA), 2024)

This demographic phenomena will produce the biggest cities in human history, with populations far bigger than 10 million people like shown in Table 1. From the top 20 megacities in 2100, 13 will be in Africa, while 7 in Asia (Desjardins, 2018).

Table 1 - World's Twenty Largest Megacities in 2100

Rank	Population (2100)	City	Country
# 1	88.3 million	Lagos	Nigeria
# 2	83.5 million	Kinshasa	DRC
# 3	73.7 million	Dar Es Salaam	Tanzania
# 4	67.2 million	Mumbai	India
# 5	57.3 million	Delhi	India
# 6	56.6 million	Khartoum	Sudan
# 7	56.1 million	Niamey	Niger
# 8	54.3 million	Dhaka	Bangladesh
# 9	52.4 million	Kolkata	India
# 10	50.3 million	Kabul	Afghanistan
# 11	49.1 million	Karachi	Pakistan
# 12	46.7 million	Nairobi	Kenya
# 13	41.4 million	Lilongwe	Malawi
# 14	40.9 million	Blantyre City	Malawi
# 15	40.5 million	Cairo	Egypt
# 16	40.1 million	Kampala	Uganda
# 17	40.0 million	Manila	Phillippines
# 18	37.7 million	Lusaka	Zambia
# 19	36.4 million	Mogadishu	Somalia
# 20	35.8 million	Addis Ababa	Ethiopia

Source: (Desjardins, 2018)

While the disruption of our current global supply chain and the emerging nearshoring phenomena will gradually reduce our greenhouse gas emissions, and slightly improve the energy efficiency of the industrial sector, the residential sector will face an even bigger challenge. A rapid increase in energy demand due to urbanization process ahead of us in many developing countries, will raise concerns about security of energy supply. This transition must be based on solid technologies and best practices, both to safeguard people’s health, while guaranteeing energy efficiency.

One possible solution for the upcoming energy demand shock is a worldwide pursue of a Zero Energy Buildings (ZEB) in the construction sector. Where a ZEB is a building that uses less than or equal to zero energy by the building on-site renewable energy sources on annual basis (Kilkis, 2007). However, in order to achieve it, one of the most important aspects that determine the energy consumption of a building besides human behavior is its HVAC (Heating, Ventilation, and air conditioning) system. HVAC systems today accounts for more than 40% in building's total energy consumption in commercial buildings, while space heating represents 33% of the total energy use in residential buildings (Best Practices in HVAC System Maintenance to Optimize Efficiency, 2016). Commercial heating and cooling energy use are expected to account to up 84% of energy use in buildings till 2050, while for residential buildings it is expected to be around 79% in the same period (Ürge-Vorsatz *et al.*, 2015, p. 97).

In order to achieve such high standard of energy efficiency, new buildings and refurbished ones must achieve Passive House standard with an airtight and high insulation envelope, coupled with mechanical ventilation with heat recovery (MVHR), without affecting its indoor air quality (Rode *et al.*, 2016a, p. 1). Indoor air quality in buildings is an extremely important factor for human health, since people typically spend 80% to 90% of their time indoors (Liang; Qin, 2017; Liu *et al.*, 2021, p. 1). While in big cities like London and Beijing the external pollution factor are driven by outdoor pollution and traffic (e.g. Micro-particles and NO_2) (Burman *et al.*, 2018, p. 839), the in indoor pollution is mainly due to short-term sources, such as environmental tobacco smoke and cooking, and long-term sources like building materials, such as furniture and painting (Liang; Qin, 2017, p. 3). Particulate Matter ($PM_{2.5}$) and NO_2 can get indoors from outdoor sources, however it can also have indoor sources, like gas or wood stoves. While particle filters and NO_2 filters can help to reduce those pollutants from outside sources, most VOCs are driven by internal sources (Burman; Stamp, 2019, p. 1009).

Many common materials present in modern dwellings are sources of pollutants. The lack of characterization of VOCs in building materials and the increasing usage of those materials such as medium-density fiberboard (MDF) in indoor furniture, increases the concentration of formaldehyde in indoor air (Burman; Stamp, 2019, p. 1008). The authors (Burman; Stamp, 2019, p. 1008) also bring attention to the lack of building regulations in UK regarding formaldehyde.

> Formaldehyde is currently not regulated in the UK Building Regulations. Given the potential health impact of high formaldehyde concentrations and the empirical evidence, it is necessary to cover formaldehyde in the next edition of the Building Regulations. This study points to the significance of improving the existing regulations and standards to clearly define maximum permissible emission factors for various VOCs in building material and indoor furniture.

The role of seasons into indoor air quality is also another important factor. In an experimental study (Burman; Stamp, 2019, p. 1013) noticed higher levels of formaldehyde during winter, even though emissions factors were expected to increase with temperature in summer. The explanation is that during summer the combination of natural ventilation through windows, doors and balcony, coupled with background ventilation by MVHR (Mechanical Ventilation Heat Recovery) systems, provided higher air change rates compared to winter.

Even though natural ventilation, together with MVHR can reduce pollutants in the time of the year when they are expected to have its highest indoor pollutant emissions. Buildings that have low air permeability and high levels of insulation coupled with MVHR are the best option to find balance between energy efficiency and indoor air quality (Burman *et al.*, 2018, p. 839). The focus on mechanical ventilation is due to the fact that natural ventilation is recommended when outdoor environmental conditions are favorable (Taheri *et al.*, 2016). In case of big cities where outdoor conditions are not favorable due to high concentrations of PM, the use of mechanical ventilation with filters are recommended (Rojas, 2019, p. 920). Indoor air quality is also a challenge when outdoor conditions are not favorable, since the building envelope must be insulated, indoor environments can have high concentrations of volatile organic compounds (VOCs) due to indoor sources (Liu *et al.*, 2021, p. 1). Aside of VOCs, PM can also have an indoor source from cooking, however it can also be mitigated by cooking hood systems (Rojas, 2019, p. 920).

The indoor pollutants can be separated in two different groups (U.S. Department of Health and Human Services; U.S. Department of Housing and Urban Development, 2012).

- **Biologic:**

Such as bacteria, molds, viruses, animal dander, animal saliva, dust mites, cockroaches, pollen, etc.

- **Chemical:**

Such as CO_2, ozone, environmental tobacco smoke, Volatile Organic Compounds (VOC), radon, pesticides, etc.

In modern day buildings we have numerous air pollution sources, and the level could increase if there is no exchange of fresh air from outside to dilute the emissions of those pollutants and carry them out from the indoor environment. Bellow, there is a list of seventy nonbiological pollutants that (Logue *et al.*, 2012) had sufficient toxicological and epidemiological data to calculate their health impact using the disability-adjusted life-years (DALY) method. In their study, the researchers considered the population-mean exposure concentrations exposed in the Table 2.

Table 2 - Pollutants assumed population-average concentrations (µg/m3)

Pollutant	Concentration	Pollutant	Concentration
1.1.2,2-Tetrachloroethane	0.42	Cyclohexane	5.2
1,1,2-Trichloroethane	0.46	Di(2-ethylhexyl) adipate	1.6_x10^{-2}
1.1-Dichloroethene	1.2	Dibenzo[a,c+a.hjanthracene	1.4_x10^{-5}
1,2-Dibromoethane	0.14	Dibromochloromethane	0.44
1,2-Dichloroethane	0.34	*d*-Limonine	23
1,3-Butadiene	0.46	Ethanol	860
1.4-Dichlorobenzene	50	Ethylbenzene	3.9
2-Butoxyethanol	2.6	Formaldehyde	69
2-Ethylhexanol	3.7	Hexachlorobutadiene	1.7
2-Ethoxyethanol	0.43	Hexane	7.3
2-Methoxyethanol	0.12	Isopropylbenzene	0.4
Acetaldehyde	22	Manganese	3.3_x10^{-3}
Acrolein	2.3	Methyl ethyl ketone	7.4
Acrylonitrile	0.27	Mercury	1.6_x10^{-4}
Ammonia	28	Methyl methacrylate	0.27
Arsenic	9.8_x10^{-4}	Methylene chloride	8.2
Atrazine	59_x10^{-4}	Methyl isobutyl ketone	1,2
Benzaldehyde	2.5	Methyl tert-butyl ether	12
Benzene	2.5	Naphthalene	1,2
Benzo[a]pyrene	9.1_x10^{-5}	NO_2	13.1

Benzyl chloride	0.5	*o*-Phenylphenol	0.13
Beryllium	1.6_x10^{-6}	Ozone	17.2
Bis(2-ethylhexyl) phthalate	0.14	Pentachlorophenol	2.9_x10^{-3}
Bromodichloromethane	0.49	PM_{25}	15,9
Bromoform	0.39	Styrene	5,9
Cadmium	2.6_x10^{-3}	SO_2	2.9
Carbon disulfide	0.34	Tetrachloroethene	1.7
CO	810	Tetrahydrofuran	15
Carbon tetrachloride	0.68	Toluene	2.3
Chlorobenzene	0.68	Trichloroethene	0.16
Chloroethane	0.26	Vinyl chloride	1.7
Chloroform	1.5	Xylene, *0*	8.2
Chloromethane	1.8	Xylene, *m/p*	9.7
Chromium	2.2_x10^{-3}	Xylenes	7.4
Crotonaldehyde	4.7		

Source: (Logue *et al.*, 2012, p. 217)

The understanding of how those pollutants behave inside building environments is key for the design and operation of future buildings that will require minimum energy consumption for its operation while guaranteeing indoor air quality. (Liang *et al.*, 2017, p. 219) explains, that the most effective approach is through the emission source control, ventilation and air cleaning, which is often a post-processing method after the completion of building construction. However, the effort to bring those assessments to the design stage can help us find the best design solution, getting us closer to the goal of ZEB buildings. (Liang *et al.*, 2017, p. 219) complements.

> IAQ pre-assessment and control is mainly achieved by IAQ simulations. However, even there are a series of IAQ simulation programs have been developed, such as RISK [1], MCCEM [2], MEDB-IAQ [3], CHAMPS [4] and ACCESS-IAQ [5], their engineering applications in actual buildings are rather rare due to the limitation of the empirical emission source/sink models, the lack of emission database or the over-simplify and insufficient consideration of the influencing factors.

The modelling of indoor pollutants is a very complex task, not only due to the many influence factors represented in Figure 3, but also because of the different molecular weights of pollutants.

Figure 3 - Influence Factors of VOC Concentrations

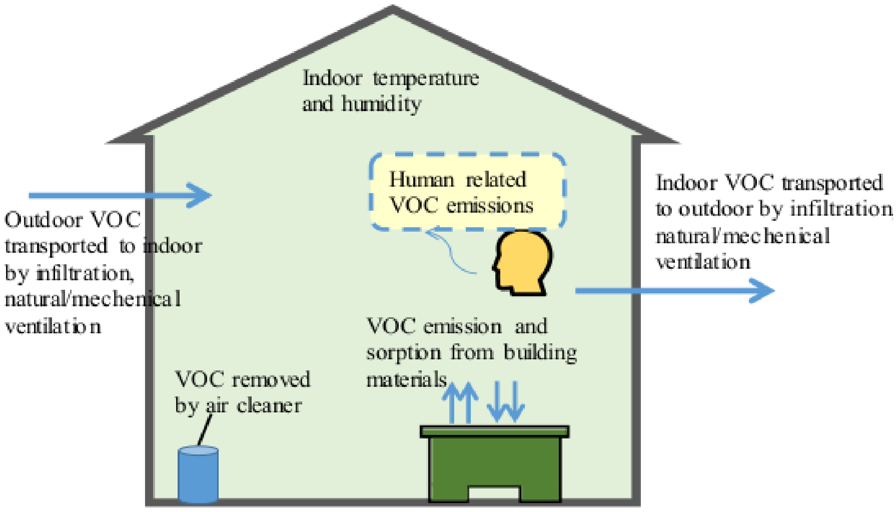

Source: (Liang *et al.*, 2017, p. 220)

The molecular weight of a pollutant together with the change in emission and sorption behavior of different materials due to temperature and humidity (Liang *et al.*, 2017, p. 221), can affect the spatial concentration of specific groups of pollutants.

The majority of modeling techniques consider the indoor air and the pollutants in a well-mixed situation, where the spatial concentration of a pollutant is evenly distributed throughout the control volume. This approach makes the simulation less computational costly and enables long simulation horizons, usually a one-year simulation period with a time-step of minutes. This type of modelling techniques are important for specific cases, when the highest pollutant concentration is often due to prolonged periods of exposure. As an example the case of (Burman *et al.*, 2018, p. 839) that points to a considerable gap between the design projections and operational use, when concentrations in benzene and formaldehyde were higher three years after construction.

The fast simulation techniques are essential to reduce the time to analyze different ventilation solutions in a possible design stage. However, since the simulation is only time-dependent, it does not give the designer a better understanding of higher concentration gradients inside the geometry, but rather the average concentration within the control volume. This could mislead the designer in certain situations, for instance, when pollutants have a high molecular weight. In those cases the designer might choose a ventilation solution that gives the average concentration within the limits of the environmental standards, but due to spatial differential concentrations, the designer's simulations assumptions might mislead during the decision-making process.

In order to find the perfect solution for a nearly zero-energy target in Europe, the standards' criteria for airtightness and fabric heat loss are reaching their technical and economic limits, according to (Burman *et al.*, 2018, p. 839). The risk could be an exacerbated focus in reducing ventilation with focus on energy efficiency, but neglecting the adverse impacts on health and wellbeing. Such buildings require mechanical ventilation due to their airtightness, which is already dominant type of ventilation system in Europe (Bocanegra-Yanez *et al.*, 2017, p. 831). However, its main barrier is that such ventilation systems requires a high capital cost, space, and duct routing (Bocanegra-Yanez *et al.*, 2017, p. 831), things that are barriers for European standards, and can be an even bigger barrier for low income and developing countries, as (Zukowska *et al.*, 2021, p. 8) points in the following passage.

> For example, one HVAC planner in the province of Vorarlberg stated that they used to have a legal requirement to build all publicly built housing according to the Passive House (PH) standard, which required MVHR ventilation. After removing this requirement, implementation of MVHR dropped drastically and most new housing projects in that province installed a simple extract air system or solely relied on NV.

And continues with.

> That planner explained that "Non-public housing developers were put in a tight spot" having to argue why social housing had "higher standard" than their buildings. He added that the situation was distorted due to the housing subsidies received by the social housing developers and that consequently the private constructors were able to promote their views that MVHR ventilation is questionable and capital and operation costs are too high.

The conflict between reduction of energy consumption, indoor air quality and its economical viability is the problem that the Annex 68 research project tries to address, since its focus is on low-energy residential buildings.

1.2 ANNEX 68

The annex 68 is an international collaboration of fifteen countries and twenty-five research institutions under the umbrella of the International Energy Agency - Energy in Buildings and Communities Program (IEA-EBC) (Participants - Indoor Air Quality Design and Control in Low Energy Residential Buildings (IEA-EBC Annex 68), [*s. d.*]).

The project goal is to find solutions for energy efficient residential buildings to achieve comfortable and healthy indoor environments, through ideal balance between energy efficiency and the need for ventilation while considering indoor pollutants. To achieve it, the annex is divided in five subtasks, as (Rode *et al.*, 2016b, p. 2) explains:

1 – Defining the metrics

Subtask 1 was designated set up the metrics for required performances which combine the aspiration for very high energy performance with good indoor environmental quality.

2 – Pollutant loads in residential buildings

Subtask 2 gathered existing knowledge or provided new data about indoor air pollutants as well as combined heat, air, and moisture transfer.

3 – Modelling – review, gap analysis and categorization

Subtask 3 identified and/or further developed modelling tools that can assists designers and managers of buildings.

4 – Strategies for design and control of buildings

Subtask 4 built upon the fundaments laid by previous subtasks and developed a guidebook on design and control strategies for energy efficient ventilation in residential buildings that will not compromise indoor air quality.

5 – Field measurements and case studies

Subtask 5 identified and investigated relevant case studies and did field measurements where the above-mentioned strategies could be examined and optimized. The different subtasks are presented in more detail in the following sections.

The interrelations between each subtask are shown in Figure 4 bellow, where solid lines indicate direct relations, while dotted lines indicate indirect ones:

Figure 4 - Schematics of Annex 68 Study Branches

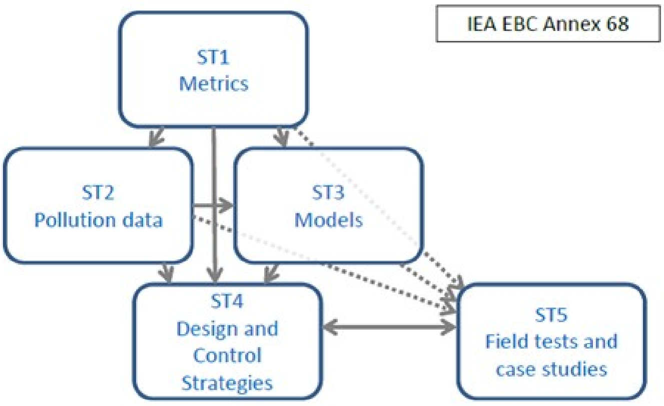

Source: (Subtasks - Indoor Air Quality Design and Control in Low Energy Residential Buildings (IEA-EBC Annex 68), [*s. d.*])

The workflow between each Substask seeing in Figure 5 shows its aim, which is to fill all the gaps for the full comprehension of indoor pollutants, model tools, field experiments and stakeholders with experience on the market.

Figure 5 - Work flow between subtasks

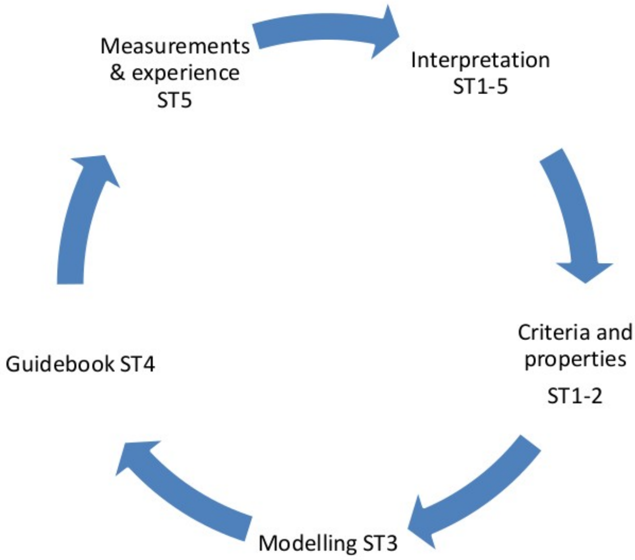

Source: (Rode, 2017, p. 8)

The annex 68 aimed to provide guideline for design and control strategy of energy efficient residential buildings. That will guarantee the quality of indoor environments, also setting up metrics for required performance which combines high energy performance and good indoor environmental quality. To achieve it, the project goals were to identify or further develop tools that designers and managers could use throughout the building life-cycle.

The target audience according to Rode (Rode, 2015, p. 2) is:

- Building designers (engineers and architects),
- Suppliers of HVAC and control systems
- Suppliers of materials used for building constructions and indoor furnishing,
- Providers of building management systems.

Another focus of the Annex 68 were to gather existing data or provide new information on indoor pollutants under different heat, air, and moisture transfer conditions. This will be used for sensor technology and controls. The research in this field will improve the performance of smart devices responsible to enhance indoor air quality while maintaining minimal energy consumption during operation. Also, the research project intended to identify relevant case studies where energy efficiency and indoor air quality performances can be examined and optimized.

This thesis is based on the subtask 5 and 3, where the Subtask 5 deals with physical tests of pollutant dispersion inside different buildings and the Subtask 3 with modeling tools. The field tests in Subtask 5 are divided in five different scenarios:

1) Passys Cell
2) Dormitory
3) House
4) Office
5) Dual Building

In all of them many sensors collected data about pollutant load, relative humidity and indoor (and/or outdoor) temperature. This subtask aimed to understand the behavior of common pollutants such as CO_2 and Hexane in normal daily life airtight environments. From the first field test to the last one, the complexity increases, not only the furniture inside, but the volume, indoor geometry of the building and transport phenomena.

While the Subtask 5 focus on collecting empirical data on pollutant dispersion, the Subtask 3 deals with a big challenge faced by the construction industry nowadays, which is the gap between building design and building simulation. The industry in the next decade needs to incorporate building simulation into design process from start where the cost of design changes is low and the gain in energy efficiency and indoor air quality is high. However, the current workflow of building design in many industrialized countries and developing countries has a huge gap between designers (engineers and architects) and simulation experts. This gap in the design process makes the design expensive and add too much noise between designers and simulation experts, making the cooperation difficult. In the subtask 3 the goal was to find the best tools and methods for building simulation, which can be easy to use and could reduce the gap between the two group of professionals.

The reason behind all this effort is summarized by Rode (Rode, 2015, p. 2) as following.

> The rationale of carrying out the proposed Annex is that buildings in the future will have to be optimized just to the limit in order to become as close as possible to being zero energy buildings. This means that the ventilation will also be reduced to just the absolutely necessary, while the quality of the indoor air must not be sacrificed.

In additon, within the scope of subtask 3, this study is based on the common exercise 1 from the Annex 68, where different researchers used different tools to replicate the first field experiment. The experiment is the dispersion of hexane inside the Passys Cell, where the field experiment is the benchmark to compare different modelling techniques. The tools used in this exercise are the following:

- Matlab HAMFitPlus
- TRNSYS
- Matlab ODE23S
- CONTAM-TRNSYS
- DELPHIN6

All the above methods for modelling the Passy Cell field experiment are time-dependent, which means that the simulation assumes that the pollutant is well-mixed within the indoor environment and the only variable is time. Even though inside the Passys Cell there was a fan for mixing the pollutant (hexane), the hexane molecular weight is high, and it tends to settle close to the floor because of density difference in relation to the indoor air.

In this study the simulation of the Passys Cell was performed by means of a differential approach, that considers the spatial behavior of the chemical dispersion through time. The spatial analysis of pollutant dispersion in buildings is important to determine specific regions inside a modelled house or office, where the pollutant load exceeds the maximum accepted by healthy authorities.

The spatial analysis can bring more data during the design process, which can be complementary to the time dependent methods. While the time dependent method can produce a cheaper analysis and can simulate long time horizons, the differential analysis would enhance the capacity of building designers to understand spatial distribution of pollutants. Thus, changing the way ventilation solutions can be chosen, while concentrating only in volume exchange of air, the differential analysis will help to find the best spatial solutions for ventilation design.

Another field where differential analysis can contribute is during field tests of existing buildings operating under new indoor air quality standards. One of the field methods used to analyzing pollution in indoor environments is the gravimetric methods, where air filters are placed in specific locations inside the room to collect particles of pollutants and weight it later. If the filters are placed only in certain locations where the pollutant is less concentrated, the empirical analysis can give wrong results, this could cause the categorization of a hazardous environment as a healthy environment for long term human occupation.

In order to simulate the Passys Cell field test, the Computational Fluid Dynamics (CFD) method is used in this study in contrast to the Lumped Parameter Model used by other researchers.

1.3 HEXANE

Hexane is a hydrocarbon made from crude oil, which in its purest form is a colorless liquid with a petroleum-like odor. Its use ranges from extraction of edible oils from vegetables and seeds, to cleaning agent in printing, textile, furniture, and shoemaking industries (n-Hexane | Toxicological Profile | ATSDR, 2024, p. 1).

It consists of a chain of six carbons bonded to fourteen hydrogen molecules (C_6H_{14}), represented in the Figure 6 in its spatial form. The hexane molecule is less dense than water and insoluble in water due to its stable molecular form. Its vapor is heavier than air and explosive, while its liquid form is highly inflammable, with flash points at around -22 ºC (N-HEXANE | CAMEO Chemicals | NOAA, 2024).

Figure 6 - Hexane 3D Chemical Structure Model

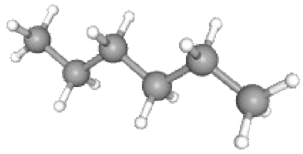

Source: (Boese; Blaeser; Weiss, 1999)

Due to its broad use in industry, humans can be exposed to hexane in different forms. In high concentrations in industrial facilities or laboratories, and also in low concentrations, but long exposure within built environments, such schools, offices, and dwellings.

According to the PANDORA database (Pandora, 2024), there are 91 hexane emission data from nine different studies (Alevantis, 2003; Bluyssen, 1997; DE TOXICOVIGILANCE, 2014; Doyun; Shaw, 2004; Kozicki; Guzik, 2021; Marie-Lise; FCBA; BATIMENT, 2013; Offermann, 2009; Oliveira Fernandes, 2001; Zheng *et al.*, 2024) as described in the Table 3.

Table 3 - Hexane Emission Sources in Buildings

Sub-Category	# of Sources	Location
Carpeting	8	Homes, Offices, and Schools
Acoustical Materials	4	Homes, Offices, and Schools
Finishes	16	Homes, Offices, and Schools
Flooring	14	Homes, Offices, and Schools
Installation Materials	8	Homes, Offices, and Schools
Interior Panels	11	Homes, Offices, and Schools
Structural Materials	17	Homes, Offices, and Schools
Cushions	4	Homes, Offices, and Schools
Insulation Materials	1	Homes, Offices, and Schools
Day-nursery furniture	1	Day-Care
Painting, drawing, doing plastic arts	4	School
Homes	1	Residence

Mattress	2	Day-Care

Source: The Author

Since hexane is highly volatile, the most common exposure is through inhalation, even though dermal and oral exposure might also occur, yet in a much rarer situation. Human hexane exposure in building environments can happen from indoor and outdoor sources. The main external source of hexane comes from motor fuel, making the population living in denser urban areas more exposed. However, even in dense urban areas the average concentrations are in the parts per billion range (n-Hexane | Toxicological Profile | ATSDR, 2024, p. 1).

According to (n-Hexane | Toxicological Profile | ATSDR, 2024, p. 1), the majority of studies focused on human exposure to hexane have evaluated chronic-duration inhalation exposure, while animal studies have focused on acute and intermediate-duration inhalation as shown in Table 4. Those studies show that neurological, respiratory, developmental, and reproductive effects are the most important health concerns related to hexane intoxication.

Table 4 - Health Effects Found in Animals Following Inhalation Exposure to n-Hexane

Concentration (ppm)	Effects in Animals
12,500	**Intermediate**: Decreased number of live pups, impaired development of reproductive system.
2,500-5,000	**Acute**: Decreased body weight, decreased motor nerve conduction, testicular lesions. **Intermediate**: Peripheral nerve degeneration; testicular lesions.
800-1,200	**Acute**: Decreased litter weight. **Chronic**: Leydig cell hyperplasia.
400-500	**Intermediate**: Central and peripheral neuropathy, severe clinical signs of neurotoxicity; skeletal muscle atrophy; decreased body weight; decreased fetal body weight; chronic nephropathy
6 ppm	**Provisional Acute** Minimal Risk Levels
0.4 ppm	**Provisional Intermediate** Minimal Risk Levels

Source: Adapted from (n-Hexane | Toxicological Profile | ATSDR, 2024, p. 2) Figure 1-1.

The early documented cases on the toxicity of hexane in humans were occupational epidemiological studies and reports examining workers in Italian and Japanese shoe industries in the 1960s and 1970s. The workers reported numbness in the feet and hands followed by weakness in the lower legs and feet, later developed into peripheral neuropathy. The investigation reveled that those symptoms and later illness were linked with high exposure to the hexane presented in glues and solvents in poor ventilated environments (n-Hexane | Toxicological Profile | ATSDR, 2024, p. 11).

The number of studies examining the health effects of hexane is more expressive with animal subjects than humans as shown in Figure 7. From those 73 studies with humans and animals, 80% are from inhalation exposure route, 16% oral and 4% dermal. While 51% had an intermediate exposure duration, 30% acute and 19% chronic (n-Hexane | Toxicological Profile | ATSDR, 2024, p. 13). Nevertheless, one important point is the considerable number of studies related to neurological effects in humans.

Figure 7 - Number of Studies Examining n-Hexane Health Effects

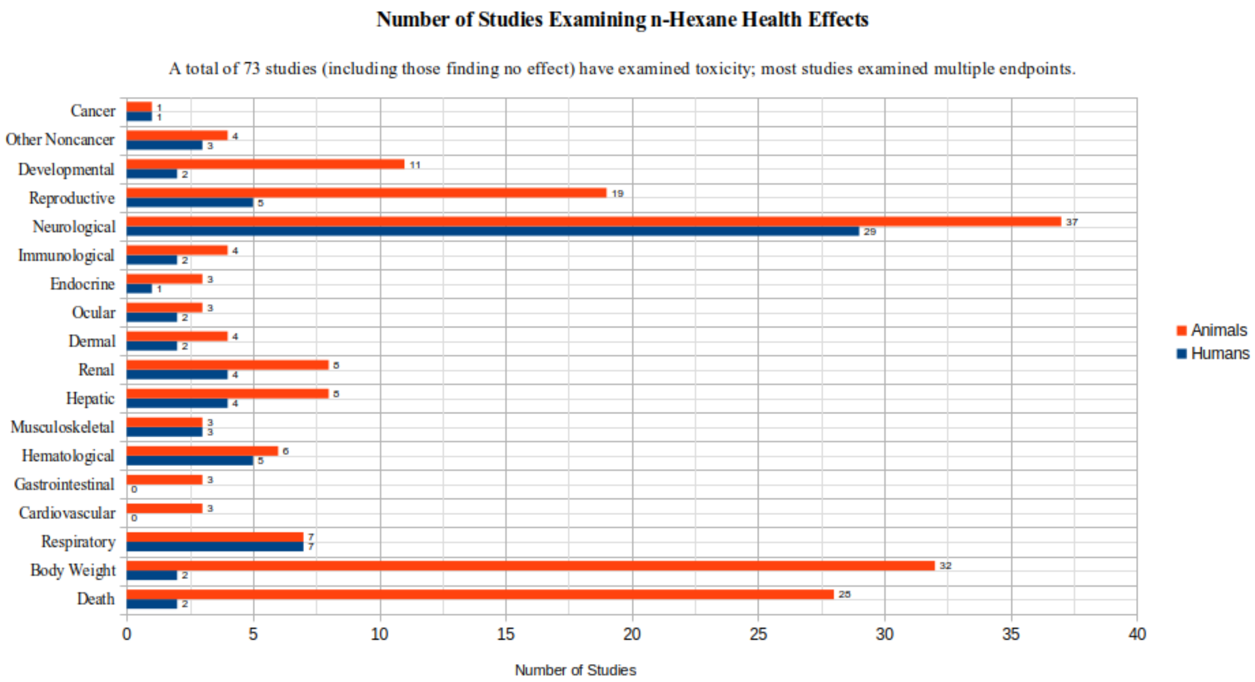

Source: Adapted from (n-Hexane | Toxicological Profile | ATSDR, 2024, p. 13) Figure 2-1.

The understanding of hexane behavior in close environments is highly essential in the field of building physics due to its known neurological (and other) effects in humans, and its widespread presence in building environments.

1.4 OBJECTIVES

1.4.1 General Objectives

The general objective of this master thesis is to model the common exercise number one from the Annex 68 project using the Computational Fluid Dynamic (CFD) method. Later, compare the CFD results with other time-dependent methods used by other researchers of the project, and analyze the quality of the CFD results in comparison with other methods by using the field experiment as a benchmark.

1.4.2 Specific Objectives

With the general objective in mind, it is intended to achieve the following specific objectives:

(a) Identify the pros and cons of the CFD method in comparison with other methods.
(b) Identify which method can better describe the field experiment.
(c) Understand how important a spatial analysis of the pollutant dispersion can improve the building design process.
(d) Understand whether a pure CFD approach is recommended or a hybrid analysis can bring more value to the design process.

1.5 DOCUMENT STRUCTURE

This study comprises five chapters. The first chapter walks through the current challenges humanity faces as specie and the importance of energy efficiency in modern buildings without sacrificing the indoor air quality. The second chapter presents the literature review regarding indoor pollutant modelling with CFD, its findings and limitations. In the third chapter is exposed the methodology used for the modelling of the common exercise number one, from the Annex 68. The fourth chapter brings the results of the CFD modelling and the comparison with other numerical methods used by other researchers. The fifth and final chapter analyzes the results, its strengths and weaknesses and proposal of future work.

The study also has two appendices, the first is about the numerical solution convergence and the geometry of the fan blade while attempting to use dynamical mesh to model the effect of the fan in the hexane dispersion using volume of fluid. And the second shows the convergence of the numerical solution.

CHAPTER 2
LITERATURE REVIEW

2.1 INTRODUCTION

Indoor environments are a key factor in human survival since the dawn of our species. From caves at Lascaux in France, dwellings made from mammoth bones at Mezhirich in Ukraine, until Burj Khalifa in Dubai. All of them share the same basic principle, a close environment that offers shelter from the weather and other animals.

The investigation of the time-activity patterns of modern humans in 12 European countries, USA and China, shows that 90% of the time, humans spent indoors, including buildings and transportation vehicles. While the average daily intake of mass (water, food, and air) by a human with 80 kg of body mass is around 15 kg, more than 80% of it, is air inhaled indoors (circa 13 kg) (Zhang; Hopke; Mandin, 2022, p. 5). Thus, the indoor air quality is one of the most important elements of human health, and its understanding can provide the foundations for a broad number of actions in public health guidelines and preemptive measures during building design process. This can have positive effects on our life expectancy, reduce public health expenditure and increase productivity.

The beginning of our understanding of breathing in modern scientific terms spans from XVIII century until XIX century. Scientists like Priestley (1733–1804), Scheele (1742–1786), Lavoisier (1743–1794) and later Pettenkofer (1818–1901), set the foundations of this field. Priestley and Scheele independently discovered the oxygen, while Scheele and Lavoisier realized that air is a mix of different gases. The relationship between oxygen inhale and CO_2 exhale was first understood by Lavoisier, and from that moment the concentration of CO_2 became the benchmark to classify the freshness of air. In the XIX century Pettenkofer understood that CO_2 was not the cause of bad qualitative human perception of air freshness, but just a correlation indicator of many organic species emitted by humans' lungs into the environment. In 1858 Pettenkofer published a book on ventilation in dwellings and set the 1000 ppm number as the maximum concentration of CO_2 in order to keep inhabitants comfortable (Zhang; Hopke; Mandin, 2022, p. 5).

During the first half of the XX century the field experienced a rapid development with many indoor pollutants being found and its correlation with respiratory diseases. However, only during the 1970s that the field experienced a significant shift in perspective, and the modern indoor air science was born (Zhang; Hopke; Mandin, 2022, p. 6). The main contributors to that change was the oil crisis of 1973 due to the embargo by the Organization of Arab Petroleum Exporting Countries (OAPEC) towards nations supporting Israel during the Yom Kippur War. This geopolitical scenario forced western countries to think about building energy conservation. The second big factor, was the understanding of modern diseases associated with new chemicals found indoors.

Advances in field data collection such as gas chromatography-flame ionization detection (GC-FID), and gas chromatography-mass spectrometry (GC-MS) (Zhang; Hopke; Mandin, 2022, p. 7) were developed about the same time with the Imperial College investigation program to predict simple shear flows, free and confined jet flows in early 1973 (Khalil, 2021, p. 43). This is when modern Computational Fluid Dynamics (CFD) was born as a science.

2.2 COMPUTATIONAL FLUID DYNAMICS

The Navier-Stokes equations are the backbone of the Computational Fluid Dynamics (CFD) field. It comprises the conservation of mass, the conservation of momentum (Newton's Second Law) and the conservation of energy (Second Law of Thermodynamics) for problems involving heat transfer (Bhattacharyya *et al.*, 2021). In an incompressible and isothermal condition, the gradient of the velocity vector must be equal to zero in the continuity equation, which means that mass do not ceased to exist in the continuum, while in the conservation of momentum we have three separate components. The first is the mass times the acceleration, which equals to the sum of forces, both internal (gradient of pressure and viscous stress) and external (gravity, electromagnetism, or Coriolis force). Its solutions are non-linear and requires the simultaneous consideration of momentum in all three coordinates, conservation of mass, conservation of energy and often the addition of turbulence models and species conservation/reaction equations. Due to the inherent computational complexity of this process, an analytical solution it is not possible (Chen; Srebric, 2000, p. 22). Therefore, the need for computers to solve it numerically.

When the first paper applying Computational Fluid Dynamics (CFD) into indoor air field was published in 1974 (Zhang; Hopke; Mandin, 2022, p. 11) with the title “Predictions of air distribution in a ventilated room”, a new field was born, the use of CFD for indoor design and assessment. However, the use of CFD for such application requires a good understanding of important variables such as air velocity, air temperature, contaminant concentrations, relative humidity, and turbulence quantities. Those are the key variables to solve fluid flow, heat transfer, and chemical specie transport.

A Direct Numerical Simulation (DNS) solves the Navier-Stokes equations without approximations. Nevertheless, this method requires a grid resolution as fine as the Kolmogorov microscale, and since a normal wind flow has a Reynolds number around 10^6 and indoor air flows approximately 10^5, the total grid number for such airflow is approximately 10^{13} (Chen; Srebric, 2000, p. 3). This is still not viable for the majority of modern hardware. Average computers are not powerful enough to represent the rich details of velocity fields from the Navier-Stokes equations. Since turbulence is a consequence of non-linear terms in the Navier-Stokes equations and appears to have a deterministic cause, it is not a product of purely stochastic behavior. Thus, it is not possible to simply use a statistical analysis in order to solve the turbulence (Kim; Leonard, 2024, p. 22). Mathematical models were developed to average the velocity fields and reduce its complexity. The main turbulence models are the following:

- RANS → Reynolds Average Navier-Stokes
- LES → Large Eddy Simulation

RANS model works by ensemble-averaged Navier-Stokes equations by using turbulence modeling. It can be divided into turbulent viscosity models and Reynolds-stress models. The most widely used turbulent viscosity model is the standard k-epsilon model, where the k equation is the kinetic energy and the epsilon equation is the dissipation rate of turbulent kinetic (Nielsen, 1974, p.

220). Meanwhile the LES approach consists on the separation large-eddies and small-eddies, since its separation does not have a significant impact on the behavior of large-eddies, which is the main contributor of turbulent transport. Large-eddies are modelled by a set of filtered equations governing the three-dimensional time dependent motion, while a turbulent approximation is used for small-eddies, that are modeled independently of the flow geometry (Chen; Srebric, 2000, p. 3).

The RANS method is divided in k-epsilon and Reynolds-stress models, both are further divided in many variations. The standard k-epsilon is the most used, since it is easy to program and produce fair results for a broad range of applications. Different variations of k- epsilon models are common practice in the field since modifications are easily made in the source code. The majority of those modifications were developed for simple turbulent flows. In order to understand the difference in those models (Chen, 1995) compared five of them to predict natural, force, and mixed convection in rooms:

- standard k-epsilon model
- low-Reynolds-number k-epsilon model
- two-layer k-epsilon model
- renormalization group (RNG) k-epsilon model

These models failed to predict the anisotropic turbulence and secondary recirculation of indoor airflow. The performance of the models were unstable, except for the standard k-epsilon model and RNG k-epsilon model, where the second performed slightly better. The author in another work (Chen, 1996) compared the standard k-epsilon model with three different Reynolds-stress models:

- Isotropization of production models (RSTM-IP)
- Isotropization of production models (RSTM-GY) (different from RSTM-IP in empirical coefficients)
- Quasi-isotropic model (RSTM-QI) (different from RSTM-IP in equation which applies proposal by (Rotta, 1951))

Among the Reynolds-stress models, the RSTM-GY model performed slightly better than the others. However, the performance of those models were not much better than the standard k-epsilon model and since the Reynolds-stress models computed nine additional transport equations needed to solve a three-dimensional non-isothermal problem (six Reynolds-stress equations and four heat flux equations, without the k equation) the computing effort of the Reynolds-stress models were 5-20 times greater than that with the standard k-epsilon model in the study. In addition, the computations with Reynolds-stress models were less stable.

Another study (Murakami, 1998) compared three different models to a flow around a body:

- DNS → Direct Numerical Simulation
- LES (standard and dynamic) → Large Eddy Simulation
- RANS (Reynolds-stress model, standard k-epsilon and revised k-epsilon) → Reynolds Average Navier-Stokes

The study showed that LES gave the best accuracy and the standard k-epsilon model the worst. This could be explained due to the fact that LES simulates airflow in a three-dimensional, time-dependent manner, making the computing time needed much longer than that by RANS. Another important point is that in LES the transport terms (e.g. Reynolds stresses) are treated with full empiricism, making it superior to RANS. While in comparison with DNS, LES is more affordable in terms of computational cost, since it can be performed on a large and fast workstation (Chen; Srebric, 2000, p. 4). Consequently, the turbulent models can be ordered from the most computational intense to the least as followed:

- DNS → Direct Numerical Simulation
- LES → Large Eddy Simulation
- RANS → Reynolds Average Navier-Stokes

RANS models are more suitable to simulate indoor environments, while LES for external environments. Hence, in the first paper in indoor air field using CFD (Nielsen, 1974), the author used a RANS k-epsilon model from 1972 (Hunt, 1973) to predict the flow inside a room and compare the results with its scale model. The results were fairly accurate and opened up a new frontier of possibilities to use CFD as a tool to improve indoor design and assessment.

2.3 INDOOR EMISSION SOURCE MODELS

The indoor pollutant emission behavior depends on accurately description of some phenomena, such as evaporation, desorption, diffusion, and convection. Those processes are affected by factors like molecular size and structure, temperature, relative humidity, ventilation rate and air velocity. Thus, the pollutant emission is another important model that must be well represented. (Sparks, 1991) categorized emission sources in three groups:

- Long term steady state sources
- On/off sources
- Decaying sources

There are two groups of VOC emission models, physical (deterministic) and empirical (statistical). While empirical methods are based on curve-fitting of experimental data collected from small-scale chamber tests, physical methods take into account elemental internal and external mass transfer process of source materials (Murakami; Kato; Ito, 1998, p. 19). A review of various IAQ models was conducted by (Austin *et al.*, 1992). Physical models can better simulate the underlying processes causing emissions, with some assumptions, like the disregard of factors that are less influential in a particular context. Empirical models on the other hand present some disadvantages, since the equations lack physical significance and may produce qualitatively inaccurate results. Another significant point is that those models fail to incorporate essential factors that may affect the emission rate, which reflects on the struggles to account for the extremities of the emission curve when dealing with rapid emissions (Haghighat; Jiang; Zhang, 1994, p. 277). Within the physical methods, VOC emissions from source are classified into two types according to its emission control, one regarding internal diffusion and the other with external diffusion (in the interaction with the surface boundary layer) (Murakami; Kato; Ito, 1998, p. 19).

The physical models applied to decaying sources are divided between two groups (dry and wet) as explained by (Yang; Chen, 2001):

Dry materials emit volatile organic compounds (VOCs) primarily through two diffusion processes, molecular and Knudsen diffusion. To simplify complex diffusion processes, continuum models are often used to treat the material as a homogeneous medium with an effective diffusion coefficient. Such models have been used to estimate emissions from various materials like vinyl flooring and carpet backing.

However, various authors have identified shortcomings in these simplified approaches and proposed more advanced models that better capture the underlying physical and chemical processes. For instance, (Yang *et al.*, 2001) developed a numerical model accounting for both internal and interfacial mass transfer processes. Their findings indicated that for long-term IAQ studies, it is acceptable to use simplified models that only consider diffusion coefficient and initial VOC concentration. Conversely, complex models may be necessary for accurate short-term emission simulations.

Success in using these models is highly dependent on accurate data for key material properties, namely the diffusion coefficient and partition coefficient. Many researchers have conducted experiments and published data on these properties for various materials including vinyl flooring, carpet backing, plywood, and wall paper. These correlations have enabled more robust and reliable predictive modeling of VOC emissions from buildings and their impact on indoor air quality.

The complex and multiphase nature of VOC emissions from petroleum-based solvents in "wet" materials, such as paints, varnishes, and wood stains, can emit a variety of VOCs that can degrade indoor air quality. Prior research suggests that there are three primary phases of VOC emission from such materials. Initially, high emission rates are observed as the material is still wet but not fully dried. The dominant emission mechanism appears to switch from evaporation at the surface to an internal-diffusion controlled phase. In the final phase, the material is relatively dry and the emission rates and decay rates are significantly lower. Researchers have found that the use of simplified emission source models may not adequately capture the complex interactions between the material and its environment.

For instance, (Sparks *et al.*, 1999) found that neglecting internal diffusion in models like the Vapor pressure and Boundary model can lead to significant errors in predicting emission rates, particularly in the later phases of drying. Meanwhile, more advanced semi-empirical models have been developed to better capture the complex multiphase nature of "wet" material emissions. However, the empirical relationships inherent in such models limit their generalization.

An example of physical model for decaying “wet” emission source is demonstrated in the study conducted by (Haghighat; Jiang; Zhang, 1994), where the author used CFD to model a newly painted office with two different internal layouts. The objective was to assess the impact of different workstation layouts on the dispersion and further flushing of a contaminant concentration under different ventilation regimes. The office’s partitions were 1.5 m high and 0.05 m thick and disposed in two different layouts (side and central layout). And it was painted in a non-uniform way, with 2.0 kg for each of the northern and southern walls, 1.8 kg for the western wall and 0.8 kg for the eastern wall. This type of situation imposes a non-uniform concentration distribution of contaminant.

A physical mass transfer model developed by (Guo, 1992) called VB (Vapor pressure and Boundary layer) was further improved by the author to model the VOC emitted by the wall paint. The VB model assumes that the vapor pressure is the same for all surfaces with wet product, which means that the same vapor pressure is considered independent of the amount of coating applied; As the coating ages the vapor pressure decreases gradually, thus, during the aging process the vapor pressure is proportional to the mass of VOCs left; A simplification is considered, the average diffusivity of solvent’s molecules is represented by the most abundant component in the mixture. Since the VB model requires a detail information of air movement within the room, it was coupled with a k-epsilon model. The CFD model provided an approximate solution of the governing equations (momentum, energy, and mass) in Cartesian coordinates using the finite-volume method, the data was then used by the VB model to simulate the VOCs emission.

The simulation accounted with six different combinations of scenarios, two layouts and three ventilation rates (1.7 ach, 3.4 ach, and 6.8 ach). Its results showed that the time difference between the chambers to have the highest and lowest concentrations were 3 to 8 h, and that the different layouts under the same ventilation rate required different times to reduce the contaminant's concentration. However, the same layout in different ventilation rates also have different times to reduce concentration rates. Hence, internal obstacles and air velocity have direct influence over VOC concentrations.

In another study conducted by (Murakami; Kato; Ito, 1998), the author used a physical model for decaying dry source, where the author used CFD to analyze the behavior of an indoor pollutant. The Total Volatile Organic Compound (TVOC) emission source was a polypropylene styrene-butadiene rubber (SBR) plate covering the floor of a single room. The objective was to model the emission of the chemical compound and its diffusion in a room under different conditions of ventilation rate and temperature. The study aimed to assess the concentration distribution of the contaminant and the ventilation efficiency in the room.

The model represents a 2D single room with 4.5 m of length and 3.0 m of hight with a variable inlet velocity of 0.1 m/s with no flushing, and 1 m/s in flushing state. Both openings were placed on the top of the room with 0.06 m opening each. The study applied a physical method for the pollutant emission based on internal diffusion control, which substitutes the various chemical compounds emissions and diffusions coefficient in the SBR for the virtual representative compound TVOC. The mechanism of the diffusion process is modeled by a single one-dimensional diffusion equation considering the equivalent air phase concentration, effective diffusion coefficient of the TVOC and initial concentration distribution. To respect the conservation law the TVOC emission rate at the material surface is set as the same value as the transportation rate by internal diffusion. The contaminant is transported by the room air flow, its molecular diffusivity and turbulent diffusivity. So for the modelling of the flow field, a Low Reynolds Number k-epsilon model is used.

The results from the mean velocity using the low Reynolds number k-e model compared against experimental data appeared to be in a good agreement. Though, some key findings concerning the TVOC emissions are the following:

1. The room-averaged TVOC concentration remains almost constant throughout the simulation period of 14 days due to the extremely short duration in comparison to the characteristic time for internal diffusion, which is approximately 680 years.

2. As the flushing duration is significantly shorter than the characteristic time for internal diffusion at around 6.8 years, the flushing impact is limited to only during the flushing phase.

3. The TVOC emission rate is increased by a factor of four when the temperature is 30 °C compared to 23 °C.

4. The TVOC concentration near the SBR floor, representing the source of contamination, is eight times higher than the overall room-averaged concentration.

5. In this investigation, the TVOC emitted from the SBR floor and dispersed into the breathing area of individuals sitting in the room is decreased by roughly a multiple of 8.1 before dissipating.

In some physical situations it is necessary to not only describe some materials as emission sources such as the two previous examples, but also as a sink. This complex phenomena can happen when considering porous materials, since the internal diffusion and permeation phenomena is possible within the pores. Its diffusive transport is a complex phenomenon caused by the molecular and Knudsen diffusion in the vapor phase that occur through its pores due to concentration gradients (Kondo; Fujimura, 2024, p. 2).

2.4 CONCLUSION

The field of Computational Fluid Dynamics (CFD) applied to Indoor Air Quality (IAQ) is a fairly new field of study that blends physics, computation and chemistry. Despite the recent developments in hardware in the last few decades, most of the physics required to properly describe common phenomena in building physics still prose a big challenge for modern computers. The battle between indoor environment control and energy efficiency is extremely important for our civilization, thus, new numerical methods and couple solutions must be developed while Moor's Law slowly approaches its plateau (The Death of Moore's Law, 2024).

Study cases where hexane is being model using CFD is practically inexistent, meanwhile pollutants with similar molecular weight are found in many slow decay materials. The understanding of its behavior within close environments is essential for further study about its interactions with porous materials. Therefore, this study is relevant for the further development of the field.

CHAPTER 3
METHODOLOGY

3.1 THE PASSYS TEST CELL

During the First European Communities Conference on Solar Heating in 1984, N. V. Baker, researcher at Energy Conscious Design, proposed in his paper “European Passive Solar Test Facility” the idea of a standardized test facility to be constructed in at least four test sites (Baker, 1984). The idea was to test solutions on passive solar components in four main different climate regions in Europe, the Mediterranean, Mid European (Costal), Mid European (Continental) and North European.

Within these four different sites, the test cell could provide a realistic test environment for systems and components. The standardized facility had to provide a high specific test environment where boundary conditions could be grossly simplified in order to have small range of variables. As (Baker, 1984, p. 1) stated, this test cell would be able to provide reliable data sets for validation of mathematical models. These models could be directly used as design tools or produce a generalized solution for design guidelines.

Based on Baker’s proposal, the Passys Test Cell was created. The Passys Test Cell is a common European outdoor test facility for thermal and solar building research that was implemented at the beginning of the 1990s in many European cities. Based on Baker’s design suggestions, the German Test and Research Institute for Aviation and Space Flight (DFVLR) from Stuttgart prepared the design of the test cell in 1985, which was accepted by the participants.

The PASSYS test sites are located in the following countries, Belgium, Limelette (4 Cells); Denmark, Lyngby (2 Cells); France, Sophia Antipolis (1 Cell) and Cadarache (4 Cells); Germany, Stuttgart (4 Cells); Italy, Catania (4 Cells) and Ispra (2 Cells); The Netherlands, Delft (4 Cells); United Kingdom, Glasgow (4 Cells).

The test cell used for the experimental analysis of the Annex 68 is located in Limelette, Belgium. The cell is within the BBRI site, oriented more or less along the north/south axis, with a slight rotation to the east as shown in Figure 8. It is isolated in its surroundings and usually is accompanied by a weather station outside, shown in Figure 9.

Figure 8 - PASSYS Cell Orientation

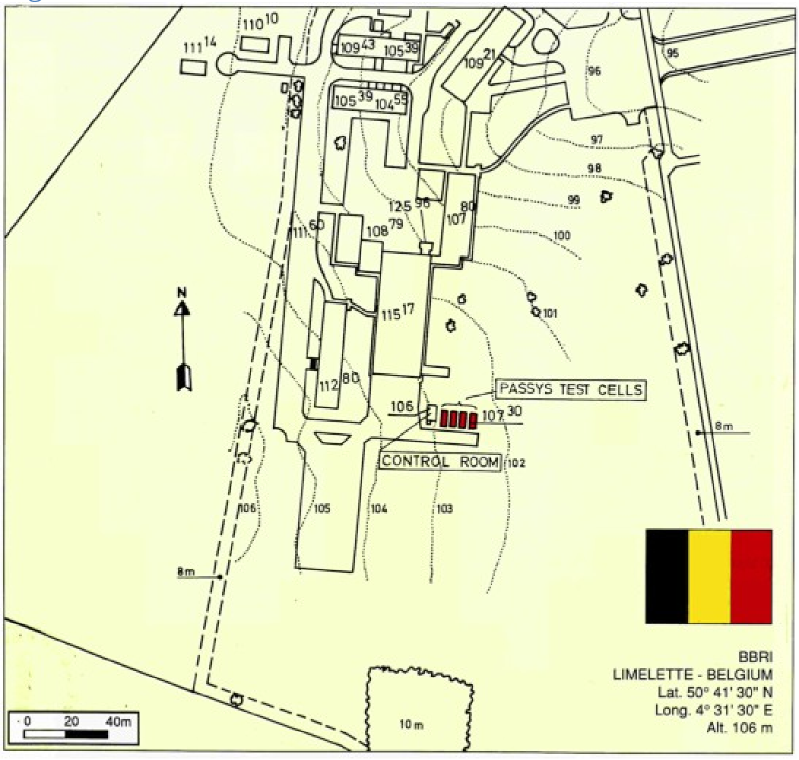

Source: (European Commission, 1990, p. 16)

Figure 9 - PASSYS Cell

Source: (European Commission, 1990, p. 33)

According to the official manual, the test cell is a hard casing built using the steel frame construction method for structural loads and stainless-steel casing for protection against exposure to the weather, where the structural elements and the inner rigid foam for thermal insulation are strictly separated. The internal part of the test cell is made of two parts, the test room and the service room, as presented in Figure 10. The service room leads to a well-insulated partition wall and door which is usually used in cooling chambers. The test room is composed by high insulated walls, floor, and ceiling with 400 mm rigid polystyrene foam and mineral wool, for a thermal conductance (U x A) of less than 12 W/K.

Figure 10 - PASSYS Cell Construction Materials

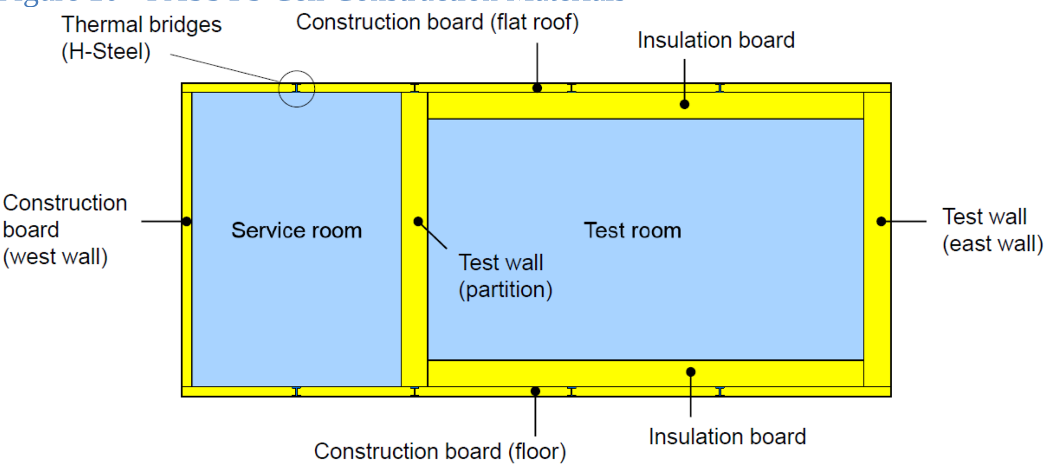

Source: (Grunewald *et al.*, 2018, p. 1508)

The room is designed to be high grade airtight and create a highly adiabatic behavior from all the walls, except from the south wall, where the passive solar elements are tested. In the Table 5 and Figure 11 it is possible to see its complete dimensions.

Table 5 - Test Cell Dimensions

	Length (m)	Width (m)	Height (m)	Area (m^2)	Volume (m^3)
Outside Overall	8.44	3.80	3.61	32.07	115.8
Test Room Inside	5.00	2.76	2.75	13.80	38.0
Service Room Inside	2.40	3.58	3.29	8.60	28.3
Total mass appr. 12,000 kg					

Source: (European Commission, 1990, p. 9)

Figure 11 - PASSYS Cell Inner Measurements

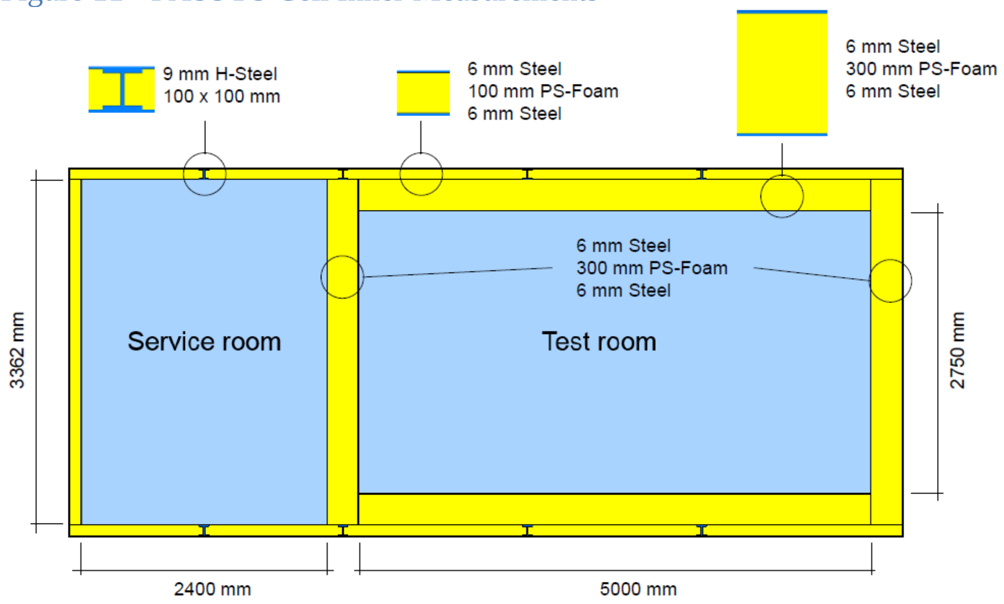

Source: (Grunewald *et al.*, 2018, p. 1508)

3.2 EXPERIMENTAL TEST SETUP

In the field experiment document, (Laverge, 2017, p. 5) explains that test cell used in the experiment suffered some changes for the common exercise 1, those changes are:

- 12 cm of additional EPS insulation material and 1 mm of stainless-steel cladding added to the interior walls.
- A "calibration" test wall that has the same changes as all the other walls, has no windows and it is placed in the south.

These two changes affected the internal dimensions from 2.75 m of height and width to 2.46 m, and the length from 5 m to 4.86 m.

The door separating the service room and the test room received a concreteplex panel with a flexible PU foam with 2mm thickness and clips to preserve the air tightness of 1.7 ACH50. Two circular openings in the door are the only inlet and outlet of fresh air to the test room. The inlet is an

80 mm opening 15 cm above the floor with an axial fan to provide controlled inlet of air, while the outlet is a 150 mm flexible exhaust duct, located at 15 cm from the top of the door panel. The indoor air is then expelled to the service room through a service opening at the front of the test cell at ceiling height. During the experiment a small window in the service room in front of the test cell is opened for fresh air supply, while the inlet fan keep it pressurized. In Figure 12 it is possible to better visualize the spatial disposition of the cell.

Figure 12 - PASSYS Cell Perspective Cross Section

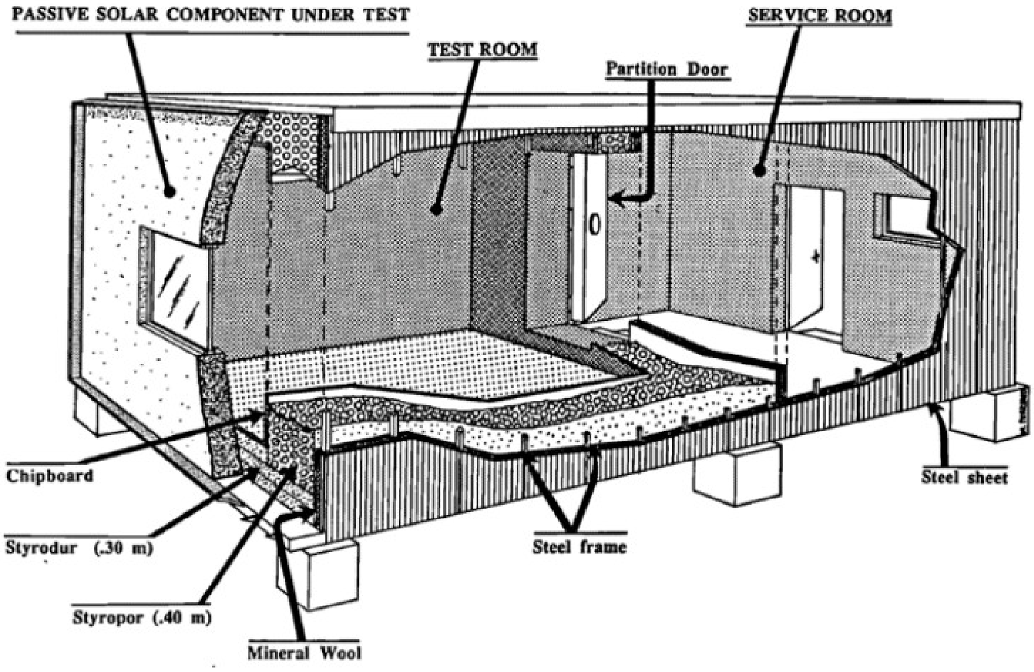

Source: (European Commission, 1990, p. 5)

Inside the test room a mixing fan is placed in the south-east corner and a concrete block with a height of 50 cm is placed at 1.20 m from the south wall. On top of the concrete block there is the pollutant source, a glass bottle with freely diffusing hexane. Right behind the concrete block a single electric convector is placed at 0.5 m from the south wall, keeping the room heated at 27.5 °C throughout the whole experiment by a thermostat with an external temperature probe with a 0.1 °C dead band. The temperature was chosen since a heated indoor air helps the diffusion of the hexane. The external probe is positioned at the exact midpoint of the room (1.25 m height, 1.25 m from the side wall and 2.35 from the south wall).

During the experiment the temperature is measured at four different heights at two locations. One at the midpoint where the thermostat probe is located and the second at 40 cm from the south west corner. They are spaced by 60 cm interval starting at 35 cm from the ceiling using Onset HOBO U12-012 loggers. The hexane concentration is measured at the midpoint where the thermostat probe is, using a Rosenmount NGA2000 FID sensor. The whole physical setup is shown in Figure 13. The test field follows the protocol described in the Table 6, during the whole experiment the source condition remains open. For more information about the field experiment, see Appendix A.

Table 6 - Field Test Protocol

Phase	Time	Supply Ventilation Rate
1. Startup	Until steady state	1 ACH
2. High	Day 1 00:00:00 (11/04)	1 ACH
3. Low	Day 2 17:20:00	0.1 ACH
4. High	Day 8 14:12:00	1 ACH

Source: (Laverge, 2017, p. 5)

Figure 13 - Field Test Disposition

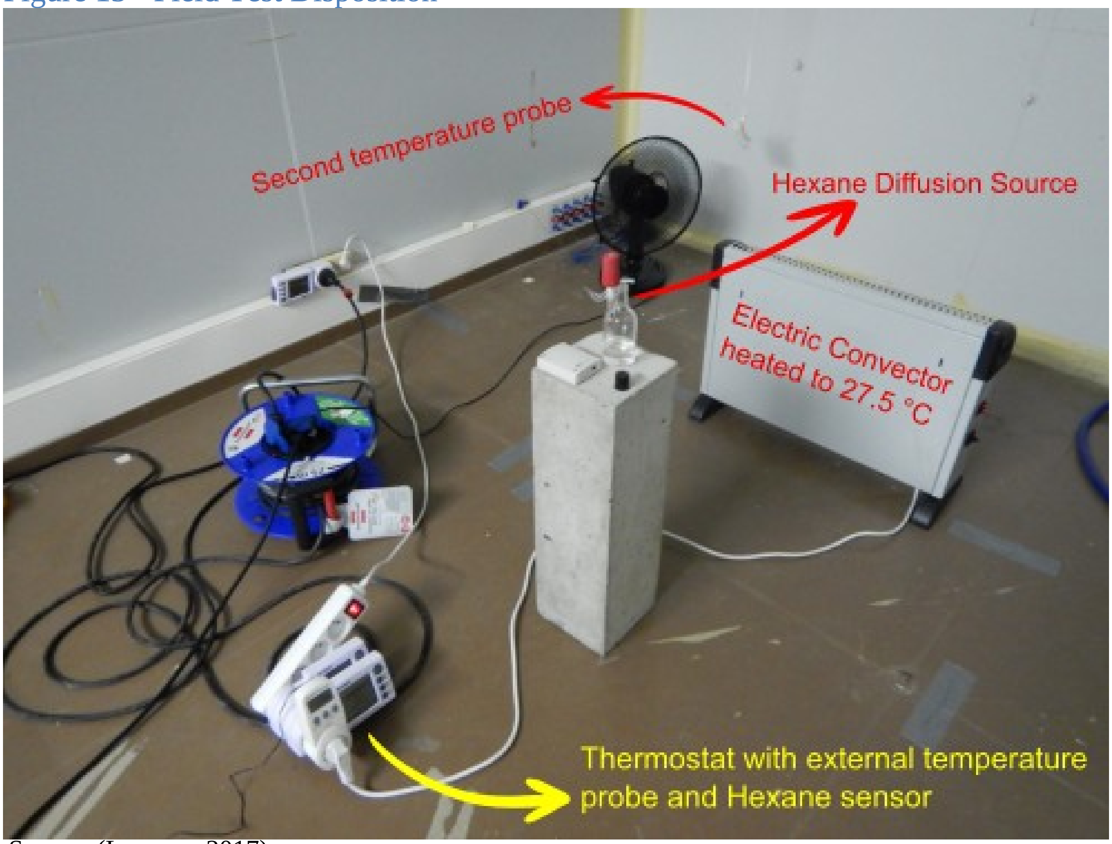

Source: (Laverge, 2017)

3.3 GEOMETRY AND CARTESIAN COORDINATE SYSTEM

The geometry for the simulation was created in AutoCAD Figure 14, based on the additional information provided by the experimental test setup document, where the original internal Passys cell geometry has been changed due to extra internal insulation.

Figure 14 - Geometry Reproduction of Field Experiment

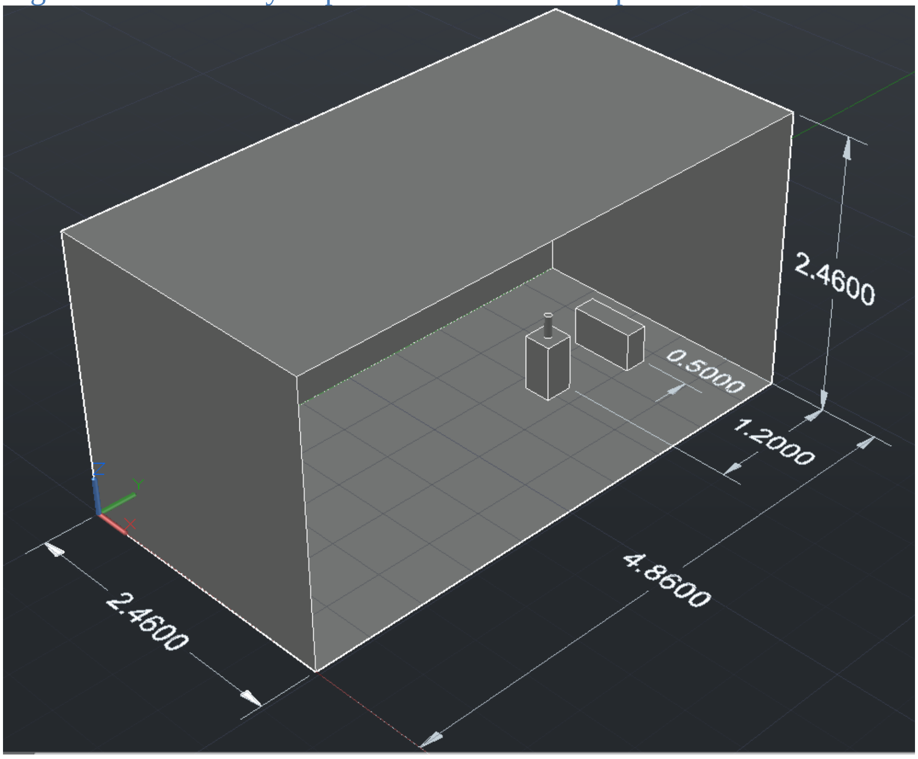

Source: From the Author

The geometry created was then exported to ANSYS Design Modeler, where the extraction of the negative volume from the original AutoCAD geometry has been made. In this process is extracted a solid corresponding to the internal air, which later will be applied the meshing process.

After the negative volume were extracted, one inlet and one outlet were placed in the north wall as presented in Figure 15, a simplification of the inlet of fresh air and the outlet, detailed in the experimental setup document.

Figure 15 - North Wall with Inlet and Outlet

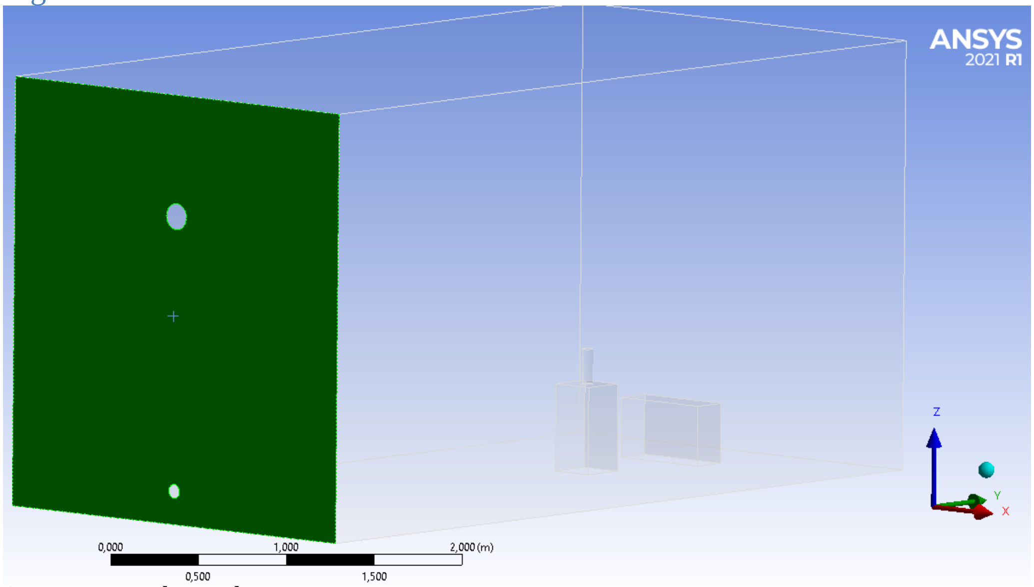

Source: From the Author

The origin of the Cartesian coordinate system in the internal geometry is located in the left corner of the north wall, where the x-axis is positive in the direction of the left corner; the y-axis is positive in the direction of the south wall and the z-axis is positive in the direction of the ceiling. All the results are based on this convention.

3.4 MESH

In order to choose the right mesh for the problem, some constrains had to be in mind. The first one was the student version limitations of ANSYS, which limits to 128k Nodes/Elements for the simulation. The second is the big simulation horizon, where the field experiment took 12 days in total and the goal was to simulate the first 8 days to compare the maximum concentration of hexane. The third and last constrain was the conformity of the geometry, since the original idea was to also simulate the fan blades inside the test cell, shown in Appendix B.

The first choice was hexahedral mesh, since this mesh geometry uses fewer nodes to reach the same accuracy of fine tetrahedral meshes, however, the geometry of the blades was complex, making the geometry conformation difficult. Thus, having in mind the need of good conformity to the geometry, fewer nodes to make the simulation less computationally intensive and at the same time allow big simulation horizon, the tetrahedral mesh was the final choice (Hefny; Ooka, 2009, p. 1). The overview of the mesh can be see in Figure 16.

The first simulations considering the effect of the fan blade in the hexane mixture required a much finer mesh and smaller time-steps in order to reach convergence, thus the limitation of the student version and the need to simulate big time horizons made it nonviable. Nevertheless, the choice for tetrahedral was also considered for the simulation without the fan geometry in order to reach convergence while simulating the mixture of hexane with volume of fluid, which is not a perfect mixture and expose the difference in molecular weight of the different gases.

Figure 16 - Mesh of Entire Air Domain

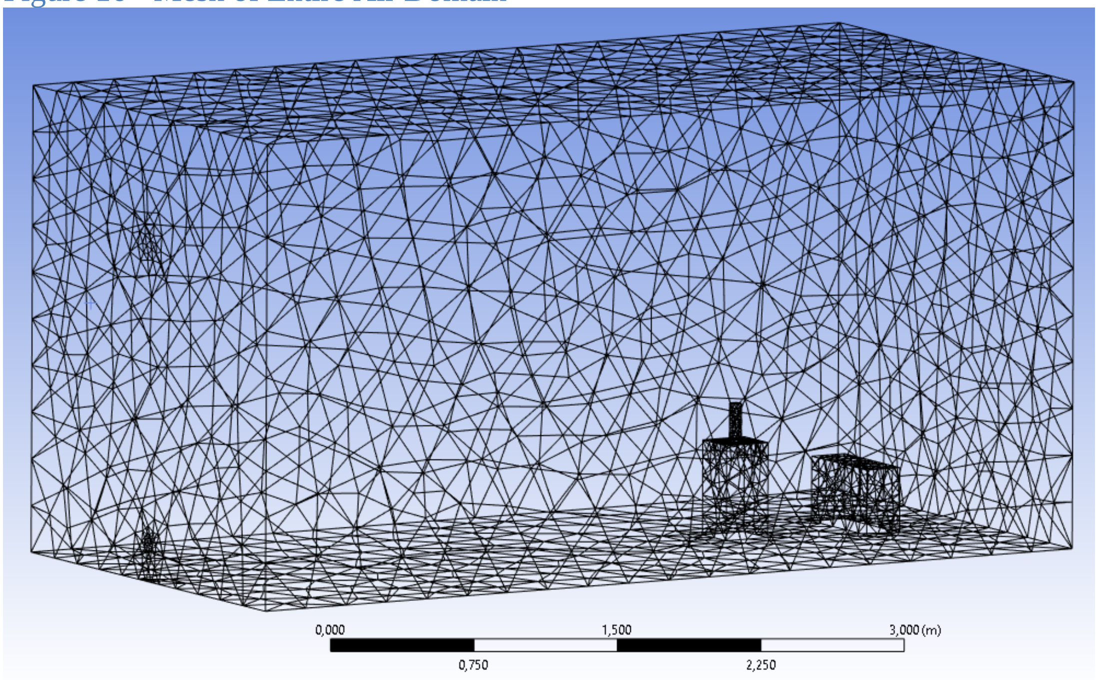

Source: From the Author

In order to analyze the mesh quality, it is important to have in mind three characteristics, which is element quality, skewness, orthogonal quality and aspect ratio.

Element Quality

The element quality ranges from 0 to 1, and it is based on the ratio of the volume and the square root of the cube of the sum of the square of the edge lengths for 3D elements. A value of 1 indicates a perfect cube, while a value of 0 indicates that the element has a zero or negative volume.

For three-dimensional brick elements the formula to calculate the Element Quality is represented by Equation 1:

$$Quality = C\left[\frac{Volume}{\sqrt{\left[\sum \left(Edge\ Length\right)^2\right]^3}}\right] \tag{1}$$

Where the constant C for Tetrahedron mesh is 124.70765802.

Skewness

The skewness determines how close to an ideal equiangular quad a 3D cell is (Figure 17). The value ranges from 0 to 1, where 0 means that the cell has the highest quality and 1 the worst, the whole gradation can be better understood in the Table 7.

Figure 17 - Skewness Quality Example

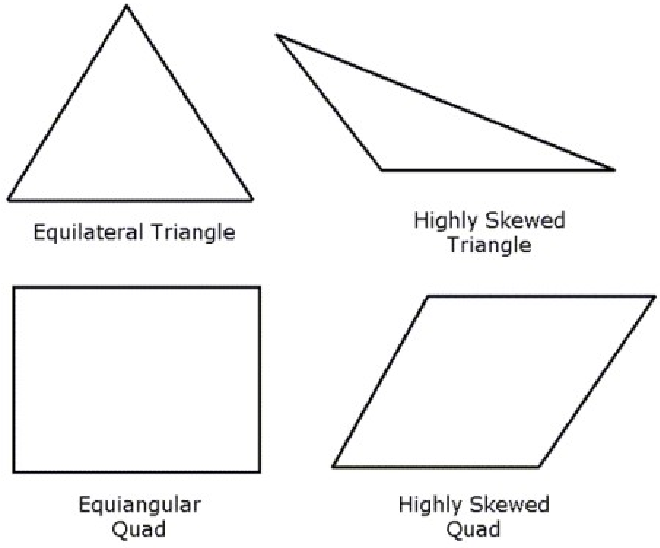

Source: (ANSYS, Inc., 2017, p. 121)

Table 7 - Skewness Quality

Value of Skewness	Cell Quality
1	Degenerate
0.9 – < 1	Bad (Sliver)
0.75 – 0.9	Poor
0.5 – 0.75	Fair
0.25 – 0.5	Good
> 0 – 0.25	Excellent
0	Equilateral

Source: (ANSYS, Inc., 2017, p. 121)

In order to increase the accuracy of the results, it is important to reduce the value of skewness of the cells. This improves the work of the solver, since the equations being solved assume the cells to be relatively equiangular, thus making it converge more the solution.

Orthogonal Quality

The Orthogonal Quality ranges from 0 to 1, where 0 is the worst quality and 1 the best. The cosines of the vectors A_i and C_i and A_i and f_i are calculated for each face of the cell, the smallest value of cosine is the orthogonality of the cell as presented in Figure 18. However, orthogonality also depends on type of cell, for tetrahedral cells, the Orthogonal Quality is the minimum of the orthogonality and (1 – Cell Skewness).

Figure 18 - Orthogonal Quality Example with Vectors

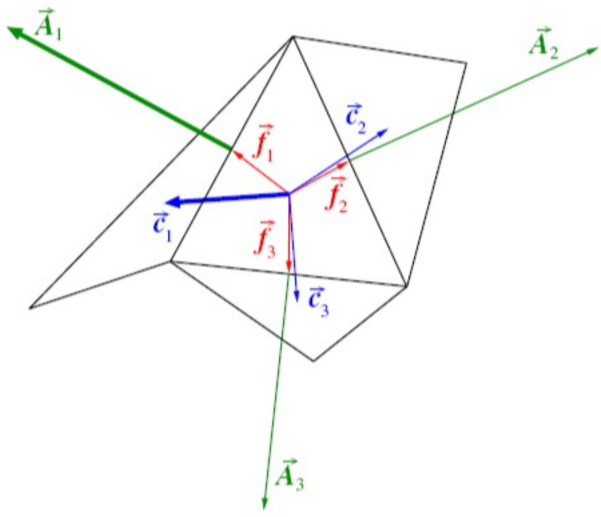

Source: (ANSYS, Inc., 2017, p. 123)

The scale is inverse between the Orthogonal Quality in the Meshing application in ANSYS and Fluent Meshing, it can be calculated according to Equation 2:

$$Inverse\,Orthogonal\,Quality = 1 - Orthognal\,Quality \tag{2}$$

It is important to keep the minimal Orthogonal Quality of the mesh above 0.1, otherwise those cells can be too much squished and this is not good for the Fluent solver, the solution tend to not have a good convergence.

Aspect Ratio

The Aspect Ratio is the ratio of the longest edge of a cell and the shortest length, it can be used to determine how close the cell is to the ideal shape as presented in Figure 19. The number ranges from 1 to numbers greater than 1, where 1 means the cell is equilateral and numbers above >1 means the cell is less regularly-shaped.

Figure 19 - Aspect Ratio Example

Source: (ANSYS, Inc., 2017, p. 112)

The Figure 20, Figure 21, Figure 22 and Figure 23 represents the quality of the tetrahedral mesh used for the simulation of the Passys test cell.

Figure 20 - Mesh Average Element Quality

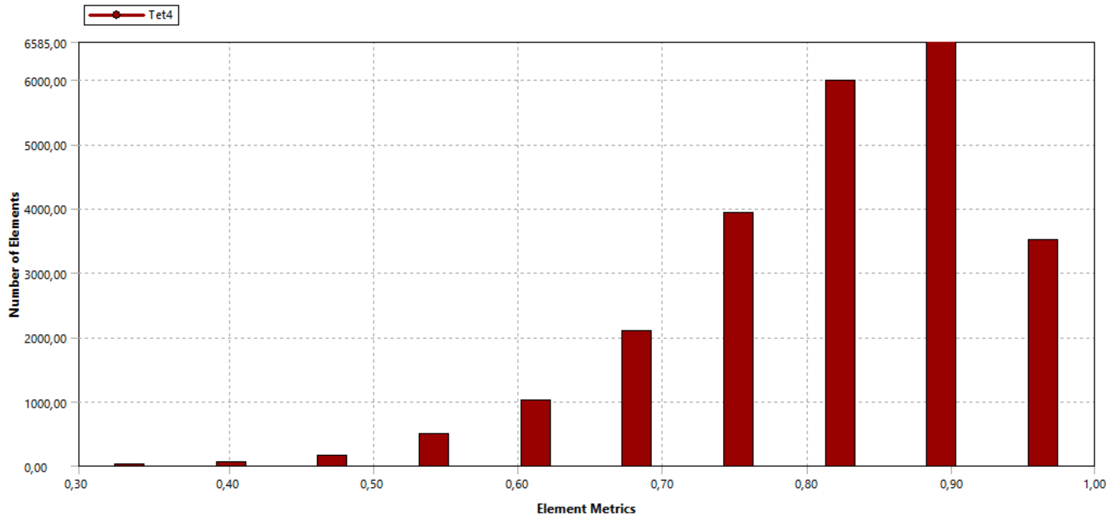

Source: From the Author

Figure 21 - Mesh Average Aspect Ratio

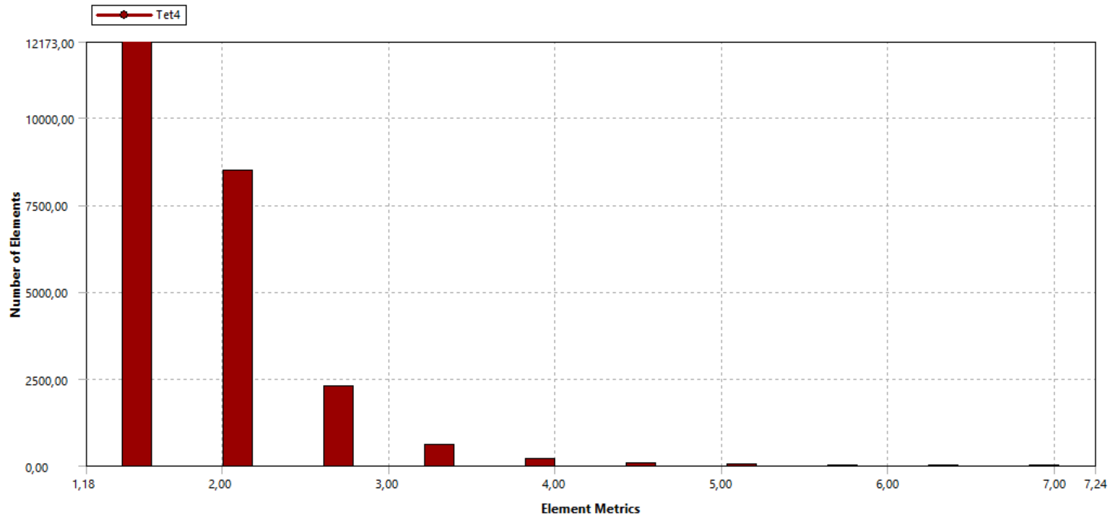

Source: From the Author

Figure 22 - Mesh Average Skewness

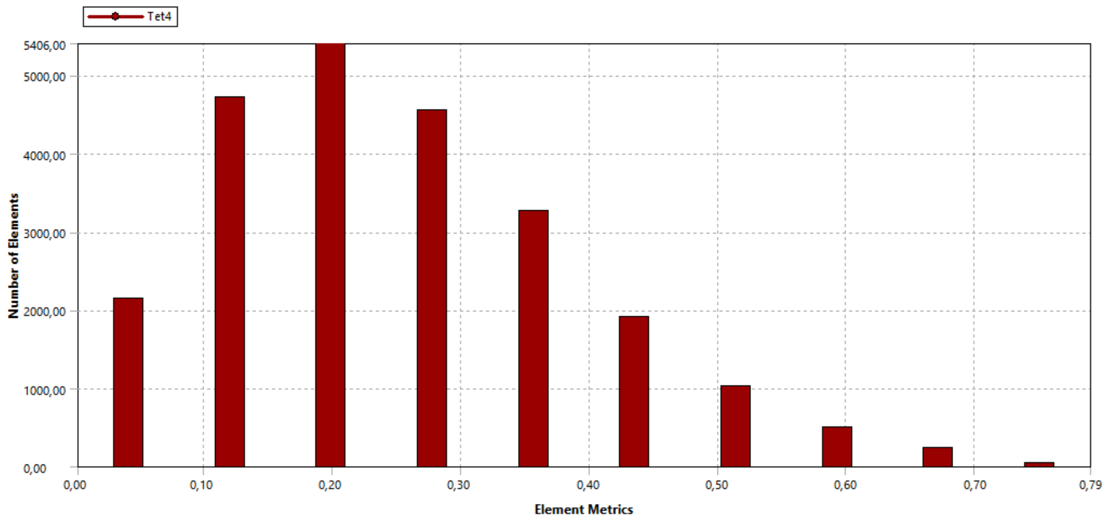

Source: From the Author

Figure 23 - Mesh Average Orthogonal Quality

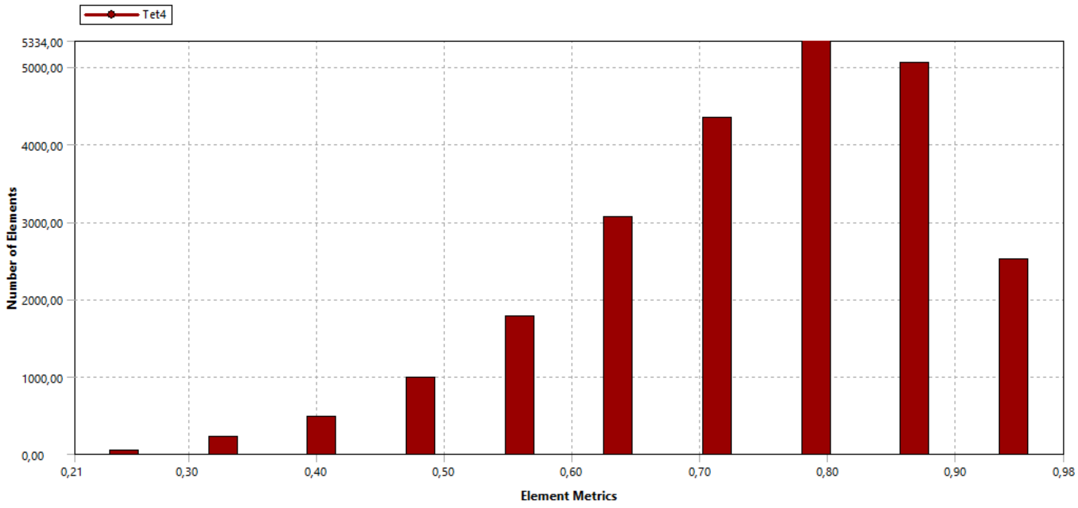

Source: From the Author

As we can see the quality of the tetrahedral mesh is the following:

- **Element Quality**

Ranging from 0.30 to 1, where the majority of the cells are located closer to 1, which means good cell shape.

- **Aspect Ratio**

Ranging from 1.80 to 3, where the majority of the cells are closer to 1, which means more regularly-shaped cells.

- **Skewness**

Ranging from 2.2e-3 to 0.79 as shown in Table 8, categorized from Good to Excellent.

- **Orthogonal Quality**

Ranging from 0.21 to 0.98, categorized from Good to Excellent.

Wall Distance Estimation (Y+)

The wall distance estimation parameter is a non-dimensional measure of distance from the wall (first cell thickness) (Dimensionless wall distance (y plus) -- CFD-Wiki, the free CFD reference, 2024). The desire value is 1, however in some extremely well behavior simulations it is possible to have a value of 2, since the estimated wall distance was 2e-4. Meanwhile, the smallest mesh size in the proximity of the boundary layer being 2.46e-3 m, thus, Y+ between 1 and 2. Far from the walls, the mesh size went to a maximum value of 0.246 m. The two main limitations for a further refining of mesh in this setup, was the student license and the extremely long time horizon of the simulation, with the last being the main factor.

Table 8 - Inner Air Geometric Domain

Object Name	*inner_air*
State	Meshed
Definition	
Suppressed	No
Coordinate System	Default Coordinate System
Treatment	None
Reference Frame	Lagrangian
Material	
Fluid/Solid	Defined By Geometry (Fluid)
Statistics	
Nodes	4773
Elements	23779
Mesh Metric	Skewness
Min	2,20E-03
Max	0,79005982
Average	0,252139813
Standard Deviation	0,13965966

Source: From the Author

3.5 SIMULATION SETUP

The assumptions for the simulation are:

- **Newtonian Fluid** (Air and Hexane).

In this simulation, the fluid is assumed to be a Newtonian fluid, both air and hexane, this refers to a fluid whose viscosity is constant and does not change with the rate of deformation or the gradient of velocity. In this case, both air and hexane, exhibit Newtonian behavior, since at standard temperature and pressure conditions, this assumption is generally valid.

- **Fluid flow incompressible**

The fluid flow is modeled as incompressible. Incompressible flow means that the density of the fluid remains constant during the flow process. This assumption is reasonable for many engineering applications involving air or hexane at normal temperature and pressure conditions, as they experience very small changes in density under moderate pressure and temperature variations.

- **Transient Regime where the inlet velocity of air varies over time**

The simulation is considered transient, since the air inlet flow change with time. In the transient regime, the flow field and other flow properties vary with time. This assumption is relevant when studying the time-dependent behavior of fluid flows, such as in the case of unsteady or pulsatile flows.

- **Three-Dimensional**

The simulation takes into account all three spatial dimensions, meaning it considers the variation of flow properties in the x, y, and z directions. This assumption allows for a more accurate and realistic representation of the fluid flow phenomena under investigation.

- **Boussinesq Approximation for buoyance forces**

The Boussinesq approximation is applied. This is an assumption used to simplify the solution of fluid flow problems involving density variations due to temperature or concentration gradients. It is an approximation because it neglects the rate of strain in the flow field, which simplifies the governing equations considerably and saves computational resources.

- **Gravitational acceleration in the negative z-direction**

The gravitational acceleration is imposed as constant and uniform in the negative z-direction with a magnitude of 9.81 m/s^2.

- **Adiabatic Walls**

The system is assumed to have adiabatic boundaries, meaning there is no heat exchange between the fluid and its surroundings. This assumption significantly simplify the complex physics governing fluid flows and simplify the computational effort required to simulate the system accurately.

For this simulation, some physical characteristics were considered for the fluids (air and hexane) and the boundary layer (walls) as presented in Table 9. Air is used as the primary fluid. The material of the walls are considered as aluminum, since it was the only metal available in the list of standard materials for Ansys Fluent.

Table 9 - Physical Characteristics of Species and Wall

Air	
Density	1.225 kg/m^3
Cp (Specific Heat)	1006.43 J/(kg K)
Thermal Conductivity	0.0242 W/(m K)
Viscosity	1.7894×10^{-5} kg/(m s)
Molecular Weight	28.966 kg/kmol
L-J Characteristic Length	3.711 Angstrom
L-J Energy Parameter	-194.55 C

Aluminum	
Density	2719 kg/m^3
Cp (Specific Heat)	871 J/(kg K)
Thermal Conductivity	202.4 W/(m K)
N-Hexane-Air	
Mixture Species	Names
Density	Incompressible Ideal Gas
Cp (Specific Heat)	Mixing Law
Thermal Conductivity	0.0454 W/(m K)
Viscosity	1.72×10^{-5} kg/(m s)
Mass Diffusivity	Kinetic Theory

Source: From the Author

In the Figure 24 is possible to visualize the localization of the two inlets and outlets to better understand the physical assumptions for them.

In this simulation, the fluid flow is modeled using an absolute reference frame for both the inlet and outlet boundary conditions. The inlet specifies a mass flow rate of 0.0082 kg/s at a temperature of 27.5°C and an initial gauge pressure of 0 Pa. The flow direction is described using a Cartesian coordinate system with components in the x, y, and z directions. The turbulent intensity is set to 5%, and the turbulent viscosity ratio is 10. The simulation assumes stationary walls with a uniform thickness of 0 m and a constant wall roughness coefficient of 0.5. The walls are treated as stationary and non-reactive surfaces, with no specified species boundary conditions.

The inlet flow conditions are defined in the absolute reference frame with a uniform temperature of 27.5°C and an initial gauge pressure of 0 Pa. The flow direction is identified using the Cartesian coordinate system with components in the x, y, and z directions. The inlet velocity magnitude is defined by a User Defined Function (UDF). The fluid is assumed to be incompressible and in steady-state conditions. Further information refer to Table 10.

Figure 24 - Geometry of Air Domain with Inlet, Outlet and Hexane Inlet Highlighted

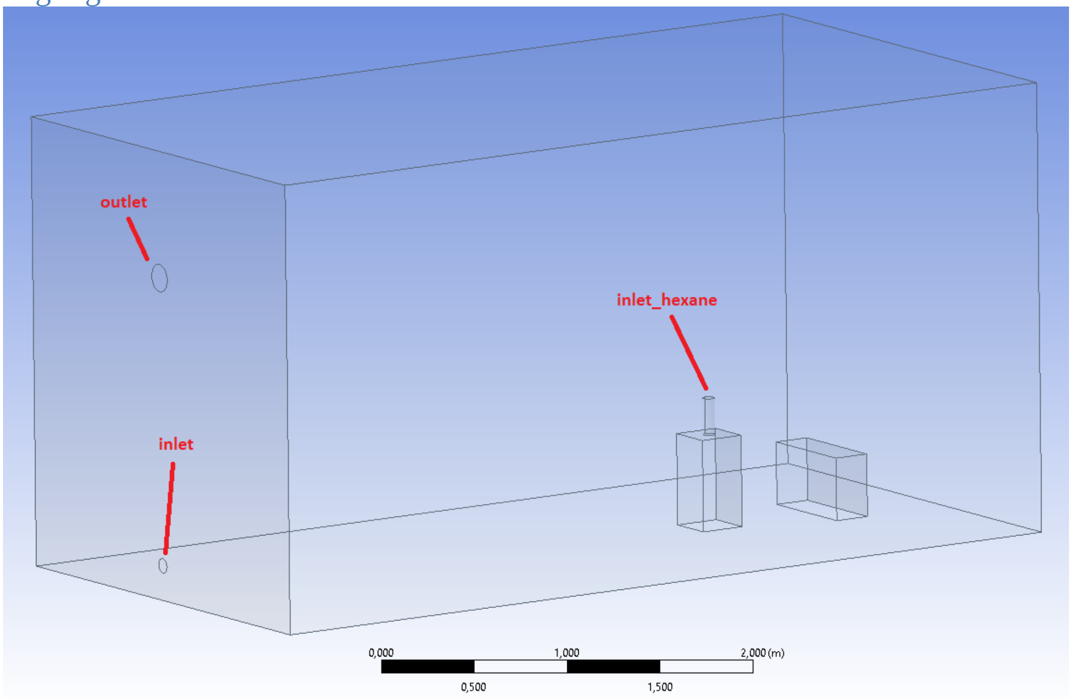

Source: From the Author

Table 10 - Boundary Conditions

inlet_hexane	
Reference Frame	Absolute
Mass Flow Specification Method	Mass Flow Rate
Mass Flow Rate [kg/s]	0.0082
Total Temperature [°C]	27.5
Supersonic/Initial Gauge Pressure [Pa]	0
Direction Specification Method	Direction Vector
Coordinate System	Cartesian (X, Y, Z)
Component of Flow Direction (x, y, z)	(0, 0, 1)
Turbulent Specification Method	Intensity and Viscosity Ratio
Turbulent Intensity [%]	5
Turbulent Viscosity Ratio	10
Specify Species in Mole Fraction?	No
outlet	
Backflow Reference Frame	Absolute
Gauge Pressure [Pa]	0
Pressure Profile Multiplier	1
Backflow Total Temperature [°C]	27.5
Backflow Direction Specification Method	Normal to Boundary
Turbulent Specification Method	Intensity and Viscosity Ratio

Backflow Turbulent Intensity [%]	5
Backflow Turbulent Viscosity Ratio	10
Specify Species in Mole Fractions?	no
walls	
Wall Thickness [m]	0
Heat Generation Rate [W/m^3]	0
Material Name	Aluminum
Thermal BC Type	Heat Flux
Heat Flux [W/m^2]	0
Enable Shell Conduction?	no
Wall Motion	Stationary Wall
Shear Boundary Condition	No Slip
Wall Roughness Height [m]	0
Wall Roughness Constant	0.5
Species Boundary Conditions	Specified Mass Flux/Specified Mass Flux
Convective Augmentation Factor	1
inlet	
Velocity Specification Method	Magnitude and Direction
Reference Frame	Absolute
Velocity Magnitude	udf inlet-x-velocity
Supersonic/Initial Gauge Pressure [Pa]	0
Coordinate System	Cartesian (X, Y, Z)
Component of Flow Direction (x, y, z)	(0, 1, 0)
Temperature [C]	27.5
Turbulent Specification Method	Intensity and Viscosity Ratio
Turbulent Intensity [%]	5
Turbulent Viscosity Ratio	10
Specify Species in Mode Fractions?	no

Source: From the Author

The User Defined Function (UDF) is a simple C code for the air inlet velocity magnitude. It was created to properly represent the change in inlet velocity over time, following the experiment setup in Table 6. The Table 11 represents the simulation time elapse in time-steps, while the Figure 25 shows the C code.

Table 11 - Transient Air Inlet Velocity

1. Startup	0	172800	1.63 m/s
2. High	172800	321600	1.63 m/s
3. Low	321600	828720	0,163 m/s
4. High	828720	1036800	1.63 m/s

Source: From the Author

Figure 25 - User Defined Function of Air Inlet

```c
#include "udf.h"

DEFINE_PROFILE(inlet_x_velocity, thread, position)
{
    real x[ND_ND]; /* this will hold the position vector */
    real y, h, vel, tempo, factor;
    face_t f;

    h = 0.08; /* Inlet Diameter in m */

    tempo = CURRENT_TIME;

    factor = 1.63;

    begin_f_loop(f,thread)
    {
        F_CENTROID(x, f, thread);
        y = 2.*(x[1]-0.5*h)/h; /* non-dimensional y coordinate */

        if(tempo>507120) vel = factor * (1.0-y*y);
        else if(tempo>148800) vel = 0.1 * factor * (1.0-y*y);
        else vel = factor * (1.0-y*y);

        F_PROFILE(f, thread, position) = vel;
    }
    end_f_loop(f, thread)
}
```

Source: From the Author

The solver settings for the simulation is presented in Table 12. For the Volume of Fluid model, the inlet was consider to be 1 volume fraction for oxygen, while for the hexane inlet 1 volume fraction of hexane. The initialization of the simulation was standard, which reaches a steady state before start the multiphase simulation. This practice minimizes convergence errors due to truncation (truncation error tolerance was 1.5).

The initial values are 0.99 volume fraction of oxygen in the domain, meaning no hexane in the air domain at initialization.

Table 12 - Solver Settings

Equations	
Flow	True
Turbulence	True
C_6H_{14}	True
O_2	True
CO_2	True
H_2O	True
Energy	True
Numerics	

Absolute Velocity Formulation	True
Unsteady Calculation Parameters	
Number of Time Steps	1
Time Step Size [s]	5
Max Iterations/Time Step	20
Under-Relaxation Factors	
Pressure	0.3
Density	1
Body Forces	1
Momentum	0.7
Turbulent Kinetic Energy	0.8
Turbulent Dissipation Rate	0.8
Turbulent Viscosity	1
C_6H_{14}	1
O_2	1
CO_2	1
H_2O	1
Energy	1
Pressure-Velocity Coupling	
Type	SIMPLE
Discretization Scheme	
Pressure	Second Order
Momentum	Second Order Upwind
Turbulent Kinetic Energy	First Order Upwind
Turbulent Dissipation Rate	First Order Upwind
C_6H_{14}	Second Order Upwind
O_2	Second Order Upwind
CO_2	Second Order Upwind
H_2O	Second Order Upwind
Energy	Second Order Upwind
Solution Limits	
Minimum Absolute Pressure [Pa]	1
Maximum Absolute Pressure [Pa]	$5x10^{10}$
Minimum Temperature [C]	1
Maximum Temperature [C]	5000
Minimum Turb. Kinetic Energy [m^2/s^2]	$1x10^{-14}$
Minimum Turb. Dissipation Rate [m^2/s^2]	$1x10^{-20}$
Maximum Turb. Viscosity Ratio	100000

Source: From the Author

The minimum and maximum time step size were set to 5 seconds. This was the longest time step possible without convergence error. The idea behind it was to reduce as much as possible the total simulation time.

3.6 GOVERNING EQUATIONS (DIFFERENTIAL APPROACH)

After the creation of the geometry, meshing and the setup of the boundary conditions, the solver applied mathematical models in each cell of the mesh in order to describe the fluid flow inside the domain. Those mathematical models are a series of equations equivalent in number to the unknowns, where for 3D models we need four equations.

The conservative governing equations of fluid motion can be expressed in integral and differential form, they are equivalent mathematically speaking. While the integral form is used in the Finite Volume Method (FVM), the differential form is used in the Finite Difference Method (FDM). The way dependent variables are stored varies from one method to another, in Finite Difference Method, the variables are stored in the nodes, while in the Finite Volume Method (FVM) the variables are stored in the center of the Finite Volume.

The solver of the software Fluent uses the Finite Differential Method, which applies the equations of continuity, momentum, and energy in each cell of the mesh. The three governing equations originated from the Lavoisier’s law of conservation of mass, which yields to the continuity equation; The Newton’s Second Law of conservation of momentum which leads ultimately to the Navier-Stokes equation and the First Law of Thermodynamics, which leads to the Energy Equation. More on (Anderson, 1992).

Respectively in order to model fluid flows, the solver must respect the follow basic principles of physics, where the mass of an isolated system cannot be created or destroyed, however it can be transformed from one form to another. When a force is acted upon a body, the time rate of change is its momentum equals the force and finally that heat is recognized as a form of energy, so the total energy of a system plus its surroundings is conserved.

Continuity Equation in the common Cartesian coordinate form, as represented by Equation 3:

$$\frac{\partial \rho}{\partial t}+\frac{\partial (\rho u)}{\partial x}+\frac{\partial (\rho v)}{\partial y}+\frac{\partial (\rho w)}{\partial z}=0 \tag{3}$$

Where:

ρ – Fluid Density
t – Time
$u, v, w, x, y \wedge z$ – Components of the mass average velocity

Conservation of Momentum expanded in the 3D form, as represented by Equations 4, 5 and 6:

x-momentum:

$$\rho\left(\frac{\partial u}{\partial t}+u\frac{\partial u}{\partial x}+v\frac{\partial u}{\partial y}+w\frac{\partial u}{\partial z}\right)$$
$$\text{¿}=\frac{-\partial p}{\partial x}+\frac{\partial}{\partial x}\left[2\mu\frac{\partial u}{\partial x}-\frac{2}{3}\mu\left(\frac{\partial u}{\partial x}+\frac{\partial v}{\partial y}+\frac{\partial w}{\partial z}\right)\right]+\frac{\partial}{\partial y}\left[\mu\left(\frac{\partial u}{\partial y}+\frac{\partial v}{\partial x}\right)\right]+\frac{\partial}{\partial z}\left[\mu\left(\frac{\partial u}{\partial z}+\frac{\partial w}{\partial x}\right)\right]+F_{b,x} \tag{4}$$

y-momentum:

$$\rho\left(\frac{\partial v}{\partial t}+u\frac{\partial v}{\partial x}+v\frac{\partial v}{\partial y}+w\frac{\partial v}{\partial z}\right)$$
$$\text{¿}=\frac{-\partial p}{\partial y}+\frac{\partial}{\partial x}\left[\mu\left(\frac{\partial v}{\partial x}+\frac{\partial u}{\partial y}\right)\right]+\frac{\partial}{\partial y}\left[2\mu\frac{\partial v}{\partial y}-\frac{2}{3}\mu\left(\frac{\partial u}{\partial x}+\frac{\partial v}{\partial y}+\frac{\partial w}{\partial z}\right)\right]+\frac{\partial}{\partial z}\left[\mu\left(\frac{\partial v}{\partial z}+\frac{\partial w}{\partial y}\right)\right]+F_{b,y} \tag{5}$$

z-momentum:

$$\rho\left(\frac{\partial w}{\partial t}+u\frac{\partial w}{\partial x}+v\frac{\partial w}{\partial y}+w\frac{\partial w}{\partial z}\right)$$
$$\text{¿}=\frac{-\partial p}{\partial z}+\frac{\partial}{\partial x}\left[\mu\left(\frac{\partial w}{\partial x}+\frac{\partial u}{\partial z}\right)\right]+\frac{\partial}{\partial y}\left[\mu\left(\frac{\partial w}{\partial y}+\frac{\partial v}{\partial z}\right)\right]+\frac{\partial}{\partial z}\left[2\mu\frac{\partial w}{\partial z}-\frac{2}{3}\mu\left(\frac{\partial u}{\partial x}+\frac{\partial v}{\partial y}+\frac{\partial w}{\partial z}\right)\right]+F_{b,z} \tag{6}$$

Where:

ρ – Fluid Density

t – Time

$u, v, w, x, y \wedge z$ – Components of the mass average velocity

μ – Dynamic Viscosity

p – Static Pressure

With the first four equations (conservation of mass and momentum), we have four differential equations for five unknowns ρ, p, u, v and w (density, pressure, and the three velocity components). Even though the flow is incompressible, we can not simplify the density and viscosity assuming both constant. We must consider the effect of temperature of the fluid in the flow, thus, adding another unknown to the system that will require another differential equation to close the system, which is the energy equation.

Conservation of Energy in its Cartesian coordinate form, as represented by Equation 7:

$$\frac{\partial}{\partial t}(\rho c_p T)+\frac{\partial}{\partial x}(\rho u c_p T)+\frac{\partial}{\partial y}(\rho v c_p T)+\frac{\partial}{\partial z}(\rho w c_p T)=k\left(\frac{\partial^2 T}{\partial x^2}+\frac{\partial^2 T}{\partial y^2}+\frac{\partial^2 T}{\partial z^2}\right)+q'' \quad (7)$$

Where:

ρ – Fluid Density

t – Time

$u, v, w, x, y \wedge z$ – Components of the mass average velocity

T – Temperature

c_p – Specific Heat at Constant Pressure

q'' – Volumetric Rate of Thermal Energy Generation

k – Thermal Conductivity

An in depth explanation can be found on (Incropera, 2007, p. 975) and (Ahmad; Plee; Myers, 2013).

3.7 K-EPSILON TURBULENCE MODEL AND BOUSSINESQ APPROXIMATION

The CFD industry has evolved considerably the last couple of decades due to the increase in computational power. However, the industry still needs to have some best practices in order to somewhat accurately represent the natural phenomena and still keep the computational effort within the capabilities of modern computers.

Since most of the fluid flows will produce turbulence and this phenomenon is key in many analyses, ranging from fluid-structure interaction to chemical dispersion, it is crucial to accurately model this phenomenon in the best way possible. Currently, there are many turbulence models available, yet only a few currently being commercially used more often than others.

The most used in mainstream CFD analysis is Reynolds Averaged Navier Stokes (RANS), it is a simplified Navier Stokes equation which takes the average effect of turbulence and has many turbulence models available.

The Large Eddy Simulation (LES) model is better suited to large scale structures, such as offshore wind turbines, ships and buildings, where large-scale eddies caused by turbulence can influence the flow patter. Eddies bigger than the grid size will be model, while micro-eddies smaller than the grid size are replaced with turbulence models. Since it does not ignore all the turbulence, this solution is computationally intense.

An alternative to LES is the Detached Eddy Simulation (DES) which uses regular RANS near objects and LES away from objects with less mesh, also recommended for large structures.

The Direct Numerical Simulation (DNS) has no simplification of the Navier Stokes equation and models everything as it is in nature, which makes the simulation impractical, since the time-step necessary for convergence is in the order of pico-seconds and a grid resolution as fine as the Kolmogorov micro-scale (Chen; Srebric, 2000, p. 3). Also, the hardware required to simulate using this turbulence model is not yet available commercially.

While Large Eddy Simulation (LES) and Direct Numerical Simulation (DNS) are heavily computer intensive, the majority of CFD analysis nowadays uses Reynolds Averaged Navier Stokes (RANS) equation together with a two-equation models of turbulence, usually k-epsilon, which is more suitable for indoor flow analysis.

The use of k-epsilon turbulence model was chosen for this work due to the fact that is well known in literature the use of k-epsilon in steady mean flow and scalar specie transport, as stated by (American Society of Heating, Refrigerating and Air Conditioning Engineers (ASHRAE), 2017). The k-epsilon model is a two-equation model, where k is the kinetic energy and the epsilon is the dissipation rate of turbulent kinetic energy.

This method is used to predict eddy viscosity and is only valid for fully developed turbulent flow. Even though the Reynolds number will not be always high inside a room – which is the case of this study – a good prediction is obtained in areas with a certain velocity level. The k-epsilon turbulence model has three different variants, the Standard k-epsilon model, RNG k-epsilon model and the Realizable k-epsilon model. For this study it was used the Reynolds Averaged Navier Stokes with the Realizable k-epsilon turbulence model, which applies the Boussinesq hypothesis approach that has a relatively low computational cost associated with the computation of the turbulent viscosity.

In this variant of the k-epsilon model, the realizable means that the model satisfies some mathematical constrains on the Reynolds stresses on the physics of turbulent flows. The Reynolds stress in an incompressible strain mean flow is the combination of the Boussinesq hypothesis and the Turbulent Viscosity equation. More can be found on (Jiang, 2021) and (Ahmad; Plee; Myers, 2013, p. 55).

Normal Reynolds Stress in an Incompressible Strained Mean Flow, as represented in Equation 8:

$$\overline{u^2} = \frac{2}{3} k - 2 v_t \frac{\partial U}{\partial x} \tag{8}$$

The Boussinesq hypothesis equation, as represented in Equation 9:

$$-\rho\overline{u_i'}\,\overline{u_j'}=\mu_t\left(\frac{\partial u_i}{\partial x_j}+\frac{\partial u_j}{\partial x_i}\right)-\frac{2}{3}\left(\rho k+\mu_t\frac{\partial u_k}{\partial x_k}\right)\delta_{ij} \tag{9}$$

In the normal Reynolds stress expression and in the Boussinesq hypothesis equation, the turbulent viscosity term is determined by Equation 10:

$$\mu_t=\rho\,v_t \tag{10}$$

Where the second term comes from Equation 11:

$$v_t=C_\mu\frac{k^2}{\varepsilon} \tag{11}$$

Thus, the Turbulent Viscosity is represented by Equation 12:

$$\mu_t=\rho\,C_\mu\frac{k^2}{\varepsilon} \tag{12}$$

Where:

C_μ = Constant with value of 0.09

Since the C_μ is constant, only the k and ε must be determined by the two equations in the realizable k-epsilon model.

The transport equation for k in the realizable k-epsilon model is represented by Equation 13:

$$\frac{\partial}{\partial t}(\rho k)+\frac{\partial}{\partial x_i}(\rho k\,u_j)=\frac{\partial}{\partial x_i}\left[\left(\mu+\frac{\mu_t}{\sigma_k}\right)\frac{\partial k}{\partial x_i}\right]+G_k+G_b-\rho\varepsilon-Y_M-S_k \tag{13}$$

The transport equation for ε in the realizable k-epsilon model is represented by Equation 14:

$$\frac{\partial}{\partial t}(\rho\varepsilon)+\frac{\partial}{\partial x_i}(\rho\varepsilon\,u_j)=\frac{\partial}{\partial x_i}\left[\left(\mu+\frac{\mu_t}{\sigma_\varepsilon}\right)\frac{\partial\varepsilon}{\partial x_i}\right]+\rho\,C_1 S\varepsilon-\rho\,C_2\frac{\varepsilon^2}{k+\sqrt{\nu\varepsilon}}+C_{1\varepsilon}\frac{\varepsilon}{k}C_{3\varepsilon}C_b+S_\varepsilon \tag{14}$$

Where:

$S\varepsilon$ – User-defined source term.

S_k – User-defined source term.

G_k – Generation of turbulence kinetic energy due to mean velocity gradient.

G_b – Generation of turbulence kinetic energy due to buoyancy. This term is zero by default in Ansys Fluent.

Y_M – Contribution of the fluctuating dilatation in compressible turbulence to the overall dissipation rate. In this work the airflow is incompressible.

$C_3\varepsilon$ – This variable determines the degree of buoyancy effect. It is zero when buoyant shear layers are perpendicular to the gravitational vector.

$C_1\varepsilon$ – Constant with value 1.44

C_2 – Constant with value 1.9

σ_k – Constant with value 1.0

$\sigma\varepsilon$ – Constant with value 1.2

For further information on k-epsilon turbulence model refer to (Ahmad; Plee; Myers, 2013, p. 52).

3.8 SPECIES MODEL

In order to correctly analyze the spatial distribution of the hexane into the Passys test cell, the first approach was the use of multiphase fluid simulation, with the homogeneous model of Volume of Fluid. The idea behind this approach is due to the fact that hexane is a large molecule made of a chain of carbon and hydrogen, with a molecular weight of 86.18 g/mol, while the internal air – which was simulated using 99% mass fraction of oxygen – has molecular weight of 31.99 g/mol. The difference in molecular weight makes the hexane settle on the ground, since the mechanical ventilation of the inlet has a low velocity.

The multiphase approach is used when the two species are not completely miscible, since hexane is much heavier than oxygen and due to the low inlet velocity, it is possible to assume low kinetic energy for mixture. Also, the time horizon of the experiment is long enough to lead to the complete segregation of the two species over time due to sedimentation. Thus, in such circumstances it is possible to consider the interaction of the two gases as immiscible, as it is showed in Figure 26.

Figure 26 - When to Use Volume of Fluid

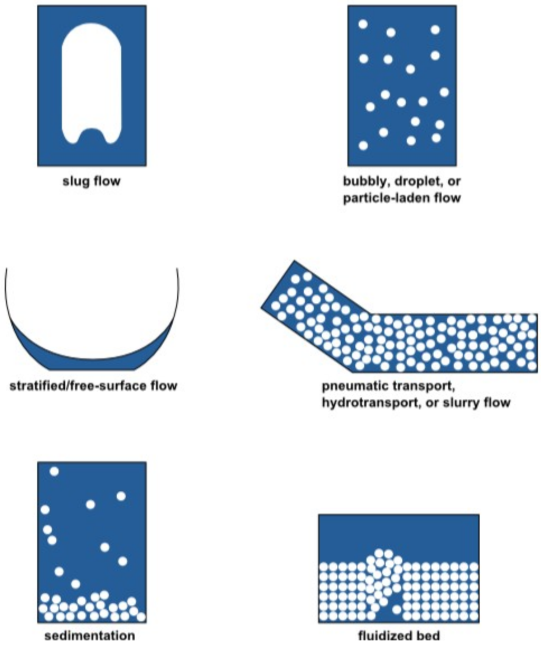

Source: (Rao, 2015)

Further analyzing the field experiment, it is possible to consider the fan placed on the south wall inside the test cell as a mixer of the two species by giving enough kinetic energy to the molecules. An attempt to simulate the direct effect of the fan into the chemical dispersion of hexane was made, yet the simulation demanded a very small time-step that would make the simulation impossible for the eight days of time horizon, and also adding an impractical computational cost into the analysis.

Since in the field experiment was added mechanical ventilation in order to mix the air and hexane inside the test cell, only the Specie Transport model was used to simulate better the mixture of hexane and internal air. Even though only the simulation with a perfect mix between hexane and oxygen was considered for further comparison with other models, the results of the spatial dispersion of hexane using Volume of Fluid is still presented, since in cases where only mechanical ventilation (with low velocity) is used, the immiscibility of the two fluids could be considered, and the simulation would give a better spatial dispersion of the two species.

Considering the fact that there is no reaction between hexane and oxygen, the goal of the simulation is to analyze the mixing of the two fluids, thus for this simulation was used only the Specie Transport model. The idea of the model is to predict the local mass fraction of each species through the solution of the convection-diffusion equation for the i^{th} species.

The general form of Species Transport, is represented by Equation 15:

$$\frac{\partial}{\partial t}\left(\rho Y_i\right)+\nabla\cdot\left(\rho \vec{v} Y_i\right)=-\nabla\cdot\vec{J}_i+R_i+S_i \qquad (15)$$

Where:

t – Time.

ρ – Density of species i.

Y_i – The mass fraction of species i.

$\vec{v}$ – The three-dimensional velocity components.

$\vec{J}_i$ – The diffusion flux of species i.

R_i – The net rate of production of species i by chemical reaction.

S_i – The rate of creation by addition from the dispersed phase plus any user-define sources.

The general equation of the species transport equation can solve any N – 1 species, where N is the total number of fluid phase chemical species in the system.

For further information, refer to (ANSYS, Inc., 2013, p. 5) and (Welahettige; Vaagsaether, 2018, p. 1).

CHAPTER 4
RESULTS

The first simulation attempt was a Volume of Fluid approach with no-mixing between hexane and the indoor air (with 99% mas fraction of oxygen), as shown in Figure 27. This assumption was taken into consideration due to the considerable difference in molecular weight between the oxygen and hexane. However, due to the effect of the heater and the fan in the field experiment, it is reasonable to assume that both can give enough thermal and kinetic energy for a perfect mix. Thus, later the perfect mixing approach was considered for the total simulation period.

Figure 27 - Hexane Molar Concentration with Volume of Fluid around 5h (North-South Walls Axis)

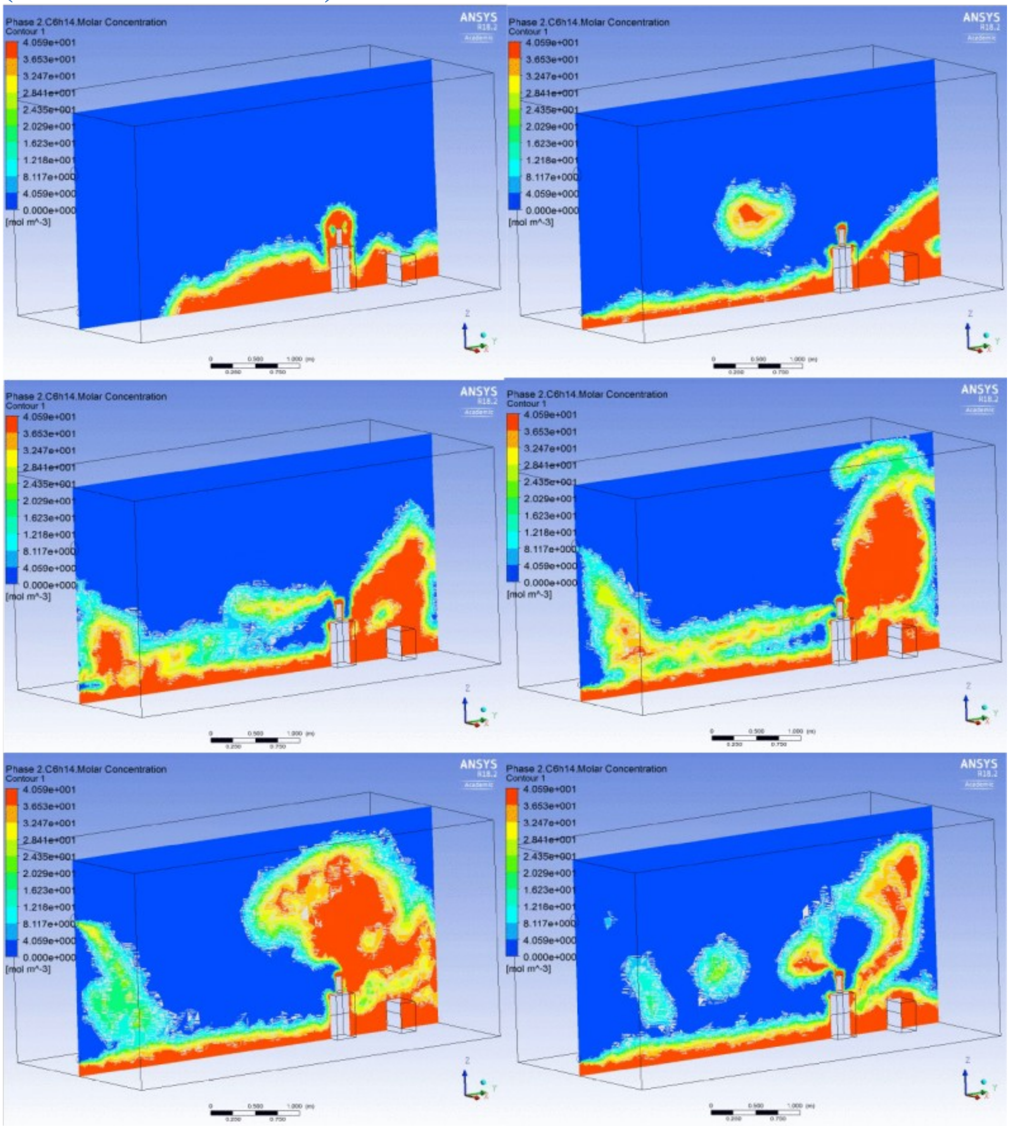

Source: The Author

However, it is worth to compare the indoor behavior of hexane between a Volume of Fluid approach without perfect mixing and with perfect mixing (Figure 28).

Figure 28 - Hexane Concentration at 1. 2 and 8 days with Fluent (North-South Walls Axis)

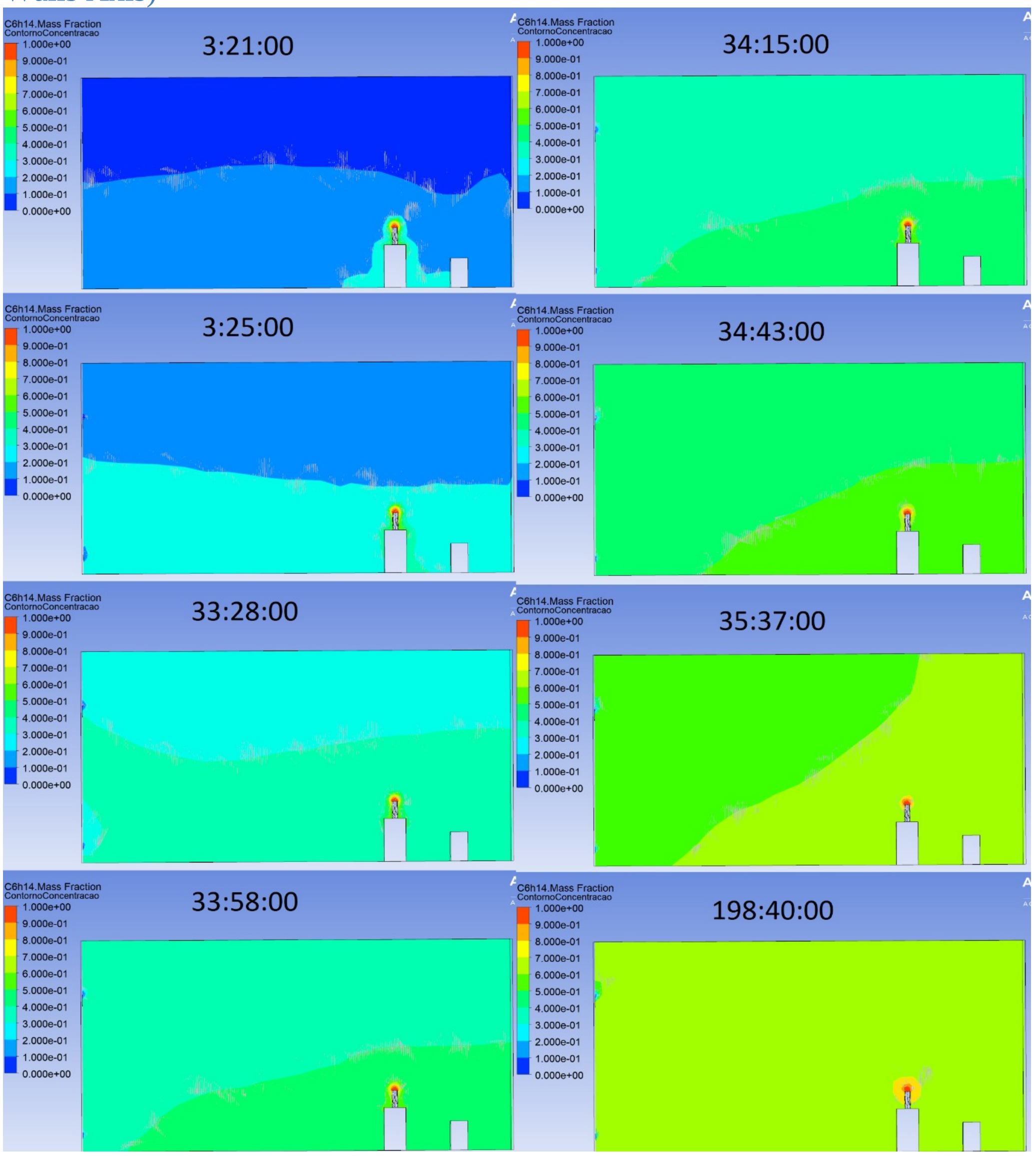

Source: The Author

As we can see, both approaches show how the hexane concentration gets higher close to the ground before it is lifted by the air inflow kinetic energy and mix with indoor air. In both figures it is possible to see the tendency in higher concentrations close to the south wall, coinciding with the direction of the air inlet flow direction (North-South), despite the time difference in both cases.

At the time of maximum concentration (198 hours and 40 min, or 8 days) the molar concentration inside the test cell in the North-South wall axis (Figure 29) also show spatial difference in the average concentration. It is possible to see a higher average concentration right at the hexane inlet and a lower average concentration close to the outlet in the north wall.

Figure 29 - Average Molar Concentration Inside Test Cell (North-South Walls Axis)

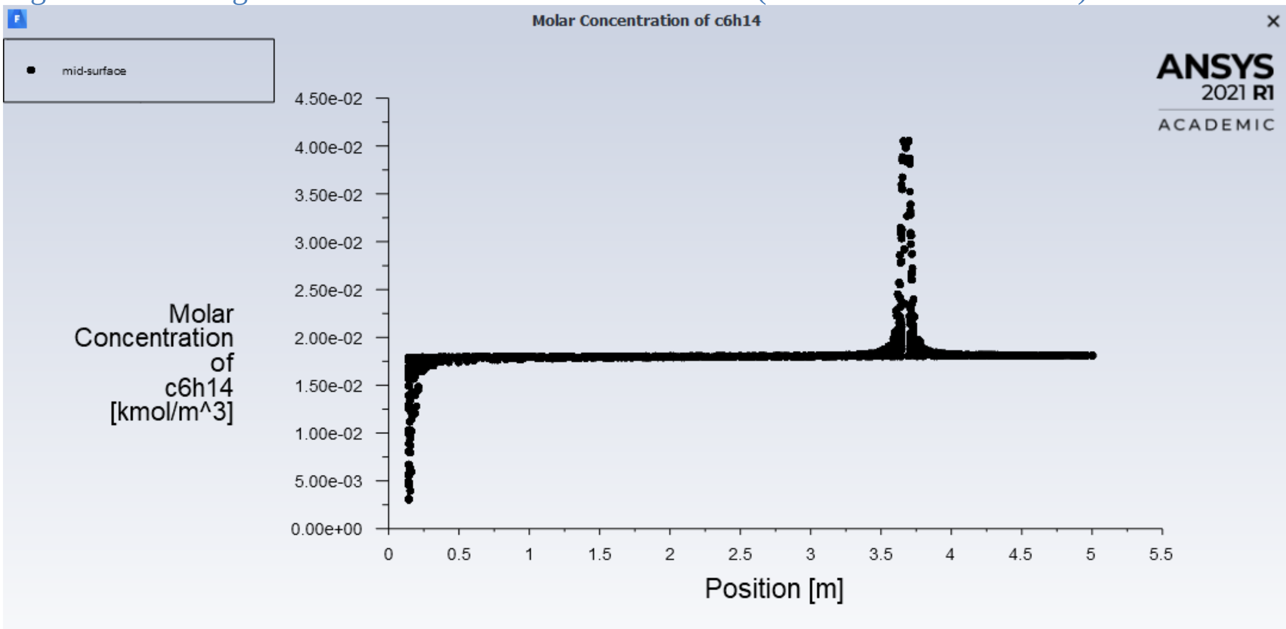

Source: The Author

Another important information is given by the hexane path-line, which is the tracing of hexane particles' movements inside the test cell. It is possible to see in Figure 27 the formation of vortices at the south wall of the test cell, right in the beginning of the simulation (5 hours, or day one) considering the immiscible interaction (volume of fluid approach) between the two chemical species. However, in Figure 30 with the perfect mixing approach, we still see that the formation of vortices persists until the final day of the simulation (198 hours and 40 min, or day eight).

Figure 30 - Hexane Particle Path (North-South Walls Axis, North Wall View, and Top View)

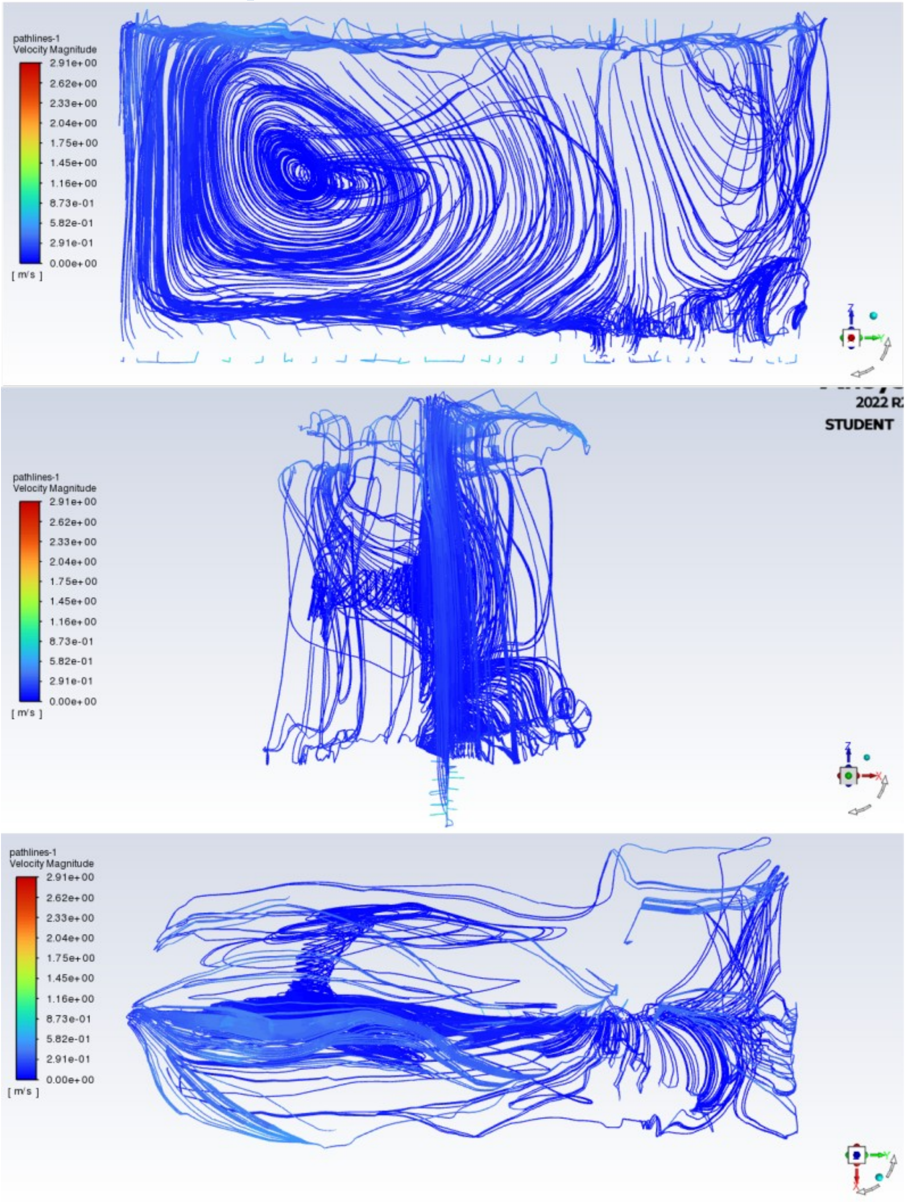

Source: The Author

These spatial visual analysis can bring a qualitative addition to the pure numerical result of total concentration, since it can give to us a hint on how the pollutant can behave when still segregated or in the process to become fully mixed. Another point worth to mention is the possibility that in the physical experiment, the fan could have created such vortices in a different location and in a different angular orientation, since the fan is not located in a symmetrical position like the air inlet. This could induce the hexane sensor placed on the center of the room to read a wrong concentration level (a lower one). Since the hexane have a high molecular weight, those vortices can create a thick vortice zone of higher concentration constantly traveling in circular motion in a specific place within the room.

In the study conducted by (Siddiqui; Jayanti; Swaminathan, 2012), the high difference in molecular weight between the pollutant (Chlorine) and the transport fluid produced an increase in concentration close to the ground and created a stratification effect between the two fluids. As we can see in the field experiment result, there is a fluctuation on the top of the Figure 31 when the maximum concentration is achieved. Could this fluctuation be the effect of a large vortice of hexane cloud changing the concentration right on top of the hexane sensor location due to its movement coupled with day-night effects? (despite the effort to keep the test cell therm-isolated, the quasi-cyclical fluctuation seems to follow a day-night pattern).

Figure 31 - Field Experiment Hexane Concentration

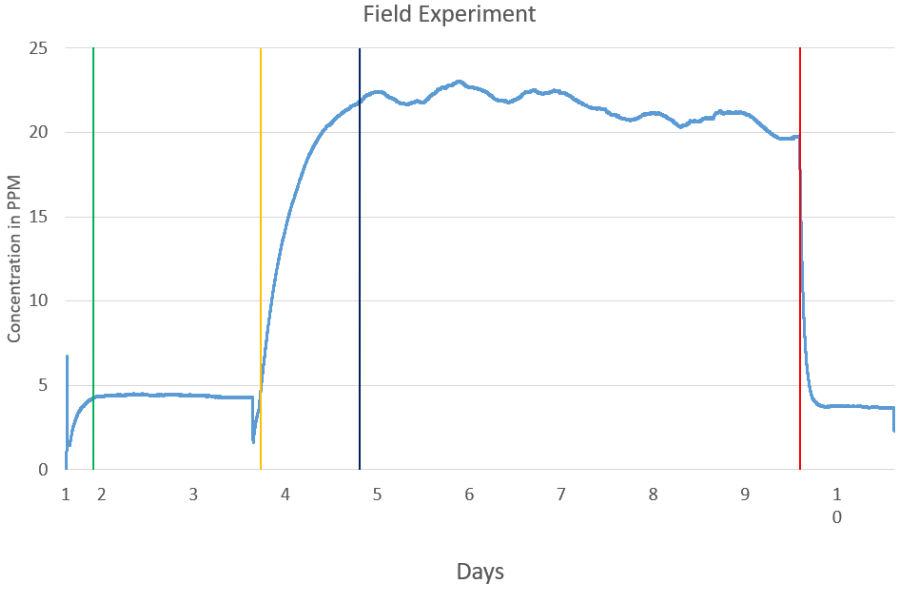

Source: The Author

When comparing the results from this thesis with the results presented in the common exercise by different authors, we can see that all models showed the correct pattern of increase in hexane concentration throughout the days, as the Figure 32 shows. However, only CFD could offer a possible answer for the cyclical fluctuation seen in the field experiment data. The field experiment raw data can be seen in the Appendix H, where the first minutes of the first day of measurement is presented.

Figure 32 - Result from all six hexane/hexanal* concentration models compared with the field experiment

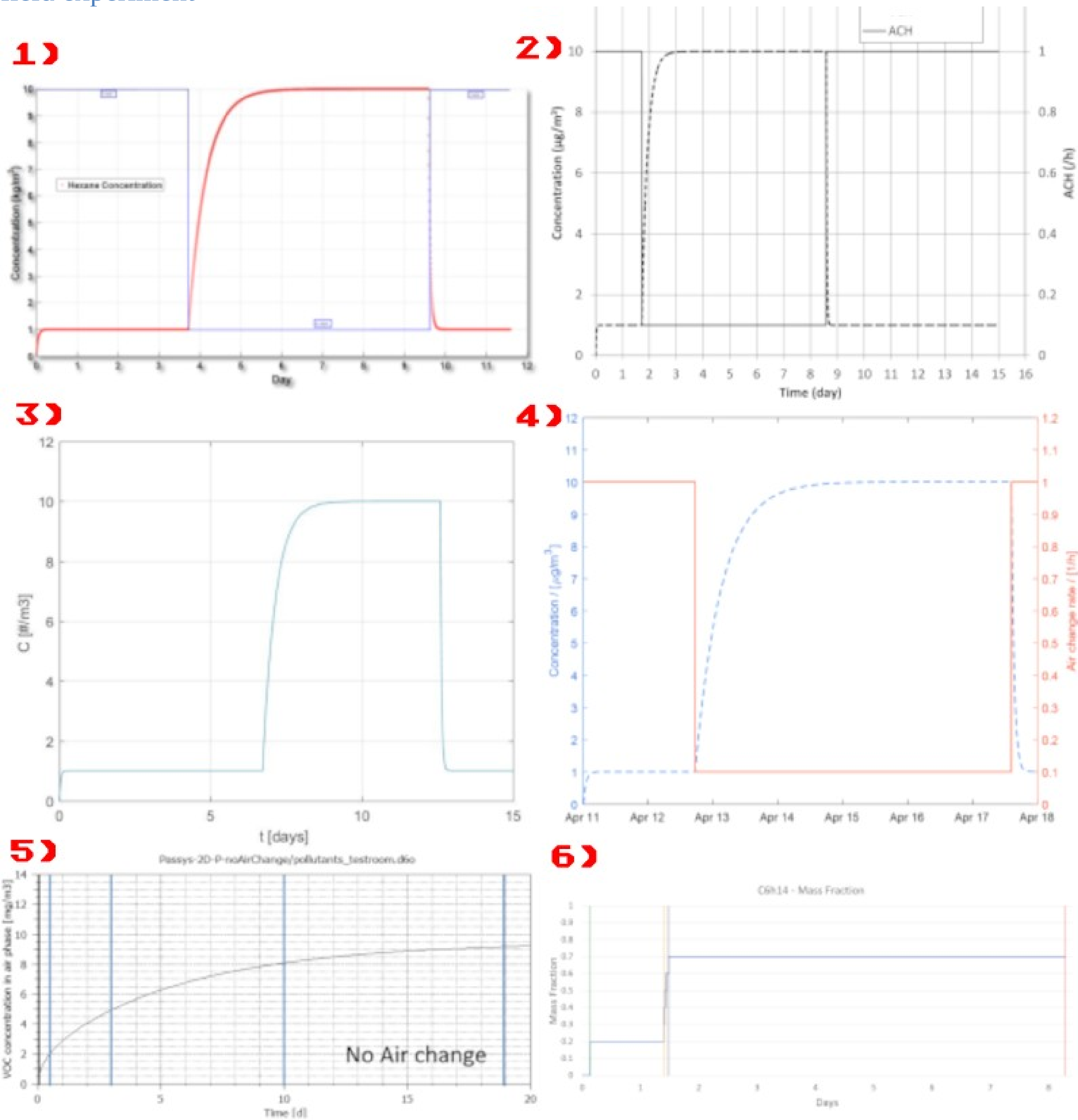

Source: 1) Fitsum Tariku - HAMFitPlus, 2) Marc Abadie - TRNSYS16, 3) Jos van Schijndel - Matlab ODE23S, 4) Toni Calabresi & Gabriel Rojas-Kopeinig - TRNSYS-CONTAM, 5) (Grunewald *et al.*, 2020) - DELHPIN6* and 6) The Author - Fluent.

The time variation shown in Figure 32 follows the same order shown in Table 13, since the table is the description of the graphs. The Table 13 follows the field experiment protocol for high air inflow and low air inflow. The field experiment protocol is described in Table 6.

The Table 14 shows the maximum concentration reached by each different model, and the Figure 34 shows the time each model took to reach the maximum concentration. All of them have the field experiment as the benchmark. For more information about Figure 32 see Appendix C, D, E and F.

Table 13 - Time Comparison of Hexane/Hexanal* Concentration Between Multiple Models

	Startup	High	Low	Max. Concentration	High	Delta Time to Max. Concentration
Field Experiment	0:00:00 [Hours]	9:22:30 [Hours]	26:42:30 [Hours]	90:56:00 [Hours]	167:34:30 [Hours]	64:13:30
	-1.8e-4 [kg/m^3]	4.363e-3 [kg/m^3]	4.17e-3 [kg/m^3]	2.31e-2 [kg/m^3]	1.98e-2 [kg/m^3]	
Matlab HAMFitPlus	0:00:00 [Hours]	3:00:00 [Hours]	90:00:00 [Hours]	134:24:00 [Hours]	229:12:00 [Hours]	44:24:00
	0 [kg/m^3]	1e0 [kg/m^3]	1e0 [kg/m^3]	1e1 [kg/m^3]	1e0 [kg/m^3]	
TRNSYS 16	0:00:00 [Hours]	2:52:48 [Hours]	40:48:00 [Hours]	72:00:00 [Hours]	205:12:00 [Hours]	31:12:00
	0 [kg/m^3]	1e-9 [kg/m^3]	1e-9 [kg/m^3]	1e-8 [kg/m^3]	1e-9 [kg/m^3]	
Matlab ODE23S	0:00:00 [Hours]	3:45:00 [Hours]	152:24:00 [Hours]	211:48:00 [Hours]	300:00:00 [Hours]	59:24:00
	0 [kg/m^3]	1e0 [kg/m^3]	1e0 [kg/m^3]	1e1 [kg/m^3]	1e0 [kg/m^3]	
CONTAM-TRNSYS	0:00:00 [Hours]	3:00:00 [Hours]	42:00:00 [Hours]	85:12:00 [Hours]	157:12:00 [Hours]	43:12:00
	0 [kg/m^3]	1e-9 [kg/m^3]	1e-9 [kg/m^3]	1e-8 [kg/m^3]	1e-9 [kg/m^3]	
FLUENT	0:00:00 [Hours]	3:25:00 [Hours]	33:28:00 [Hours]	35:37:00 [Hours]	198:40:00 [Hours]	2:09:00
	0 [kg/m^3]	4.43e-2 [kg/m^3]	4.43e-2 [kg/m^3]	1.55e-1 [kg/m^3]	1.55e-1 [kg/m^3]	
DELPHIN6*	0:00:00 [Hours]	-	-	456:00:00 [Hours]	-	456:00:00
	0 [kg/m^3]	-	-	9.25e-6 [kg/m^3]	-	

Source: The Author

From all simulations, only DELPHIN6 used Hexanal as pollutant, since the simulation considered a polystyrene board on the floor of the test room, without ventilation. This simulation is still interesting for comparison, since both used a heavy molecule pollutant and the same test cell for the simulation. The difference between molecular weight of hexane and hexanal is small in comparison with the molecular weight of the internal air, since hexane have 86.18 g/mol of molecular weight and hexanal 100.16 g/mol.

Figure 33 - Time to Reach Maximum Hexane/Hexanal* Concentration in Hours

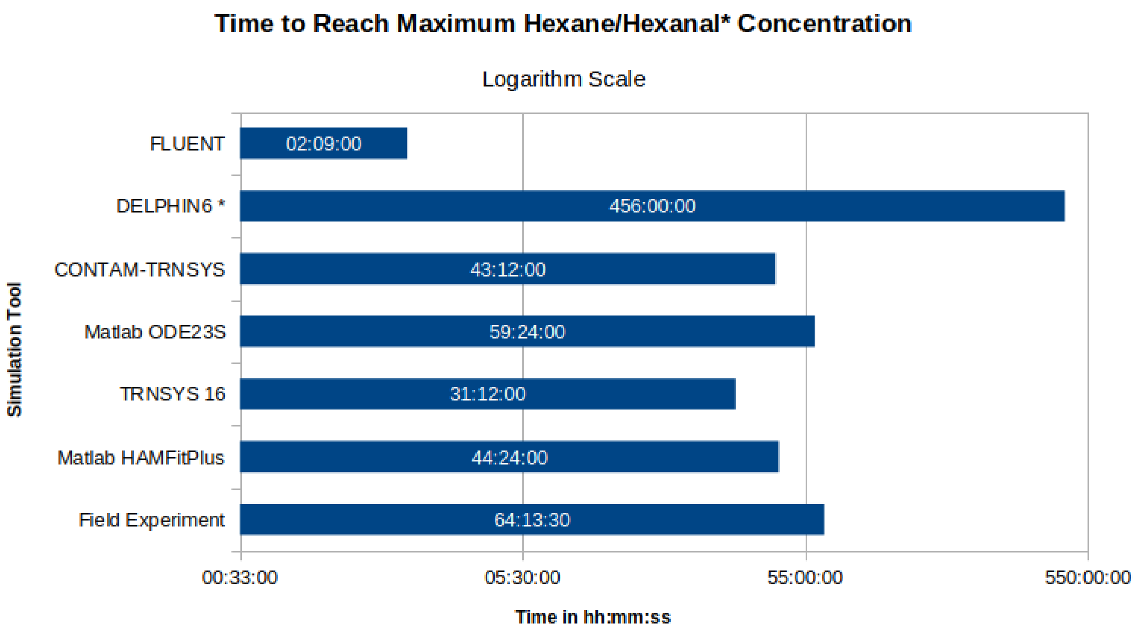

Source: The Author

Table 14 - Maximum Hexane/Hexanal* Concentration of Each Model

Field Experiment	2.31e-2	[kg/m^3]
Matlab HAMFitPlus	1e1	[kg/m^3]
TRNSYS 16	1e-8	[kg/m^3]
Matlab ODE23S	1e1	[kg/m^3]
CONTAM-TRNSYS	1e-8	[kg/m^3]
DELPHIN6*	9.25e-6	[kg/m^3]
FLUENT	1.55e-1	[kg/m^3]

Source: The Author

Figure 34 - Maximum Hexane/Hexanal* Concentration [kg/m^3]

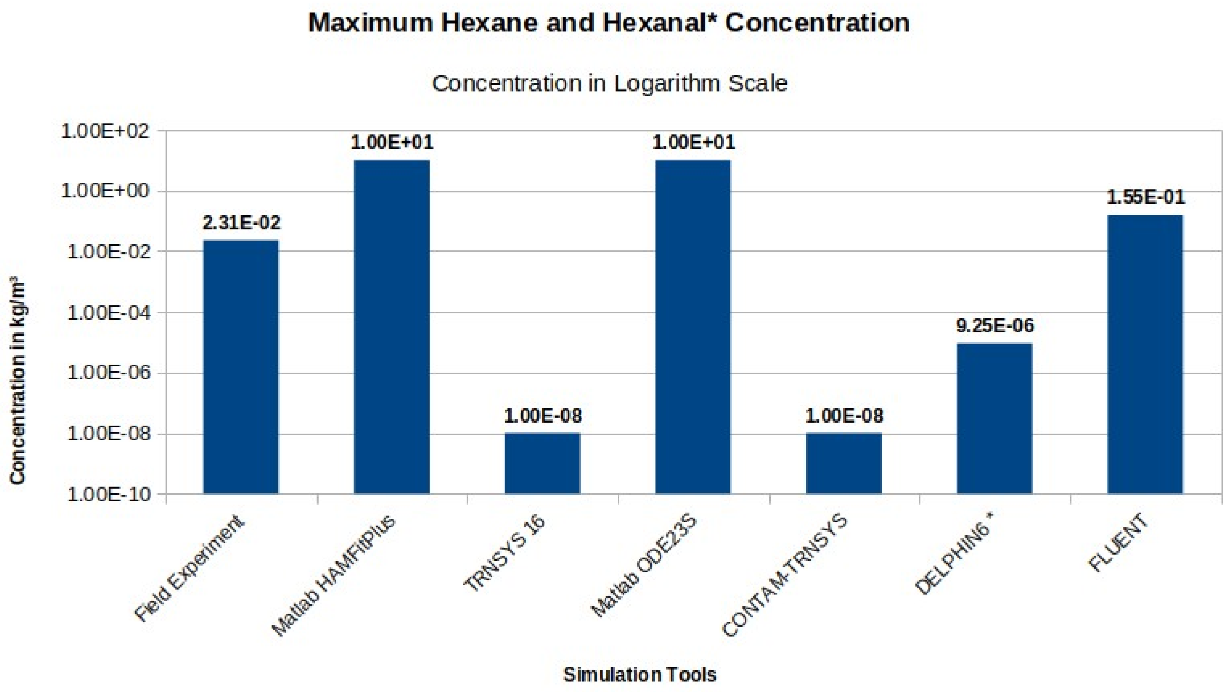

Source: The Author

CHAPTER 5
CONCLUSION

Energy is and will be a key topic for this century due to the increase of world population, despite the birthrate decline in the western hemisphere. Africa and Asia will witness an urbanization process without precedents in human history. This demographic phenomena can trigger geopolitical tensions in regions without energy security and essential trans-boundary natural resources. Since the residential sector is one of the biggest consumers of energy, this means a race against the clock for the construction and building physics fields to provide new construction techniques, energy management and simulation tools to enable energy efficient buildings without compromising the indoor air quality.

Lumped models provides fast and computational cheap solution for long time horizon simulations, however, its simplicity prevents the best description of the complex spacial distribution of pollutant behavior. Computational Fluid Dynamics (CFD) on the other hand, can provide a better description of the pollutant behavior, yet, its computational cost is extremely high compared to the first solution. While lumped models worked for a couple of hours to simulate the field experiment, the computational fluid dynamics simulation took nine months, both for the equivalent of a couple of days in a real world scenario.

From all models presented in this document, the computational fluid dynamics provided the best result for maximum pollutant concentration, while the lumped models were more accurate to describe the time to reach maximum pollutant concentration. In the Figure 35 and Figure 36 it is possible to see that both Matlab ODE23S and CONTAM-TRNSYS provided a fairly approximation regarding the time to reach maximum hexane concentration after the air change rate was adjusted to low in the field experiment. While Fluent underestimate the time to reach maximum hexane concentration, as shown in Figure 37.

Figure 35 - Comparison of Field Experiment and Matlab ODE23S on Time of Maximum Hexane Concentration

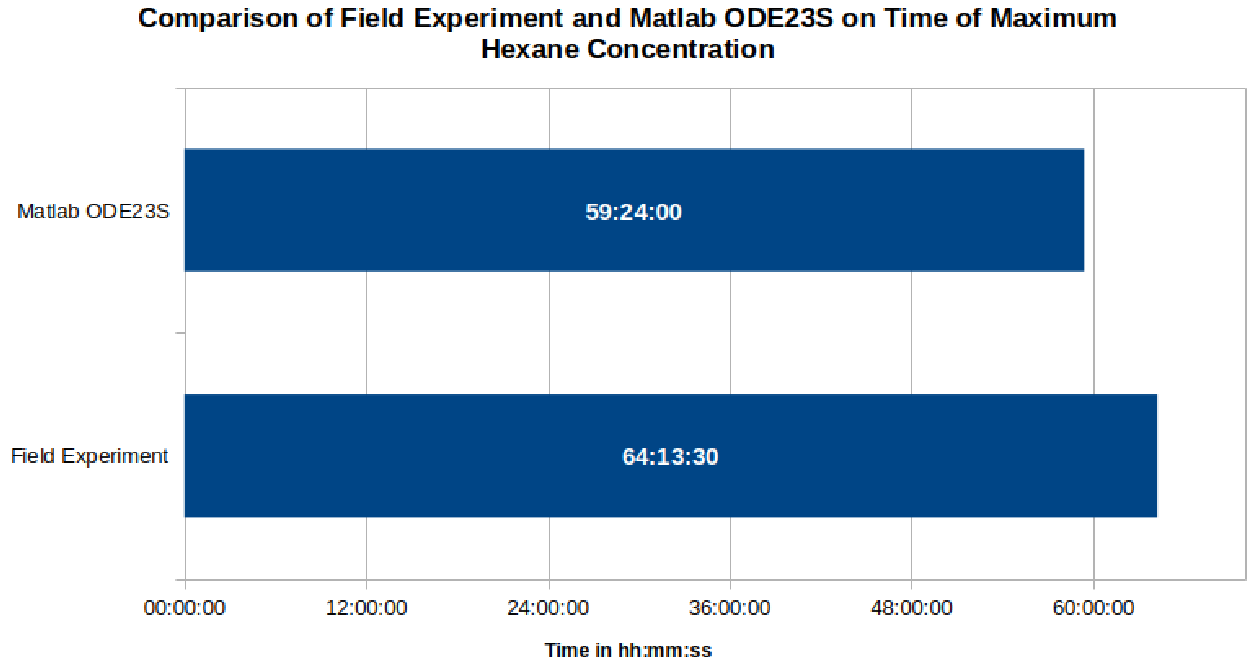

Source: The Author

Figure 36 - Comparison of Field Experiment and CONTAM-TRNSYS on Time of Maximum Hexane Concentration

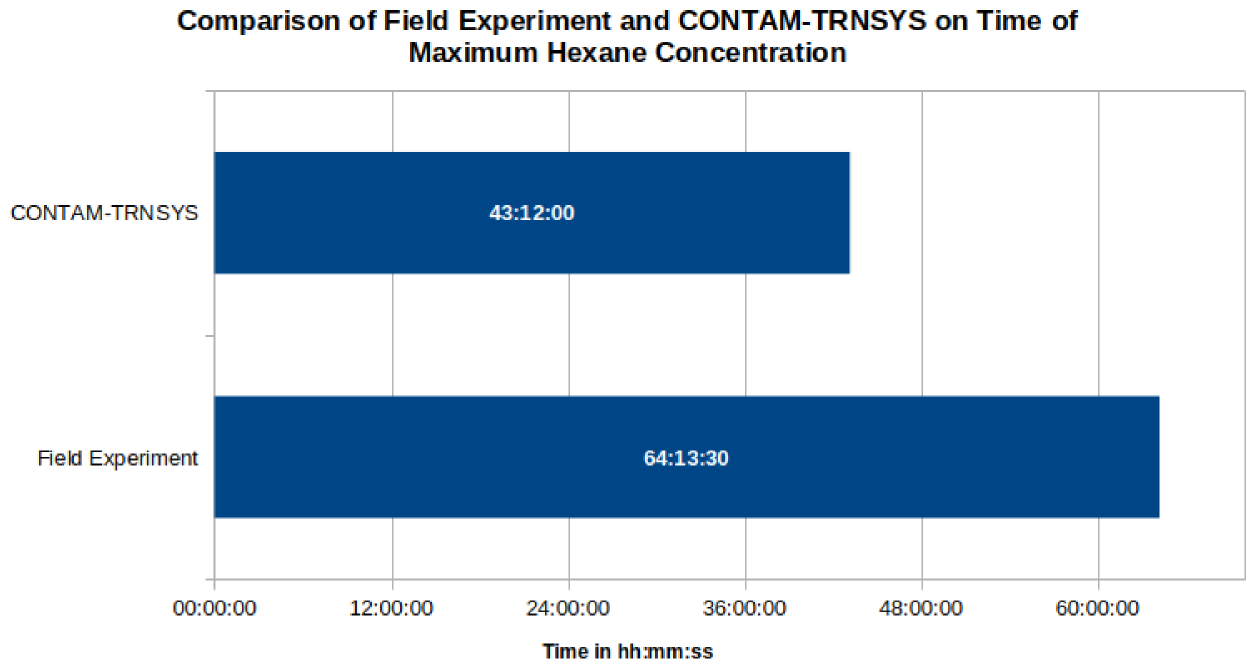

Source: The Author

Figure 37 - Comparison of Field Experiment and Fluent on Time of Maximum Hexane Concentration

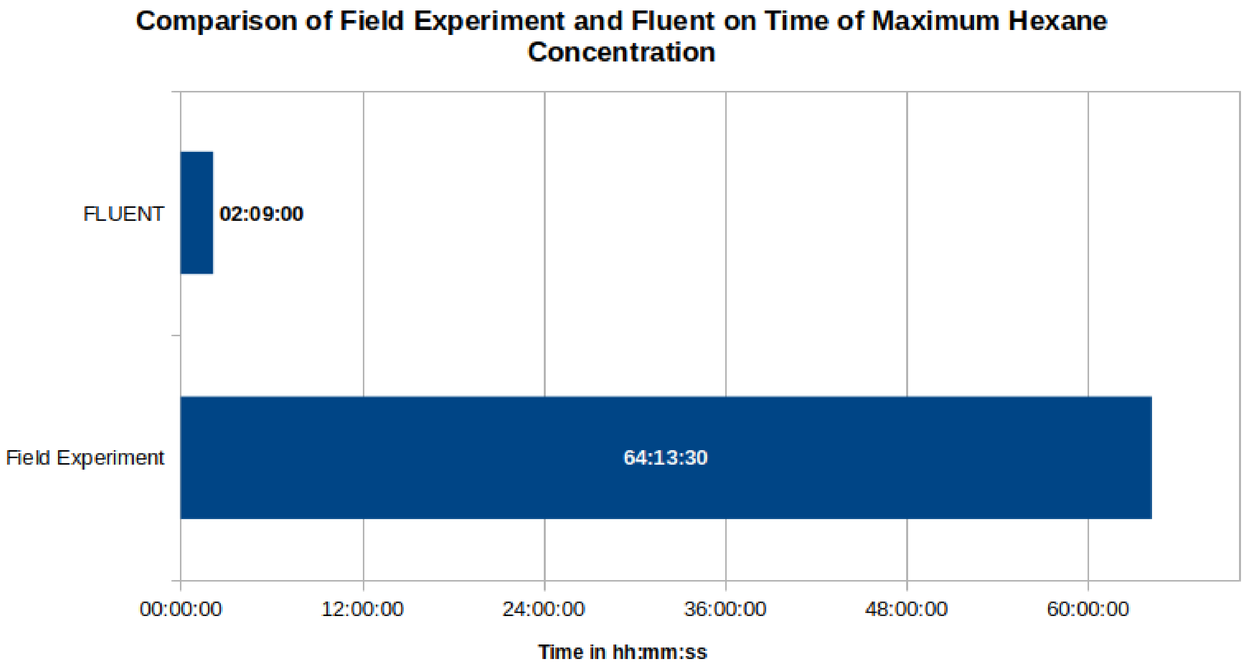

Source: The Author

However, the same lumped models exponentially overestimated and underestimated the maximum hexane concentration in the test cell as shown in Figure 38 and Figure 39 respectively.

Figure 38 - Comparison of Field Experiment and Matlab ODE23S on Maximum Hexane Concentration

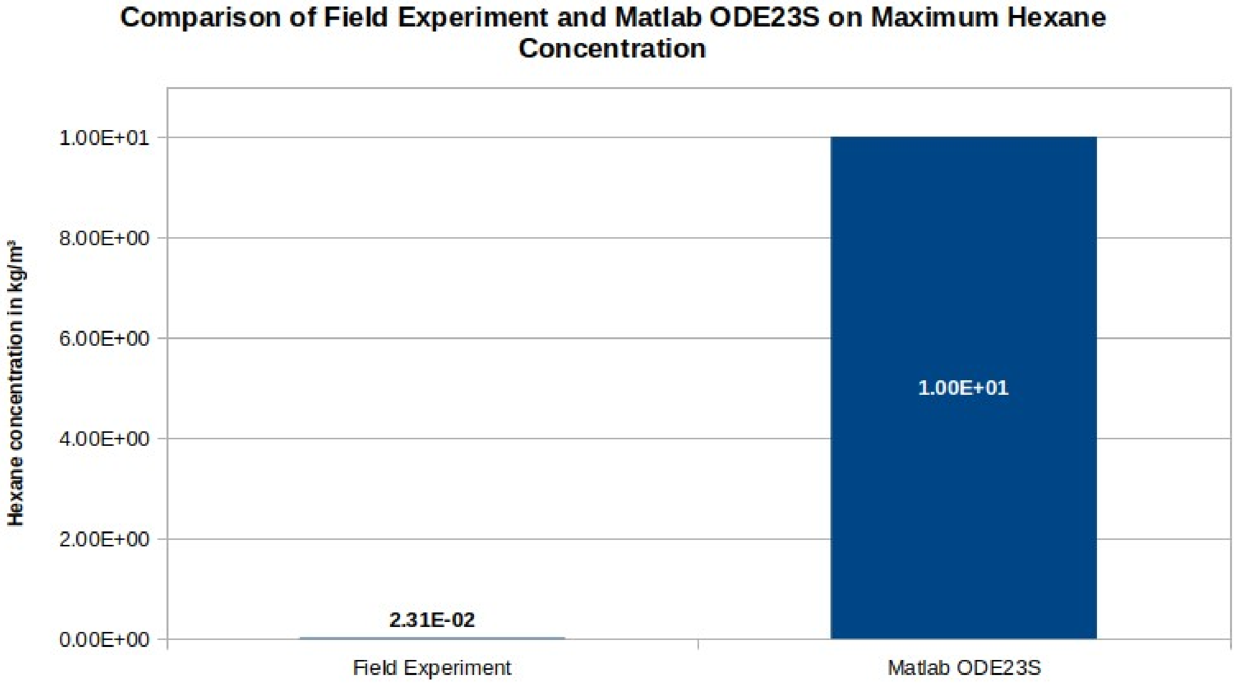

Source: The Author

Figure 39 - Comparison of Field Experiment and CONTAM-TRNSYS on Maximum Hexane Concentration

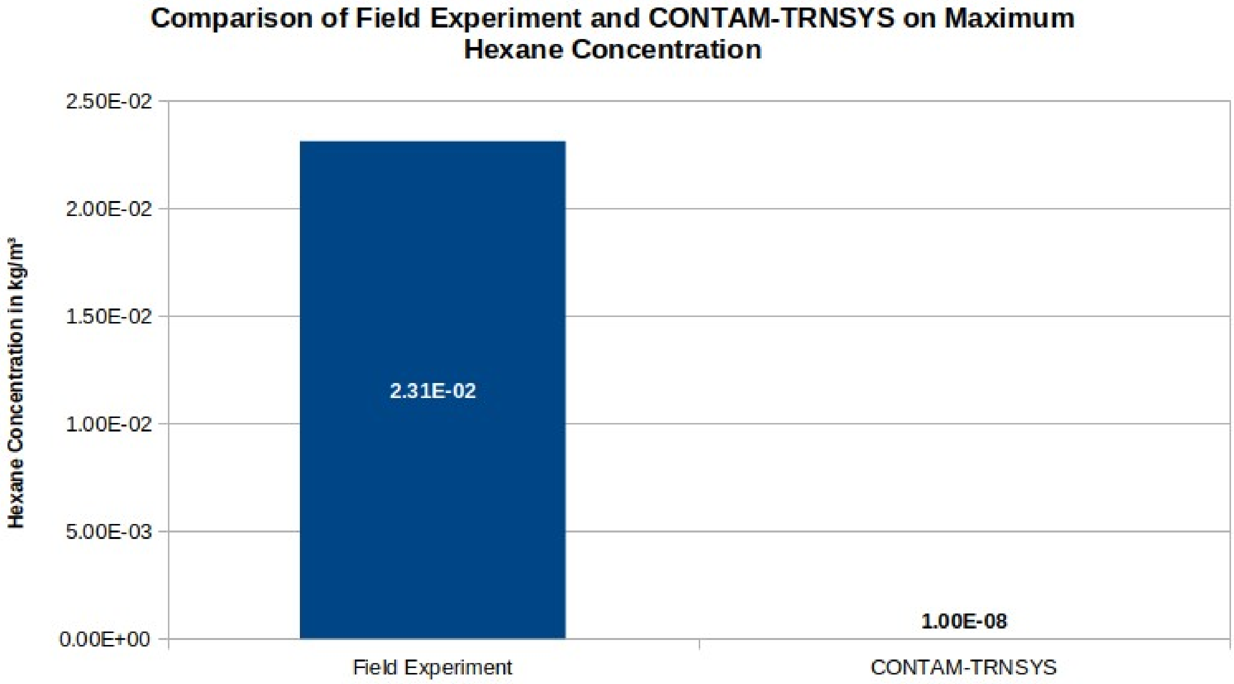

Source: The Author

While the Fluent prediction was also overestimated, it was still under a certain accuracy compared to previous lumped models as shown in Figure 40. Nevertheless, the computation fluid dynamics also gave extra spatial insights regarding the pollutant behavior within the test cell, which is even more important for certain pollutants like Hexane that have a high molecular weight.

Figure 40 - Comparison of Field Experiment and Fluent on Maximum Hexane Concentration

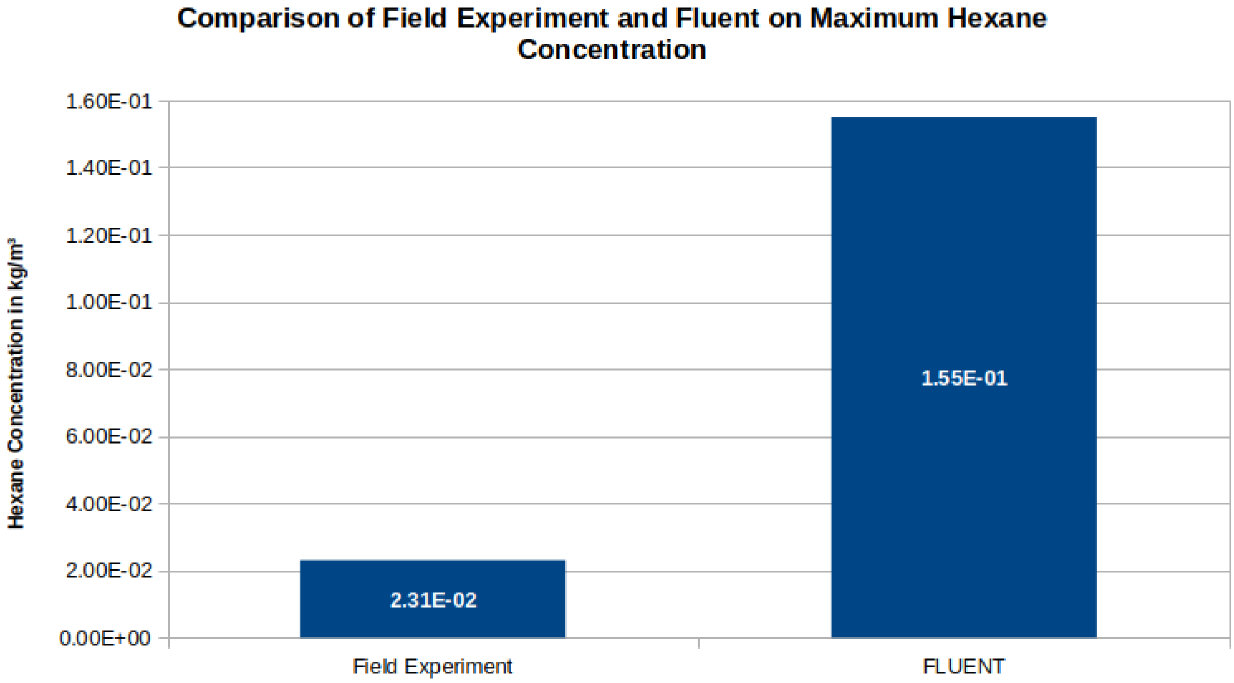

Source: The Author

Heavy molecules can behave differently under certain circumstances, such as low kinetic and thermal energy, which tends to create a stratification phenomena between the pollutant and the transport fluid as shown by (Siddiqui; Jayanti; Swaminathan, 2012). On the other hand, with high kinetic energy, a high difference of molecular weight could also produce stratified vortices of pollutants inside the indoor environment. These behaviors must be well-understood for complex situations and geometries where materials can behave both as source of pollutants or sinks. A spatial analysis of heavy molecules can determine key elements in the design process.

Other complex phenomena such as environments with presence of moisture and porous materials, can bring a high level of physical complexity that makes current computational fluid dynamics solutions impractical with current market available hardware. Thus, in our current stage the field experiment gives the best absolute results due to its possibility of full control and understanding of the variables, even with a high cost embedded. The lumped models are more practical for quick and somewhat reliable results, but lack the spatial representation that the field of study needs if we want to solve our energy challenge and preserve good IAQ. In the end, the computational fluid dynamics is a strong tool, but needs further development and optimization in order to bring the low cost and fast results that the industry needs for increasingly complex indoor environments.

The hardware used to run the computational fluid dynamic model presented in this document was a Windows machine with a CPU Intel i5-3337U quad-core 3.20 GHz with 32 GB of RAM. The total time for the simulation was around nine months for an equivalent of eight days of hexane dispersion. Many parameters were extended to the limit in order to reduce the computational cost and speed up the simulation. Parameters like number of cells, time-step size and finite volume interpolation were scarified in order to make the simulation lighter.

Some paths could further improve the simulation presented in this document, such as different turbulence models, better mesh quality and detail with at least one million cells and reduced time-steps. However, current computational power is reaching its plateau, further work must happen in the optimization of numerical methods and computational architecture. Yet, perhaps a decentralized hive computation could make computational fluid dynamics more accessible for the industry.

A decentralized network of different computers running Linux/BSD headless systems with OpenFOAM installed, could cooperate through overlay networks such as Yggdrasil or GNUnet to connect the topology in a closed network. The Yggdrasil protocol can automatically find and connect to available machines, while a custom program in the main workstation could manage the simulation by dividing groups of cells from a fluid domain and assigning each cell based on its turbulence model to different computers. Sending light computational problems for weaker machines while giving strong workstations the hardest fields of the domain.

Perhaps with such approach, and a hybrid use of lumped and computational fluid dynamics models we can address the computational cost issue by leveraging on the decentralization power of networks.

REFERENCES

AHMAD, T.; PLEE, S. L.; MYERS, J. P. **ANSYS Fluent Theory Guide**. [*S. l.*]: ANSYS, Inc., 2013.

ALEVANTIS, L. Building material emissions study. **California Department of Health Services, Report prepared for the California Integrated Waste Management Board, Publication**, [*s. l.*], p. 433–03, 2003.

AMERICAN SOCIETY OF HEATING, REFRIGERATING AND AIR CONDITIONING ENGINEERS (ASHRAE). **2017 ASHRAE Handbook: Fundamentals**. 1. ed. [*S. l.*]: ASHRAE, 2017.

ANDERSON, J. D. Governing Equations of Fluid Dynamics. *In*: WENDT, J. F. (org.). **Computational Fluid Dynamics: An Introduction**. Berlin, Heidelberg: Springer, 1992. p. 15–51. Disponível em: https://doi.org/10.1007/978-3-662-11350-9_2. Acesso em: 12 abr. 2024.

ANSYS, INC. **ANSYS Meshing User's Guide**. [*S. l.*]: ANSYS, Inc., 2013.

ANSYS, INC. **ANSYS Meshing User's Guide**. [*S. l.*]: ANSYS, Inc., 2017.

AUSTIN, B. S. *et al.* Modeling the indoor environment. **Environmental Science & Technology**, [*s. l.*], v. 26, n. 5, p. 850–858, 1992.

BAKER, N. V. European Passive Solar Test Facility. *In*: COMMISSION OF THE EUROPEAN COMMUNITIES. **First E.C. Conference on Solar Heating**. Dordrecht: Springer Netherlands, 1984. p. 73–77. Disponível em: http://link.springer.com/10.1007/978-94-009-6508-9_14. Acesso em: 6 maio 2025.

BEST PRACTICES IN HVAC SYSTEM MAINTENANCE TO OPTIMIZE EFFICIENCY. *In*: FMLINK. 13 mar. 2016. Disponível em: https://www.fmlink.com/articles/best-practices-in-hvac-system-maintenance-to-optimize-efficiency/. Acesso em: 12 abr. 2024.

BHATTACHARYYA, S. *et al.* Introductory Chapter: A Brief History of and Introduction to Computational Fluid Dynamics. *In*: APPLICATIONS OF COMPUTATIONAL FLUID DYNAMICS SIMULATION AND MODELING. [*S. l.*]: IntechOpen, 2021. Disponível em: https://www.intechopen.com/chapters/76425. Acesso em: 29 nov. 2024.

BLUYSSEN, P. **Evaluation of VOC emissions from building products: solid flooring materials**. [*S. l.*]: Office for Official Publ. of the European Communities, 1997.

BOCANEGRA-YANEZ, M. *et al.* Design and operation of ventilation in low energy residences – A survey on code requirements and building reality from six European countries and China. *In*: VENTILATING HEALTHY LOW-ENERGY BUILDINGS, 2017, Nottingham. **38th AIVC Conference**. Nottingham: [*s. n.*], 2017. p. 831–841.

BOESE, R.; BLAESER, D.; WEISS, H.-C. CCDC 103189: Experimental Crystal Structure Determination. Cambridge Crystallographic Data Centre, , 1999. Disponível em: http://www.ccdc.cam.ac.uk/services/structure_request?id=doi:10.5517/cc3gcpl&sid=DataCite. Acesso em: 16 nov. 2024.CIF

BOX, G. E. P.; DRAPER, N. R. **Empirical model-building and response surfaces.** Oxford, England: John Wiley & Sons, 1987. (Empirical model-building and response surfaces.). p. xiv, 669

BURMAN, E. *et al.* Design and operational strategies for good Indoor Air Quality in low-energy dwellings: performance evaluation of two apartment blocks in East London, UK. *In*: 7TH INTERNATIONAL BUILDING PHYSICS CONFERENCE, 2018, Syracuse. **Healthy, Intelligent and Resilient Buildings and Urban Environments**. Syracuse: International Association of Building Physics (IABP), 2018. p. 847–852. Disponível em: https://surface.syr.edu/ibpc/2018/IE4/2. Acesso em: 31 mar. 2024.

BURMAN, E.; STAMP, S. Trade-offs between ventilation rates and formaldehyde concentrations in new-build dwellings in the UK. *In*: 40TH AIVC CONFERENCE, 2019, Ghent. **AIVC**. Ghent: [*s. n.*], 2019. p. 11.

CHEN, Q. COMPARISON OF DIFFERENT *k* -ε MODELS FOR INDOOR AIR FLOW COMPUTATIONS. **Numerical Heat Transfer, Part B: Fundamentals**, [*s. l.*], v. 28, n. 3, p. 353–369, 1995.

CHEN, Q. Prediction of room air motion by Reynolds-stress models. **Building and environment**, [*s. l.*], v. 31, n. 3, p. 233–244, 1996.

CHEN, Q.; SREBRIC, J. Application of CFD tools for indoor and outdoor environment design. **International Journal on Architectural Science**, [*s. l.*], v. 1, n. 1, p. 14–29, 2000.

DE TOXICOVIGILANCE, C. D. C. ETUDE EXPLORATOIRE: CARACTERISATION DES EMISSIONS DE FOURNITURES SCOLAIRES ET DE PRODUITS D'ENTRETIEN UTILISÉS DANS UNE ECOLE ET ANALYSE DES DONNEES DE COMPOSITION. [*s. l.*], 2014. Disponível em: https://www.researchgate.net/profile/Melanie-Nicolas/publication/278630274_Etude_exploratoire_caracterisation_des_emissions_de_fournitures_scolaires_et_de_produits_d'entretien_utilises_dans_une_ecole_et_analyse_des_donnees_de_composition/links/561e365b08aef097132b340a/Etude-exploratoire-caracterisation-des-emissions-de-fournitures-scolaires-et-de-produits-dentretien-utilises-dans-une-ecole-et-analyse-des-donnees-de-composition.pdf. Acesso em: 16 nov. 2024.

DESJARDINS, J. **Animation: World's Largest Megacities by 2100**. [*S. l.*], 2018. Disponível em: https://www.visualcapitalist.com/worlds-20-largest-megacities-2100/. Acesso em: 12 abr. 2024.

DIMENSIONLESS WALL DISTANCE (Y PLUS) -- CFD-WIKI, THE FREE CFD REFERENCE. [*S. l.*], 2024. Disponível em: https://www.cfd-online.com/Wiki/Dimensionless_wall_distance_(y_plus). Acesso em: 2 dez. 2024.

DON'T PANIC - THE FACTS ABOUT POPULATION. Apresentado por Dan Hillman. London: BBC, 2013. Documentary (58:50).

DOYUN, W. O. N.; SHAW, C. Y. Investigation of building materials as VOC sources in indoor air. [*s. l.*], 2004. Disponível em: https://citeseerx.ist.psu.edu/document?repid=rep1&type=pdf&doi=f9d8f31ded9b1f41cf295c8d6279e4ef4e88dc0a. Acesso em: 16 nov. 2024.

EIA PROJECTS NEARLY 50% INCREASE IN WORLD ENERGY USAGE BY 2050, LED BY GROWTH IN ASIA - U.S. ENERGY INFORMATION ADMINISTRATION (EIA). [*S. l.*], 2024. Disponível em: https://www.eia.gov/todayinenergy/detail.php?id=41433. Acesso em: 12 abr. 2024.

EUROPEAN COMMISSION. **The PASSYS Test Cells: A COMMON EUROPEAN OUTDOOR TEST FACILITY FOR THERMAL AND SOLAR BUILDING RESEARCH**. 1. ed. Brussels: European Commission, 1990. v. 1

FERNÁNDEZ-MIGUEL, A. *et al.* Disruption in Resource-Intensive Supply Chains: Reshoring and Nearshoring as Strategies to Enable Them to Become More Resilient and Sustainable. **Sustainability**, [*s. l.*], v. 14, n. 17, p. 13, 2022.

GRUNEWALD, J. *et al.* **Subtask 3: Modelling of Energy Efficiency and IAQ - Review, Gap analysis and Categorization**. [*S. l.: s. n.*], 2020.

GRUNEWALD, J. *et al.* Using the PASSYS cell for model-to-model comparison of hygrothermal building envelope simulation tools. *In*: 7TH INTERNATIONAL BUILDING PHYSICS CONFERENCE, IBPC 2018, 2018, Syracuse. **7th International Building Physics Conference**. Syracuse: [*s. n.*], 2018. p. 6.

GUO, Z. S. Fundamental mass transfer models applied to evaluating the emissions of vapour-phase organic from interior architectural coatings. *In*: , 1992. **EPA/AWMA Symposium**. [*S. l.: s. n.*], 1992. Disponível em: https://cir.nii.ac.jp/crid/1571980074127376896. Acesso em: 30 nov. 2024.

HAGHIGHAT, F.; JIANG, Z.; ZHANG, Y. The Impact of Ventilation Rate and Partition Layout on the VOC Emission Rate: Time-Dependent Contaminant Removal. **Indoor Air**, [*s. l.*], v. 4, n. 4, p. 276–283, 1994.

HEFNY, M. M.; OOKA, R. CFD analysis of pollutant dispersion around buildings: Effect of cell geometry. **Building and Environment**, [*s. l.*], v. 44, n. 8, p. 1699–1706, 2009.

HUNT, J. C. R. Mathematical Models of Turbulence. By B. E. LAUNDER and D. B. SPALDING. Academic Press, 1972. 169 pp. £2.50 or $7.50. **Journal of Fluid Mechanics**, [*s. l.*], v. 57, n. 4, p. 826–828, 1973.

INCROPERA, F. P. **Fundamentals of Heat and Mass Transfer**. [*S. l.*]: Wiley, 2007.

JIANG, T. **CFD Modelling and Simulation of a Centrifugal Fan**. 2021. 57 f. Dissertação (Mestrado Acadêmico) - Czech Technical University in Prague, Prague, 2021.

KHALIL, E. E. CFD history and applications. [*s. l.*], 2021. Disponível em: https://www.akademiabaru.com/index.php/archives/article/view/278. Acesso em: 21 nov. 2024.

KILKIS, S. A new metric for net-zero carbon buildings. *In*: , 2007. **Energy Sustainability**. [*S. l.: s. n.*], 2007. p. 219–224. Disponível em: https://asmedigitalcollection.asme.org/ES/proceedings-abstract/ES2007/219/329276. Acesso em: 6 maio 2025.

KIM, J.; LEONARD, A. The Early Days and Rise of Turbulence Simulation. **Annual Review of Fluid Mechanics**, [*s. l.*], v. 56, n. Volume 56, 2024, p. 21–44, 2024.

KONDO, A. Y. Y.; FUJIMURA, E. J. Distribution of Chemical Pollutants in a Room Based on CFD Simulation Coupled with Emission/Sorption Analysis. [*s. l.*], 2024. Disponível em: http://www.arch.t-kougei.ac.jp/ito/pdf/pr3_2001.pdf. Acesso em: 19 nov. 2024.

KOZICKI, M.; GUZIK, K. Comparison of VOC emissions produced by different types of adhesives based on test chambers. **Materials**, [*s. l.*], v. 14, n. 8, p. 1924, 2021.

LAVERGE, J. **SUBTASK 5 – COMMON EXCERCISE 1**. Ghent: Ghent University, 2017. Technical Report.

LIANG, W. *et al.* A Pre-assessment and Control Tool for Indoor Air Quality (PACT-IAQ) Simulation in Actual Buildings. **Procedia Engineering**, [*s. l.*], v. 205, n. 1, p. 219–225, 2017.

LIANG, W.; QIN, M. A simulation study of ventilation and indoor gaseous pollutant transport under different window/door opening behaviors. **Building Simulation**, [*s. l.*], v. 10, n. 3, p. 395–405, 2017.

LIU, Z. *et al.* Development of a procedure for estimating the parameters of mechanistic VOC emission source models from chamber testing data. **Building Simulation**, [*s. l.*], v. 14, n. 2, p. 269–282, 2021.

LOGUE, J. M. *et al.* A Method to Estimate the Chronic Health Impact of Air Pollutants in U.S. Residences. **Environmental Health Perspectives**, [*s. l.*], v. 120, n. 2, p. 216–222, 2012.

MARIE-LISE, R.; FCBA, I. T.; BATIMENT, C. S. E. T. D. **Contribution de mobilier à la qualité de l'air Intérieur dans les crèches. MOBAIR-C. Juin 2013.** [*S. l.*]: FCBA. Paris, 2013. Disponível em: https://side.developpement-durable.gouv.fr/PACA/doc/SYRACUSE/341157/contribution-de-mobilier-a-la-qualite-de-l-air-interieur-dans-les-creches-mobair-c-juin-2013. Acesso em: 16 nov. 2024.

MURAKAMI, S. Overview of turbulence models applied in CWE–1997. **Journal of Wind Engineering and Industrial Aerodynamics**, [*s. l.*], v. 74, p. 1–24, 1998.

MURAKAMI, S.; KATO, S.; ITO, K. Coupled analysis of TVOC emission and diffusion in a ventilated room by CFD. [*s. l.*], 1998. Disponível em: https://www.aivc.org/resource/coupled-analysis-tvoc-emission-and-diffusion-ventilated-room-cfd. Acesso em: 19 nov. 2024.

N-HEXANE | CAMEO CHEMICALS | NOAA. [*S. l.*], 2024. Disponível em: https://cameochemicals.noaa.gov/chemical/851. Acesso em: 16 nov. 2024.

N-HEXANE | TOXICOLOGICAL PROFILE | ATSDR. [*S. l.*], 2024. Disponível em: https://wwwn.cdc.gov/TSP/ToxProfiles/ToxProfiles.aspx?id=393&tid=68. Acesso em: 16 nov. 2024.

NIELSEN, P. V. Prediction of air distribution in a ventilated room. **The Building Services Engineer**, [*s. l.*], v. 41, p. 219–222, 1974.

OFFERMANN, F. J. Ventilation and indoor air quality in new homes. **PIER Collaborative Report**, [*s. l.*], 2009.

OLIVEIRA FERNANDES, E. Materials for healthy indoor spaces and more energy efficient buildings. Final report of EEC project MATHIS, Non-Nuclear Energy Programme JOULE III. **Contract JOR3-CT97-0194, Porto (P), IDMEC, Instituto de Engenharia Mecânica**, [*s. l.*], 2001.

PANDORA. [*S. l.*], 2024. Disponível em: https://db-pandora.univ-lr.fr/. Acesso em: 16 nov. 2024.

PARTICIPANTS - INDOOR AIR QUALITY DESIGN AND CONTROL IN LOW ENERGY RESIDENTIAL BUILDINGS (IEA-EBC ANNEX 68). [*S. l.*], [*s. d.*]. Disponível em: https://www.iea-ebc-annex68.org/about-annex-68/participants. Acesso em: 6 maio 2025.

RAO, A. **Ambit of Multiphase CFD in Modelling Transport Processes Related to Oil Spill Scenario and Microfluidics**. [*S. l.*]: Louisiana State University and Agricultural & Mechanical College, 2015. Disponível em: https://search.proquest.com/openview/2ec4ff6a77b023f1c92570b10a7a2889/1?pq-origsite=gscholar&cbl=18750&diss=y. Acesso em: 6 maio 2025.

RODE, C. *et al.* An International Project on Indoor Air Quality Design and Control in Low Energy Residential Buildings. *In*: ASHRAE IAQ 2016 CONFERENCE, 2016a, Alexandria. **Defining Indoor Air Quality: Policy, Standards and Best Practices**. Alexandria: ASHRAE and AIVC IAQ 2016, 2016. p. 167–174.

RODE, C. IEA EBC Annex 68 – Indoor Air Quality Design and Control in Low Energy Residential Buildings. *In*: AIVC CONFERENCE, 2015, Athens. **AIVC**. Athens: [*s. n.*], 2015. p. 2.

RODE, C. *et al.* IEA Project on Indoor Air Quality Design and Control in Low Energy Residential Buildings. *In*: ASHRAE IAQ 2016, 2016b. **ASHRAE IAQ**. [*S. l.: s. n.*], 2016. p. 10.

RODE, C. **Indoor Air Quality Design and Control in Low Energy Residential Buildings**. [*S. l.*]: International Energy Agency, 2017.

ROJAS, G. Ambient air filter efficiency in airtight, highly energy efficient dwellings – A simulation study to evaluate benefits and associated energy costs. *In*: 6TH VENTICOOL CONFERENCE, 2019, Ghent. **From energy crisis to sustainable indoor climate - 40 years of AIVC**. Ghent: AIVC, 2019. p. 920–931.

ROTTA, J. Statistische Theorie nichthomogener Turbulenz. **Zeitschrift f�r Physik**, [*s. l.*], v. 129, n. 6, p. 547–572, 1951.

SIDDIQUI, M.; JAYANTI, S.; SWAMINATHAN, T. CFD analysis of dense gas dispersion in indoor environment for risk assessment and risk mitigation. **Journal of hazardous materials**, [*s. l.*], v. 209, p. 177–185, 2012.

SPARKS, L. E. **Exposure Version 2: A computer model for analyzing the effects of indoor-air pollutant sources on individual exposure. Documentation. Final report**. [*S. l.*]: Environmental Protection Agency, Research Triangle Park, NC (United States …, 1991. Disponível em: https://www.osti.gov/biblio/5165656. Acesso em: 2 dez. 2024.

SPARKS, L. E. *et al.* Volatile Organic Compound Emissions from Latex Paint - Part 1. Chamber Experiments and Source Model Development. **Indoor Air**, [*s. l.*], v. 9, n. 1, p. 10–17, 1999.

SUBTASKS - INDOOR AIR QUALITY DESIGN AND CONTROL IN LOW ENERGY RESIDENTIAL BUILDINGS (IEA-EBC ANNEX 68). [*S. l.*], [*s. d.*]. Disponível em: https://www.iea-ebc-annex68.org/subtasks. Acesso em: 6 maio 2025.

TAHERI, M. *et al.* A performance assessment of an office space with displacement, personal, and natural ventilation systems. **Building Simulation**, [*s. l.*], v. 9, n. 1, p. 89–100, 2016.

THE DEATH OF MOORE'S LAW: WHAT IT MEANS AND WHAT MIGHT FILL THE GAP GOING FORWARD | CSAIL ALLIANCES. [*S. l.*], 2024. Disponível em: https://cap.csail.mit.edu/death-moores-law-what-it-means-and-what-might-fill-gap-going-forward. Acesso em: 2 dez. 2024.

ÜRGE-VORSATZ, D. *et al.* Heating and cooling energy trends and drivers in buildings. **Renewable and Sustainable Energy Reviews**, [*s. l.*], v. 41, p. 85–98, 2015.

U.S. DEPARTMENT OF HEALTH AND HUMAN SERVICES; U.S. DEPARTMENT OF HOUSING AND URBAN DEVELOPMENT. **Healthy Housing Reference Manual**. [*S. l.*]: U.S. Department of Health and Human Services, U.S. Department of Housing and Urban Development, 2012.

U.S. ENERGY INFORMATION ADMINISTRATION OFFICE OF ENERGY ANALYSIS. **International Energy Outlook 2019**. [*S. l.*]: U.S. Department of Energy Washington, 2019.

WELAHETTIGE, P.; VAAGSAETHER, K. Comparison of OpenFOAM and ANSYS Fluent. *In*: PROCEEDINGS OF THE 9TH EUROSIM CONGRESS ON MODELLING AND SIMULATION, EUROSIM 2016, THE 57TH SIMS CONFERENCE ON SIMULATION AND MODELLING SIMS 2016, 2018. **Anais [...]**. [*S. l.: s. n.*], 2018. p. 1005–1012. Disponível em: https://ep.liu.se/en/conference-article.aspx?series=ecp&issue=142&Article_No=148. Acesso em: 13 abr. 2024.

WORLD POPULATION PROSPECTS 2024: SUMMARY OF RESULTS | DESA PUBLICATIONS. [*S. l.*], 2024. Disponível em: https://desapublications.un.org/publications/world-population-prospects-2024-summary-results. Acesso em: 14 nov. 2024.

YANG, X. *et al.* Numerical simulation of VOC emissions from dry materials. **Building and Environment**, [*s. l.*], v. 36, n. 10, p. 1099–1107, 2001.

YANG, X.; CHEN, Q. A coupled airflow and source/sink model for simulating indoor VOC exposures. **Indoor Air**, [*s. l.*], v. 11, n. 4, p. 257–269, 2001.

ZHANG, Y.; HOPKE, P. K.; MANDIN, C. History and Perspective on Indoor Air Quality Research. *In*: ZHANG, Y.; HOPKE, P. K.; MANDIN, C. (org.). **Handbook of Indoor Air Quality**. Singapore: Springer Nature, 2022. p. 3–33. Disponível em: https://doi.org/10.1007/978-981-16-7680-2_1. Acesso em: 21 nov. 2024.

ZHENG, H. *et al.* Species profile of volatile organic compounds emission and health risk assessment from typical indoor events in daycare centers. **Science of the Total Environment**, [*s. l.*], v. 918, p. 170734, 2024.

ZUKOWSKA, D. *et al.* Ventilation in low energy residences – a survey on code requirements, implementation barriers and operational challenges from seven European countries. **International Journal of Ventilation**, [*s. l.*], v. 20, n. 2, p. 83–102, 2021.

APPENDIX A – FIELD EXPERIMENT REPORT

FACULTEIT INGENIEURSWETENSCHAPPEN
EN ARCHITECTUUR

Annex 68

Subtask 5 – Common excercise 1

This report describes the first common exercise in the 3 exercise series developed in Subtask 5 of annex 68

School of engineering and Architecture
Vakgroep Department of Architecture and Urban Planning

E Jelle.laverge@ugent.be
T +32 9 264 37 49

Campus UFO, Technicum B4

www.architectuur.ugent.be/en/research/building-physics-construction-and-climate-control/

UNIVERSITEIT
GENT

DATE
20-04-2017

Table of content

Context

This report describes the experiment that is the subject of the first common exercise in subtask 5 of annex 68. It is the first in a series that is conceived as a set of 3 consecutive modeling exercises with increasing complexity. The goal is to validate the collective ability of the annex participants to model and reliably predict the indoor air quality in a real building, from a very simple to a more complex and realistic situation.

The tiered experiments are

- A simple 1 room outdoor testbox with an isothermal diffusion source of 1 pollutant
- A 2 room studio with a number of selected materials as sources and varying T and RH as well as solar radiation
- An occupied single family dwelling

The subsequent sections describe the first experiment. The test cell is discussed first, followed by a descriptions of the experiment and the modeling assignment. Annex participants that have a similar test cell available are also invited to perform repeated tests or perform variations on the experiment that address specific annex related issues.

Test setup

The test is executed in a PASSYS cell, situated at the Limelette test site of the BBRI.
The cell is freestanding, oriented more or less along the north/south axis (slightly rotated to the west).

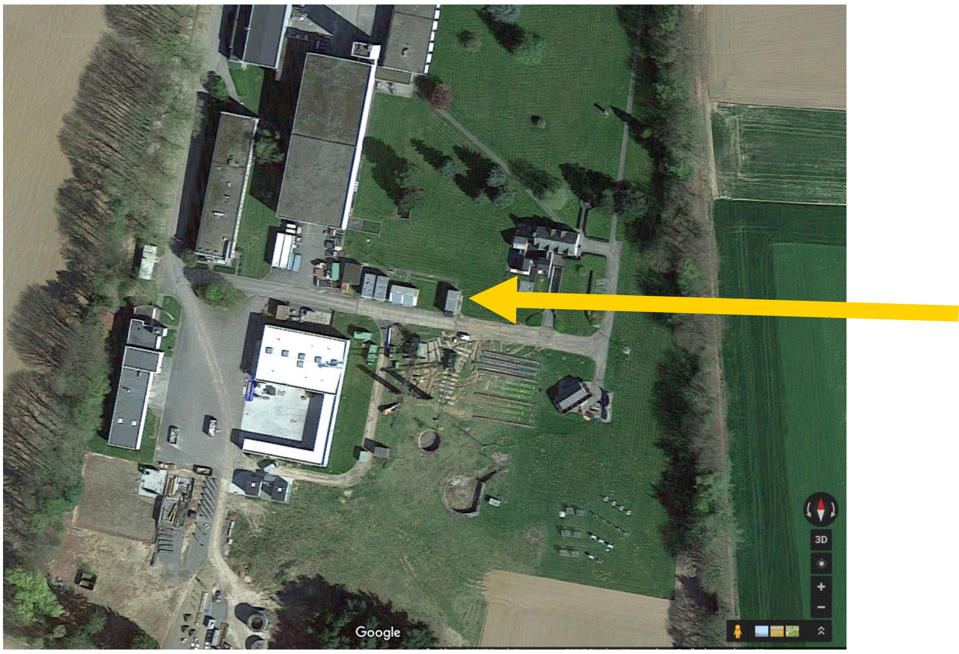

A description of the envelope and dimensions of the cell is attached in the file 'EUNA12882ENC_001.pdf'. The test cell used in this experiment is the last test cell in the original test setup described in the document that has been mounted on a mechanism that allows it to be rotated. During the test, it was in the original orientation (service room pointing north).

12 cm of additional EPS insulation and 1 mm of stainless steel cladding have been added to the interior walls, reducing the internal space to 2.46*2.46*4.86 m.
The interior walls have all been painted with an unknown acrylic paint in the early 2000's.
The cell is fitted with a 'calibration' test wall, that has exactly the same composition as the other walls and no windows.

Experiment description

A concreteplex panel has been fitted in the door between the test room and the service room. Flexible PU foam (2 mm) and clips make sure the panel fitting is airtight.

A 80 mm circular opening with a axial supply fan have been installed at 15 cm above the floor, a 150 mm flexible exhaust duct was installed at 15 cm from the top of the door panel. The exhaust duct exits the service room through a service opening at the front of the test cell, at ceiling height.

During the experiment, the small window in the front of the test cell (to the service room) is opened for fresh air supply. The test room is pressurized by the supply fan. The airtightness of the test room is 1.7 ACH50.

A mixing fan (http://www.bestron.com/en/dft27w.html?___from_store=en) is placed in the south-east corner of the test room, a concrete block with a height of 50 cm is sitting at 1,20 m from the south wall, on which the pollutant source, a glass bottle with freely diffusing Hexane, is placed.

The test room is heated to 27.5 °C by a single electric convector (http://www.produktinfo.conrad.com/datenblaetter/550000-574999/560075-an-01-ml-Konvektor_de_en_fr_nl.pdf) situated at 0.5 m from the south wall. The convector is controlled by a thermostat with external temperature probe and with a 0.1°C dead band. The external probe is positioned at the exact midpoint of the room (1.25 m height, at 1.25m from the side walls and 2.35m from the south wall.

Temperatures are measured at 4 heights at 2 locations in the test room: 1 at the mid-point (where the thermostat probe is), and one at 40 cm from the south west corner. They are measured at 60 cm intervals starting at 35 cm from the ceiling using Onset HOBO U12-012 loggers (http://www.onsetcomp.com/products/data-loggers/u12-012).

The Hexane concentration in measured at the mid-point (where the thermostat probe is), with a Rosemount NGA2000 FID.

The test protocol is as follows:

phase	time	Supply Ventilation rate	Source condition
1. Startup	Until steady state	1 ACH	open
2. High	Day 1 00:00:00 (11/04)	1 ACH	open
3. Low	Day 2 17:20:00	0.1 ACH	open
4. High	Day 8 14:12:00	1 ACH	open

Modeling exercise

The modeling exercise is very simple: model the concentration of Hexane in test cell during the experiment, using your own preferred modeling approach and tools.

Submit your modeling results to the ‘Subtask 5’ folder of the sharepoint.

Annexes

1. Test Cell description: EUNA1288ENC_001.pdf
2. FID technical sheet: FID.pdf
3. Weather data

APPENDIX B – BLADE GEOMETRY AND MESH

Figure 41 - Detail CAD of Fan Blade

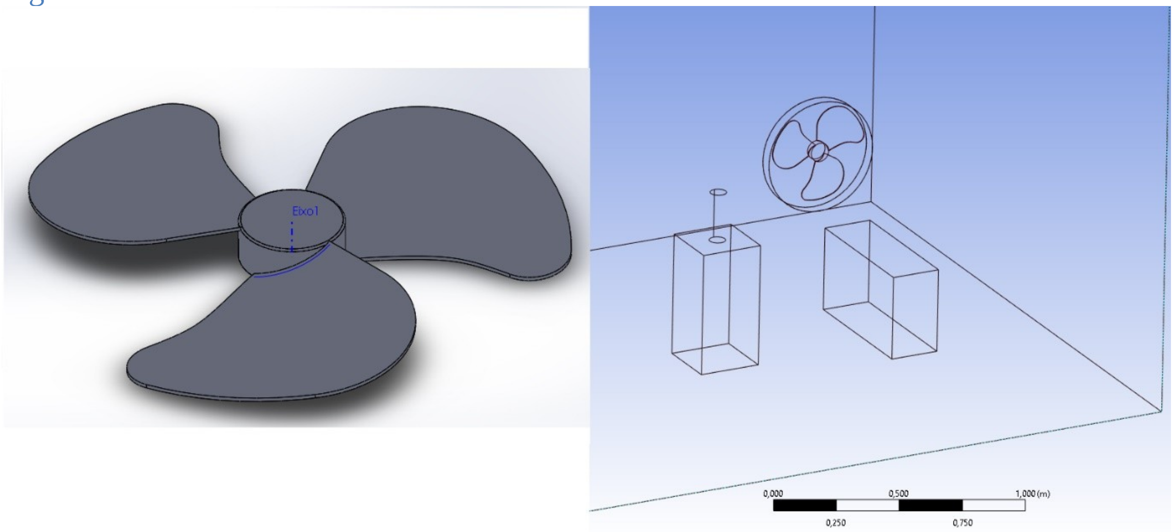

Source: From the Author

Figure 42 - High Density Mesh of Fan and Blade Geometry

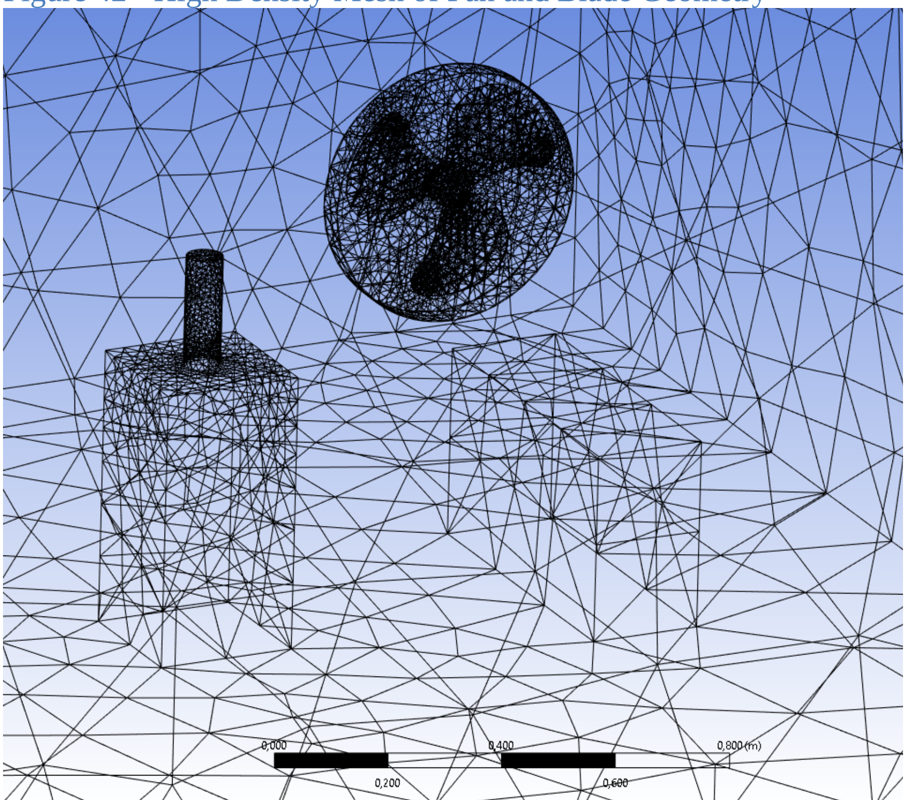

Source: From the Author

APPENDIX C – HAMFITPLUS - FITSUM TARIKU

Annex 68:

Subtask 5, Common Exercise 1.

Fitsum
Tariku

Building Science Graduate program

British Colombia Institute of

Technology Canada

Assumption:

- There is no interaction between indoor Hexane and the test cell interior surfaces/layer
- Hexane concentration in the outdoor air is assumed to be zero
- Indoor pollutant emission rate is not given. Here a 0.0082 kg/s (1 * Building Volume//hr) Hexane emission rate is assumed to compare the results with Jos and Marc results
- The indoor air is assumed to be well mixed and can be represented by node (single zone model)
- Only mechanical ventilation is considered

Method

Hexane concentration in the test cell is calculated using a Matlab function, which is incorporated in a Whole-Building hygrothermal model, HAMFitPlus (Tariku et al. 2010). The Matlab function represents a mass balance an inert gas concentration in a zone.

The Hexane concentration in the test cell can be expressed by a linear non-

homogeneous ODE. d/dt(Indoor_Hex)=[Q * (Hexane_Outdoor - Indoor_Hex) + S] /

Zonevolume (1)

Based on outdoor air assumption: Hexane_Outdoor=0, Equation (1) reduces to

Equation (2) d/dt(Indoor_Hex)=[S - Q * Indoor_Hex]/ Zonevolume (2)

The analytical solution for Equation (2) can be given as Equation (3):

Indoor_Hex=(S - exp(-(Q*dt)/Zonevolume)*(S – Q *Indoor_Hex_pv))/Q (3)

Where:

- Indoor_Hex: Indoor Hexane Concentration (kg/m3)
- S: Hexane emission rate (kg/s)
- Q: Ventilation rate (m3/s)
- dt: time step (s)
- Indoor_Hex_pv: Previous time step indoor Hexane Concentration in the zone (kg/m3)
- Zonevolume: Test cell volume (m3)
-

The Matlab function solves the analytical solution of Hexane concentration in the test cell using Equation (3).

Result:

Initial steady sate run: 2 days, 1 ACH Ventilation schedule: 0.1 ACH (Day 3, 17:20:00 till Day 9, 14:12:00) and 1 ACH for the rest of the simulation period

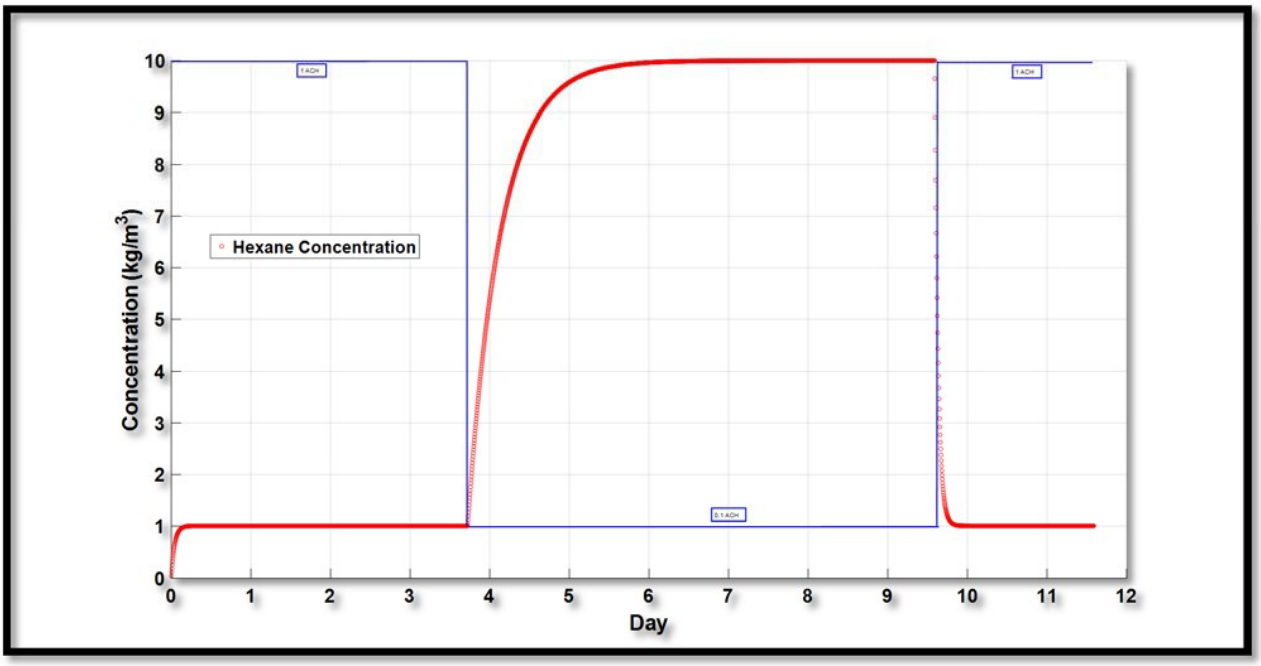

APPENDIX D – MATLAB ODE23S - JOS VAN SCHIJNDEL

Annex 68 ST5 CE1

Modeling and Simulation of Hexane in test cell

By Jos van Schijndel, July 4, 2017 Tool:

MatLab, ode23s

Interpretation of the modeling exercise description:

A lumped parameter model (No 3D information of the source), without using the climate data (No detailed information on the small window), assuming the supply ventilation rate from the table.

Appendix MatLab Files

Model Equations:

$$\frac{dm}{dt} = \dot{m}_i - \dot{m}_e + \dot{m}_s$$

$$V \frac{dc}{dt} = \dot{V} c_{in} - \dot{V} C + \dot{m}_s$$

$$\frac{dc}{dt} = \frac{\dot{V}}{V} \left(c_{in} - c \right) + \frac{\dot{m}_s}{V}$$

Simulation Result:

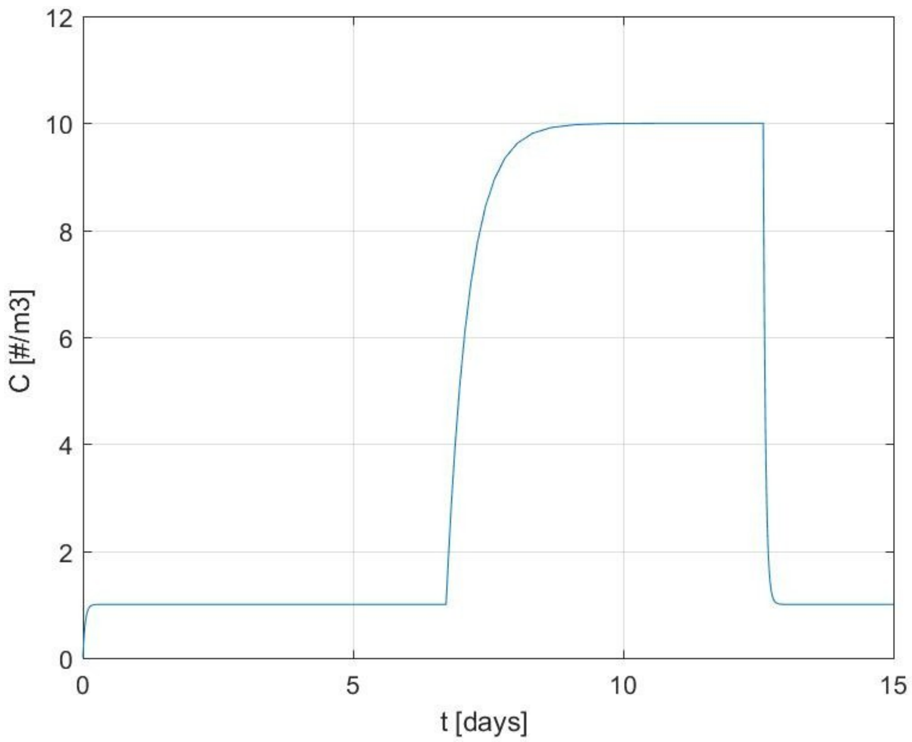

Appendix MatLab Files

```
%ODEXST ODE EXample STart Concentration
% IEA Annex 68 ST5 -1-
% JvS 2017/7


clear all


% Start/end time in seconds:
tbegin=0;
t1=5*24*3600;  %Time until Steady State
t2=t1+3600*(24*1+17.3333); t3=t1+3600*(24*7+14.2);
tend=15*24*3600;

% Initial values x0=[C0] x0=0;

% Start simulation [t,x]=ode23s(@odexfunC,[tbegin
tend],x0);
% Plot result plot(t/(24*3600),x)
xlabel('t [days] ')
ylabel('C [#/m3] ') grid
```

```
*************************************************************

%ODEXFUNC ODE FUN Concentration

% IEA Annex 68 ST5 -1-
% JvS 2017/7


function xdot=odexfunC(t,x)

%x=C  Concentration kg/m3 V=2.46*2.46*4.86;  %Volume

[m3]
Vdot=V*ACHfun(t)/3600; %Volume flow [m3/s] Cin=0;
mdotS=1*V/3600; xdot=(Vdot/V)*(Cin-x)

+mdotS/V;


function y=ACHfun(t)



%start t=0

t1=5*24*3600;  %Time until Steady State
t2=t1+3600*(24*1+17.3333); t3=t1+3600*(24*7+14.2);

te=15*24*3600;



if length(t)==1

%For odexfun t is scalar y=1;
  if ((t>t2) & (t<t3)) y=0.1;

end


else

%If t is vector nt=length(t);
y=ones(nt,1);
y(find((t>t2) & (t<t3)))=0.1; end


end
```

APPENDIX E – TRNSYS16 - MARC ABADIE

ANNEX 68

SUBTASK 5 – COMMON EXCERCISE 1

Author: Marc Abadie (ULR)

Tool: TRNSYS 16

A new TRNSYS component has been created for this CE to predict the evolution of gaseous pollutant in a room. It is based on the zonal library developed in the TRNSYS environment. It can take into account variations of airflow rate and pollutant source emission rate, as well as sorption effect using ka-kd model. See Mendonça et al. (2013, 2014) for further information about the original component.

Simulation parameters:

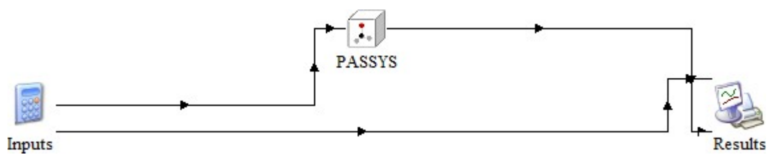

Figure 1: CE1 with Simulation Studio.

Figure 1 presents TRNSYS graphical interface called SIMULATION STUDIO where 3 components are connected together:

- Inputs: TRNSYS component "equation" where inputs can be specified,
- PASSYS: TRNSYS component "ROOM-VOC" where the calculation of the gas concentration are done.
- Results: TRNSYS component "Output" to save all results.

The inputs have been defined according to the experiment

description: RoomL = 4.86 ‘ Length of the room (m)

RoomW = 2.46 ‘ Width of the room (m)

RoomH = 2.46 ‘ Heigth of the room (m) Volume

= RoomL*Rooml*RoomH ‘ Volume of the room (m^3) Ra =

287 ‘ Air gas constant (J/(kg.K))

P = 101325 ‘ Pressure (Pa)

T = 27.5 ‘ Air Temperature (°C)

Rho = P/(Ra*(T+273.15)) ‘ Air density (kg/m^3)

t1 = 24+17+20/60 ‘ Time 1 (h)

t2 = 8*24+14+12/60 ‘ Time 2 (h)

ACH = 1*or(le(time,t1),gt(time,t2))+0.1*and(gt(time,t1),le(time,t2)) 'Air Change Rate (/h) Massflow = Rho*ACH/3600*Volume ' Air mass flow rate (kg/s)
MFR_W = Massflow ' to ROOM-VOC component – entering air (kg/s)

MFR_E = -MFR_W ' to ROOM-VOC component – leaving air (kg/s)

Source = 1*Volume/3600 ' Pollutant source emission rate (µg/s)

Note 1: the ROOM-VOC component requires airflow expressed in mass (kg/s) so that density has to be calculated but their values do not influence the results in the present CE.

Note 2: as the pollutant source emission was not possible to quantify with the current experiment description, it has been set to the value of Jos van Schijndel (TUe) to enable comparison (note of July 4, 2017).

Results:

Figure 2 presents the evolution of the pollutant concentration according to the variation of the air change rate.

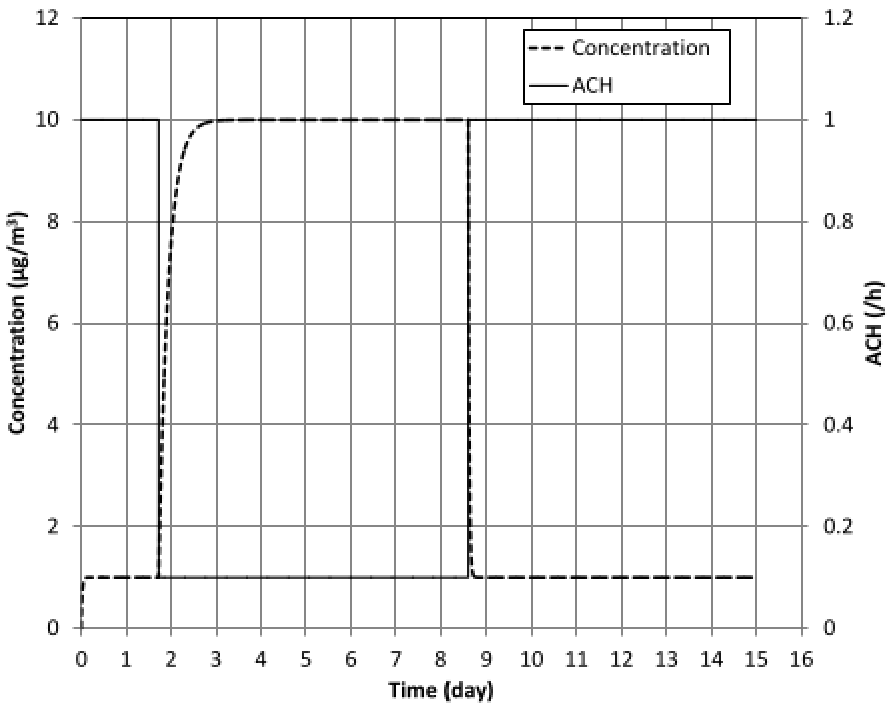

Figure 2: Pollutant concentration versus time.

References:

K.C. MENDONÇA, M.O. ABADIE, P. BLONDEAU. Modeling Gaseous Pollutant Distribution using the Zonal Approach: Case Study of an Office Space, In: ASHRAE IAQ 2013: Environmental Health in Low Energy Buildings, 15 October 2013.

K.C. MENDONÇA, M.O. ABADIE, C. BEGHEIN, P. BLONDEAU, Assessing the capabilities of the zonal model to predict the isothermal airflow induced by a linear ceiling diffuser, Building Simulation, 7(5), 2014, 489-501.

APPENDIX F – TRNSYS-CONTAM - TONI CALABRESI & GABRIEL ROJAS-KOPEINIG

ANNEX 68

SUBTASK 5 – COMMON EXCERCISE 1

Authors: Toni Calabrese, Gabriel Rojas-Kopeinig

Tools: TRNSYS, CONTAM

Introduction

A 1-zone building model (based on the Passys Cell of Limelette) with a constant source contaminant was modelled in CONTAM/Trnsys to evaluate the contaminant concentration. The energy simulation tool TRNSYS was coupled with CONTAM to perform, in addiction, energetic analysis.

Building model and boundary conditions

Figure 1 and Figure 2 show details of the model implemented in TRNSYS and in CONTAM, respectively. The building simulation tool TRNSYS works through types that represents components. The type 98 (here “PassysCell_Limelette_coupled”) allows the exchange of informations between TRNSYS and CONTAM. CONTAM is able to calculate the air flows between the different zones of a building or between the ambient and the building (i.e., infiltration, ventilation, etc.), but is not able to do any energetic analysis (e.g., calculation of temperature of the zone). TRNSYS receives as input the airflows from CONTAM and gives as output to CONTAM the temperatures of the zones. Type 9 “Experimental_data” reads the experimental weather data from an external file.

The main parameters of the simulations are:

- Volume of building: 29.4 m^3
- Climate: **Limelette (Belgium) experimental data**
- Time simulation: **1 week** (11 April **-** 17 April, experimental data available) with timestep of 1 minute
- Air change rate: **variable**, balanced ventilation system
- Contaminant: Hexane, Hexane rate: 490 ng/min (constant). A value of 490 ng/min was chosen to make possible the comparison with the results of Jos van Schijndel (Tue) and Marc Abadie (ULR)

- Hexane Ambient: 0 ppm (constant), Hexane initial of building: 0 ppm
- **No windows and infiltration** are considered
- Heating system (electric radiator, convective part: 40%) controlled with the operative temperature (Tsetpoint of **27.5°C**)

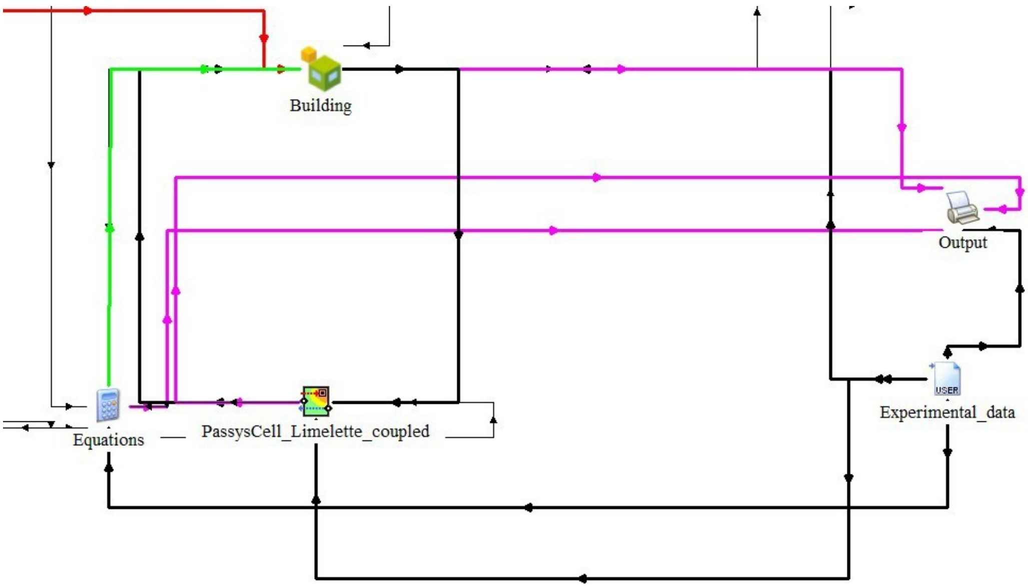

Figure 1. Detail of TRNSYS model

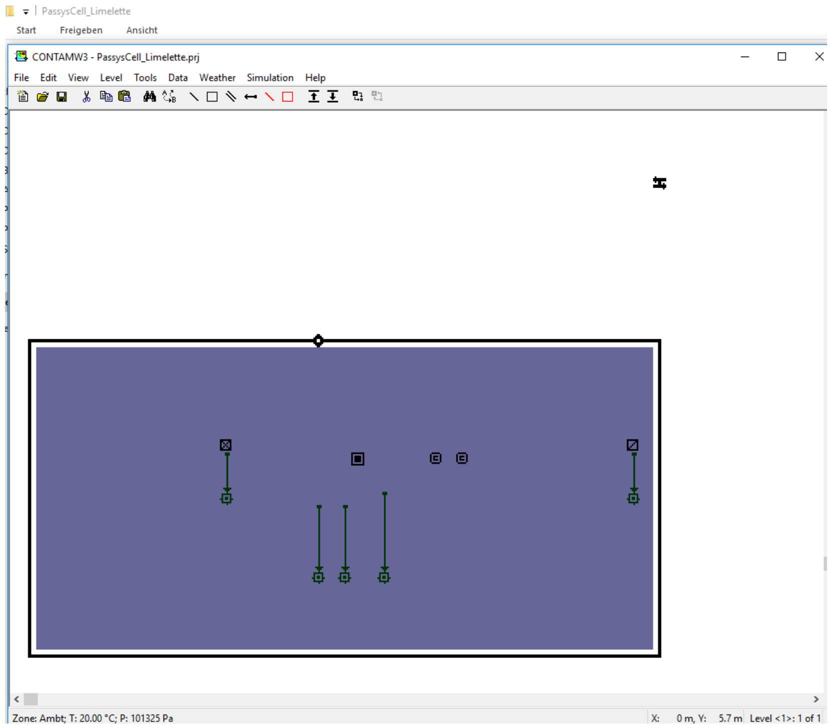

Figure 2. Detail of CONTAM model

Hexane concentration

A constant source of contaminant (Hexane) and a variable air change rate of the building was considered in the simulation in order to study the influence of the ventilation rate on the hexane concentration. Figure 3 shows the concentration of the hexane in the building. The evolution of the hexane concentration in the room is plausible and the stationary concentrations are comparable with the results obtained by the colleague Marc Abadie.

Energetic analysis

Figure 4 shows the ambient temperature and relative humidity used in the simulation. In TRNSYS a type is used to read these informations (experimental data from the site of Limelette). The experimental data were available just for the week 11Apr – 17Apr and, as consequence, just this period was simulated.

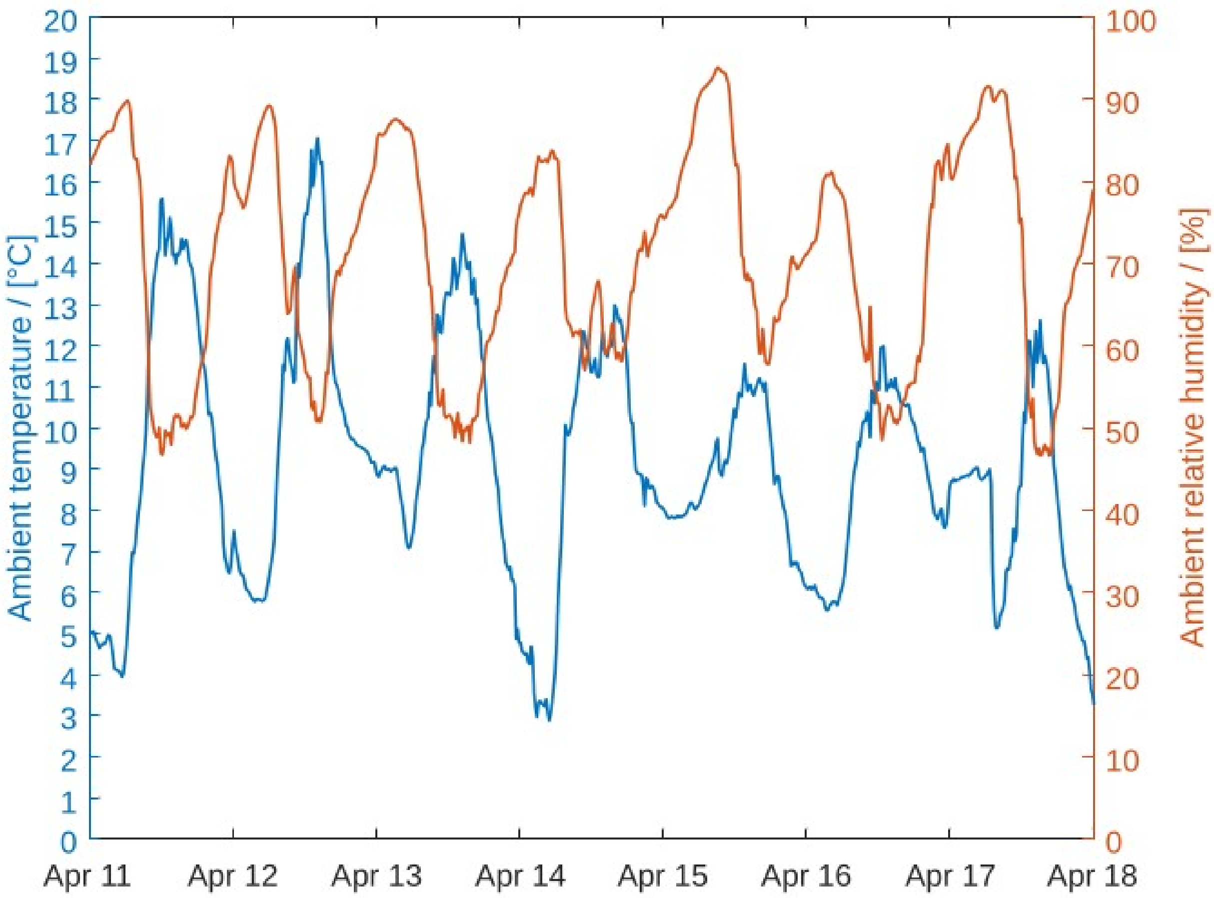

Figure 4. External temperature (left axis) and relative humidity (right axis)

Figure 5 shows the temperatures of the building and how the air change rate influences also the distribution of the heating power to the convective and radiative node. The control of the heating equipment works perfectly because the operative temperature of the building is always equal to 27.5°C and the radiative part of the total power is always 60%. The heating power has always a convective part of 40%, but the convective temperature is lower than the radiative temperature just when the air change rate is 1; when the air change rate is 0.1, the T conv is higher than the radiative temperature.

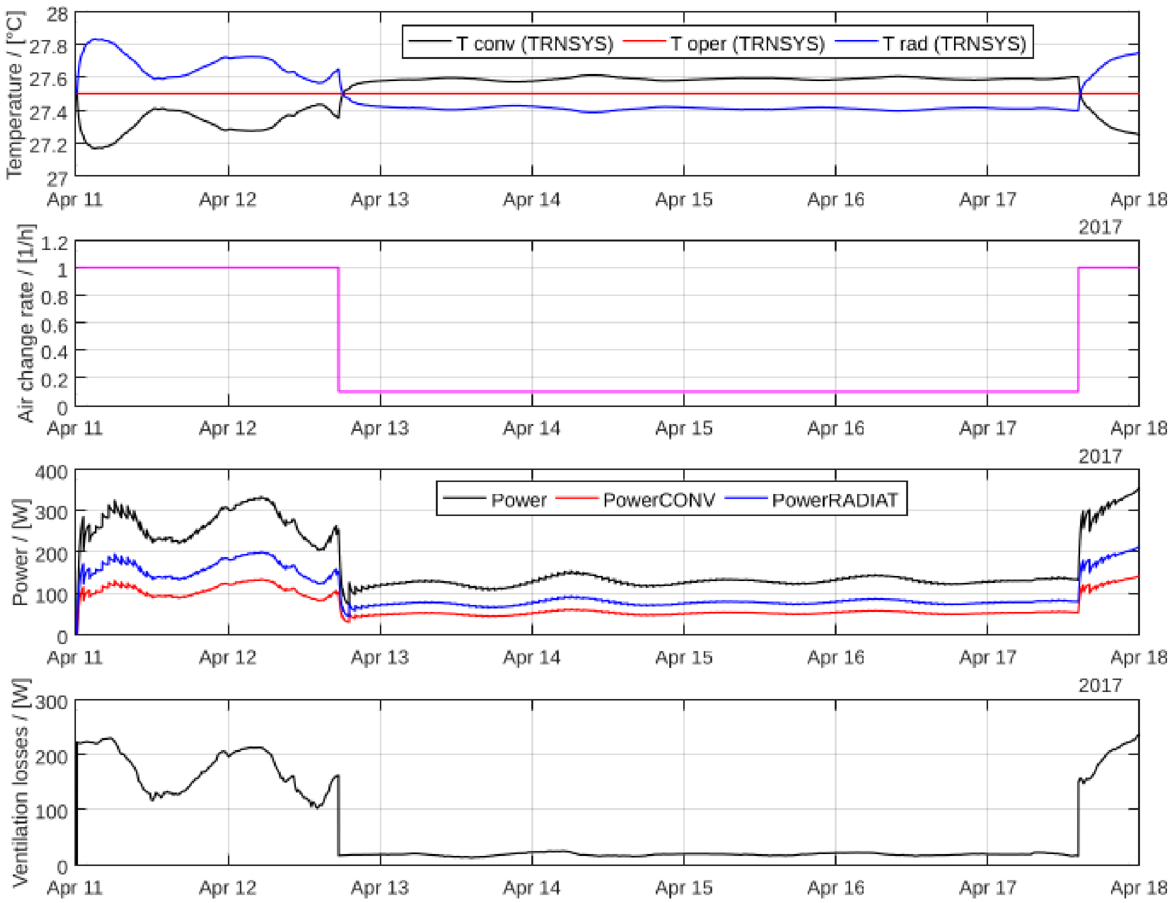

Figure 5. Temperature of the building (top), air change rate, power of electric radiator and ventilation losses (bottom) versus time

Table 1 shows the energetic balance of the building for the simulated period (1 week). As expected, the infiltration losses and the solar gains are zero.

Table 1. Energetic balance of the building

Transmission losses [kWh]	17.8
Ventilation Losses [kWh]	11.1
Infiltration losses [kWh]	/
Solar gains [kWh]	/
Heating demand [kWh]	**28.9**

APPENDIX G – NUMERICAL SOLUTION METHOD

The total Flow Time was 715200 seconds, which are 8 days, 6 hours and 43 minutes. It took Fluent 2,863,250 Iterations with a Delta-Time of 5 seconds and 143,040 Time Steps to complete.

Figure 43 - Convergency Chart of Numerical Solution

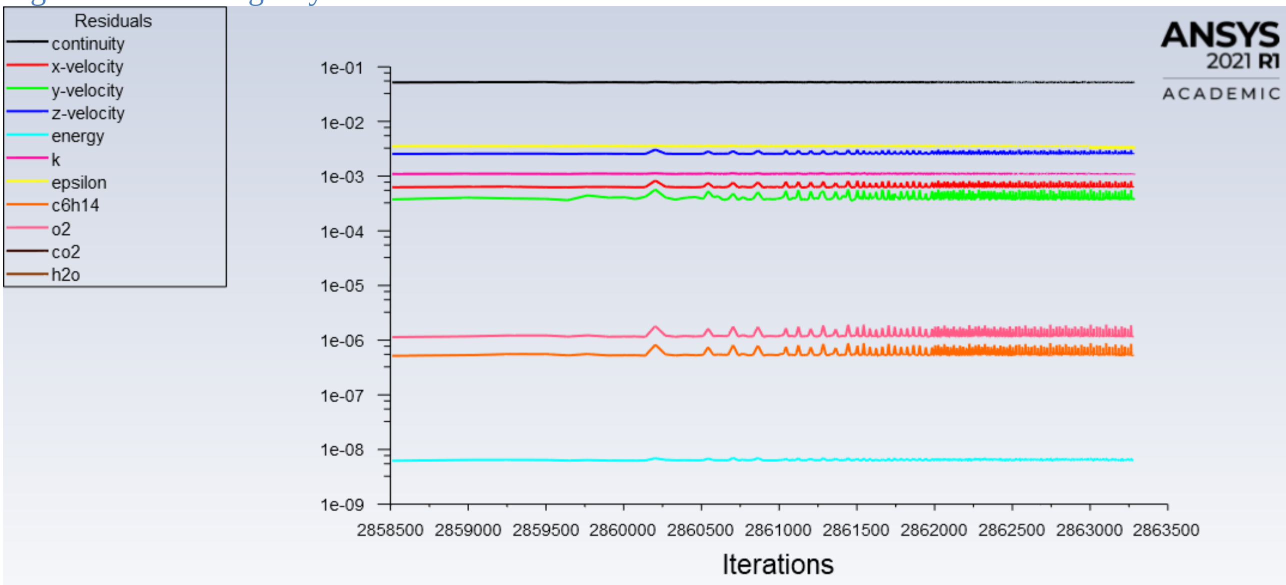

Source: From the Author

Table 15 - Convergence Status of Numerical Solution

	Value	Absolute Criteria	Convergence Status
Continuity	0.05187913	0.001	Not Converged
X-Velocity	0.0006342814	0.001	Converged
Y-Velocity	0.0004030316	0.001	Converged
Z-Velocity	0.00257777	0.001	Not Converged
Energy	6.308818×10^{-9}	1×10^{-6}	Converged
K	0.001078934	0.001	Not Converged
Epsilon	0.003187957	0.001	Not Converged
C_6H_{14}	5.410019×10^{-7}	0.001	Converged
O_2	1.185854×10^{-6}	0.001	Converged
CO_2	0	0.001	Converged
H_2O	0	0.001	Converged

Source: From the Author

APPENDX H – FIELD EXPERIMENT RAW DATA

The field experiment spreadsheet has 25962 rows of hexane concentration data. The interval of measurement was each 30 seconds for 9 days.

Figure 44 - Field Experiment Raw Data

datum	uur	C ppm	
4/10/2017	14:37:30	-0.18	4/10/2017 14:37
4/10/2017	14:38:00	-0.177	4/10/2017 14:38
4/10/2017	14:38:30	-0.18	4/10/2017 14:38
4/10/2017	14:39:00	-0.18	4/10/2017 14:39
4/10/2017	14:39:30	-0.18	4/10/2017 14:39
4/10/2017	14:40:00	-0.18	4/10/2017 14:40
4/10/2017	14:40:30	-0.178	4/10/2017 14:40
4/10/2017	14:41:00	-0.177	4/10/2017 14:41
4/10/2017	14:41:30	-0.178	4/10/2017 14:41
4/10/2017	14:42:00	-0.18	4/10/2017 14:42
4/10/2017	14:42:30	-0.178	4/10/2017 14:42
4/10/2017	14:43:00	-0.18	4/10/2017 14:43
4/10/2017	14:43:30	-0.178	4/10/2017 14:43
4/10/2017	14:44:00	-0.178	4/10/2017 14:44
4/10/2017	14:44:30	-0.18	4/10/2017 14:44
4/10/2017	14:45:00	-0.177	4/10/2017 14:45
4/10/2017	14:45:30	-0.18	4/10/2017 14:45
4/10/2017	14:46:00	-0.18	4/10/2017 14:46
4/10/2017	14:46:30	-0.18	4/10/2017 14:46
4/10/2017	14:47:00	-0.175	4/10/2017 14:47
4/10/2017	14:47:30	-0.18	4/10/2017 14:47
4/10/2017	14:48:00	-0.18	4/10/2017 14:48
4/10/2017	14:48:30	-0.18	4/10/2017 14:48
4/10/2017	14:49:00	-0.18	4/10/2017 14:49
4/10/2017	14:49:30	-0.18	4/10/2017 14:49
4/10/2017	14:50:00	-0.178	4/10/2017 14:50
4/10/2017	14:50:30	-0.18	4/10/2017 14:50
4/10/2017	14:51:00	-0.18	4/10/2017 14:51
4/10/2017	14:51:30	-0.178	4/10/2017 14:51
4/10/2017	14:52:00	0.595	4/10/2017 14:52
4/10/2017	14:52:30	0.985	4/10/2017 14:52
4/10/2017	14:53:00	1.05	4/10/2017 14:53
4/10/2017	14:53:30	1.127	4/10/2017 14:53
4/10/2017	14:54:00	1.193	4/10/2017 14:54
4/10/2017	14:54:30	6.735	4/10/2017 14:54
4/10/2017	14:55:00	4.1	4/10/2017 14:55
4/10/2017	14:55:30	1.41	4/10/2017 14:55
4/10/2017	14:56:00	1.48	4/10/2017 14:56

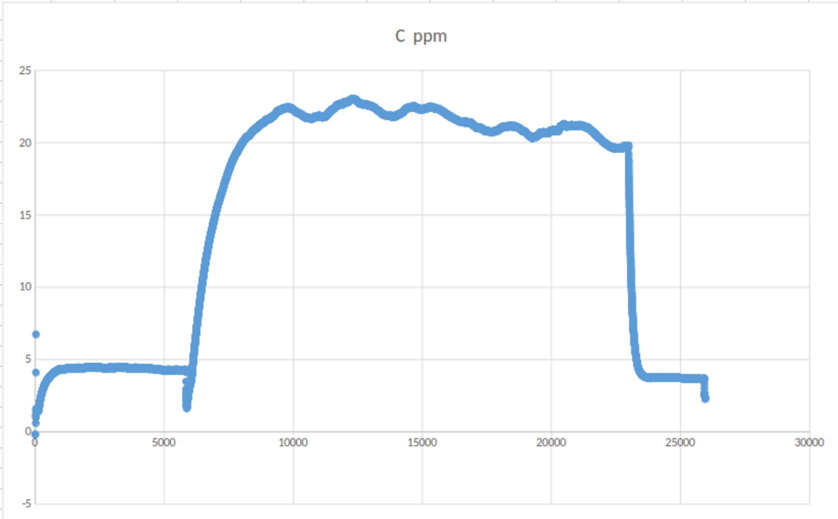

Source: Annex 68 Field Experiment